A Study on EMI Modeling of DC-DC Converter Using Noise-source Equivalent-circuit Model for Optimal Filter Design

March, 2023

Shuqi Zhang

Graduate School of
Natural Science and Technology
(Doctoral Course)
OKAYAMA UNIVERSITY

A Study on EMI Modeling of DC-DC Converter Using Noise-source Equivalent-circuit Model for Optimal Filter Design

Printed in Japan

Abstract

Electromagnetic compatibility of power electronics systems has evolved into an engineering discipline that should be considered at the beginning stage of the design process. While designing a power electronic system, switching loss and EMI problems should be taken into account simultaneously. These two issues affect system cost, size, efficiency, and quality that are a tradeoff when designing a power converter. Nowadays, power electronics are becoming more complex, and EMI is a more challenging issue.

In order to meet the requirements of power converters, an EMI model is proposed to predict conducted emissions from converters and guide EMI filter selection in the design phase.

The measurement-based equivalent circuit EMI models were shown to accurately describe EMI behavior in switched power converters. Compared to physical lumped-circuit models, these compact, linear models predict noise in the frequency domain, making simulations faster and more stable. However, the switching fluctuation affect the prediction accuracy, a method is proposed to remove the switching fluctuation effect. The prediction result is an “ideal” spectrum without switching fluctuation, which is different with the measured actual noise spectrum in reality. Moreover, to keep the model in the linear system, the load of the converter must remain fixed because any change in the load value will require re-extraction of the model parameter. In this thesis, the inherent switching fluctuation and load effect on differential-mode in DC-DC converters are investigated. A two-port noise-source equivalent circuit EMI model is used to predict conducted emissions from DC-DC converters considering the following topics:

(A) The adverse influence caused by DC-DC converter inherent switching fluctuation.

(B) The evaluation of the switching fluctuation effect in EMI prediction.

(C) The application of the proposed approach on the other types DC-DC converters.

(D) The load effect on DC-DC converter noise emissions.

The main objective of this thesis is to studied the DC-DC converter conducted emission and propose a simple, easy-to-derivate, widely applicable, and high-accuracy EMI model to predict the conducted emissions from DC-DC converters.

In Chapter 2, the waveform decomposition method is proposed to address: (A) the adverse influence caused by DC-DC converter inherent switching fluctuation is investigated. Usually, the oscilloscope averaging-mode is used for DC-DC converter conducted emission measurement to ensure both a high signal-to-noise ratio (S/N ratio) and a time-invariant linear system. However, when measured in averaging-mode, higher-frequency noise will be partially removed and the prediction accuracy of noise will be affected in higher frequency ranges. It is essential to ensure the S/N ratio, since the model based on measurement. However, the high S/N ratio for parameter identification cannot be guaranteed simultaneously with the higher frequency noise amplitude.

Through the investigation, the ripple noise is found to be not affected by switching fluctuation, only the untriggered spike noises are affected by switching fluctuation. The waveform decomposition method is proposed with the investigation. The noise signal is decomposed into ripple noise and triggered turn-on and triggered turn-off spike noises. With this method, switching fluctuations in measurement are removed without affecting higher frequency noise magnitude, while at the same time ensuring a high S/N ratio. The prediction result shows that the peak detected noise spectrum after removing switching fluctuation can be predicted within a 3-dB error up to 200 MHz.

In Chapter 2, an ideal conducted emissions prediction results are obtained, however, the prediction is different from the actual measurement condition. Thus, in Chapter 3, an experiment-based approach is used to address the switching fluctuation effect on conducted emissions from DC-DC converters, which are (B) The inherent DC-DC converter switching fluctuation is found to reduce the noise amplitude in the higher frequency range, which is the spike noise frequency range. The reduction principle is found to be similar to the frequency-modulation effect. Switching harmonics are spread by the converter's inherent switching fluctuations, which reduces the noise amplitude by several dB at each frequency. An experimental approach is proposed to address noise reduction, and a semi-empirical method is used to predict the averaged conducted noise from the converter. The prediction results show that the noise spectrum predicted by accounting for the reduction due to switching fluctuation agrees well with the spectrum obtained by averaging-mode measurement.

The general application of other types of DC-DC converter is treated in Chapter 4. Since only one commercial DC-DC buck type converter is evaluated in Chapters 2 and 3, the black-box EMI model is applicable to different type of converters. Thus, it is necessary to verify if the model is applicable to other types of converters. Besides, the general application process of the model is needed. In Chapter 4, a general application flow is described and two different type converters are used as an example to verify the model's applicability. One is a boost type converter, the other is a GaN-based buck type converter. The topologies and their EMI properties are first described. The EMI prediction results for both converters are in good accuracy. The result shows that the proposed model and approach is independent of the type of converter.

In the above work, a DC-DC buck converter used in Chapters 2 and 3 is evaluated with a fixed load. Since any change in the load would require re-extraction of the model, Chapter 5 proposes a method to make up for this deficiency. The model is extended to be applicable to normal mode noise from DC-DC converter with a variable load. The EMI prediction presupposes constant internal impedances independent of the load change with only the noise current source change dependent on the load change. Under these conditions, the noise current source at any load can be calculated by using the numerical interpolation method. Thus, in this chapter, the noise parameters for several different loads are identified. The process of parameter identification is described in Chapter 2. The internal admittances were found to be almost constant with respect to load change and only the input-port current source decreased with load. The cubic spline interpolation method is applied to fit the input-port current source and calculate it at any load. This approach was verified by predicting the input-port noise voltage for loads between 3.3 Ω and 15.6 Ω. Three load conditions are used as examples, 4.3 Ω, 6.6 Ω and 10 Ω. Below 80 MHz, the input-port current source decreased with load, and the input-port voltage predicted using input-port current source fitted by interpolation was in good agreement with the measured result.

Acknowledgments

Undertaking this PhD degree in Okayama University has been a truly life-changing experience for me and it would not have been possible to do without the support and guidance that I received from many people.

First and foremost I am extremely grateful to my supervisor, Prof. Yoshitaka Toyota and assistant professor Kengo Iokibe for their invaluable advice, continuous support, and patience during my PhD study. Prof. Toyota in particular, he is fantastic primary supervisor. Without his guidance and constant feedback this PhD would not have been achievable. Many thanks also to our assistant professor, Dr. Iokibe. He always manage lot of stuffs in lab perfectly. Thanks a lot for giving me a lot of kind advises in academic and career plan when I was anxious about my future. They have both not only guided me in many academic areas, but have also had an impact on my life philosophy. It is impressive to see how they approach their work with such a positive attitude.

I greatly appreciate my advisors Prof. Eiji Hiraki associate professor Kazuhiro Umetani, and Prof.Satoshi Denno for his helpful comments and great ideas on my research work. I am also very grateful to Prof. Hiraki for giving me the opportunity to have an internship in the EPC lab, Okayama University. This opportunity to learn about DC-DC converters and about different working processes in an entirely different environment has been extremely valuable to me.

It has been an amazing experience working at Optical and Electromagnetic Waves Lab, Okayama University. Thanks to everyone from OEW-lab past and present lab mates. From the early days, if it wasn ' t for the help of Mr. Taishi Ueimatsu, the start of my research would have been extremely difficult. Thank all the current members: Mr. Kanao Sho, Mr. Shohei Kan,Mr. Masaki Himuro, Mr. Zhenhong Xu, Ms. Yanyu Jin, Mr. Kohei Shimoda, and all bachelor students in our lab. Thanks to their kind support and assistance, I have been able to enjoy my time studying and living in Japan. Thanks also to everyone I ' ve met through the all the departments in Okayama University, your friendship and support have added a lot to my life in a different country.

Finally, thanks of course to my family for their support, my parents for their love and support throughout my life, Zhi Zhang, Xiuchuan Zhang. This thesis is dedicated to my parents. Without their tremendous understanding and encouragement in the past few years, it would be impossible for me to complete my study.

Contents

List of Figures

List of Tables

Chapter 1

General Introduction

1.1 Background

In this chapter, a brief overview of electromagnetic compatibility (EMC) is provided. The current state of EMI research in power electronics is reviewed. The motivation and objectives of this research are described. Finally, an outline of the dissertation is given.

1.1.1 The Aspect of Electromagnetic Compatibility (EMC)

Power electronics technology has advanced in recent years, allowing designers and manufacturers to decrease the size of converters by using higher switching frequencies. Therefore, it is inevitable in modern times that switches will operate in close proximity inside a power converter. These circuits often adversely affect each other, which may cause malfunctions. A very important concern has been raised as a result of this: electromagnetic compatibility (EMC). [1].

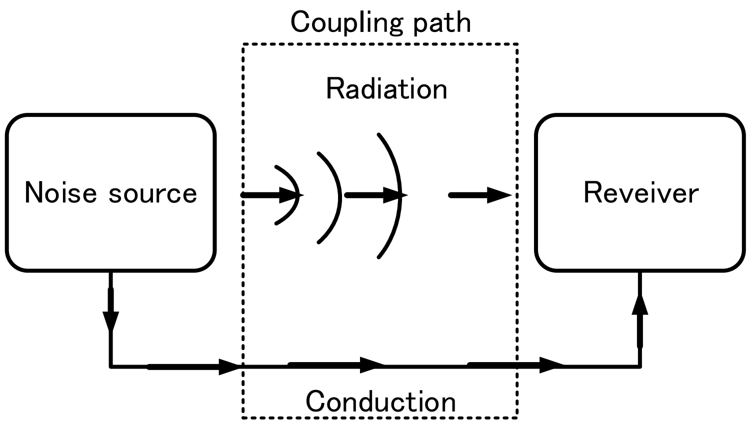

Figure 1.1 A basic illustration of the electromagnetic interference problem.

EMC is associated with generation, transmission and reception of electromagnetic energy, as shown in Fig. 1.1. It is the source that produces the emission that is transmitted to the receiver in the form of radiation or conduction through a transfer or coupling path. At the receptor, the signal is processed, which may cause undesirable behaviors.

As the the illustrated above, three aspects of EMC should be considered. The generation, transmission, and reception of electromagnetic energy. In Fig. 1.1, the noise source produce the emission, and the coupling path transfers the emission energy to the receiver. Emissions can be divided into radiated emissions and conducted emissions. If the received energy causes the receiver to behave in an undesired manner, this energy is seen as interference. This kind of interference needs to be avoided. Therefore, in order to prevent interference, there are three suggestions.

1. Suppress the emission at its source.
2. Make the coupling path as inefficient as possible.
3. Make the receiver less susceptible to the emission.

In addition to meeting the desired functional performance, devices must also meet the legal requirements of different countries. If the device cannot pass the requirements, it cannot be placed on the market for sale. Since the fast development of digital equipment, the EMC requirements will be more strict. Engineers should pay more attention to EMC aspects than before. This thesis describes serious research into modeling electromagnetic interference from switching mode power supplies (SMPS).

1.1.2 Conducted Emission from Switching Mode Power Supply

In this section, we introduce the measurement of conducted emission from a switched power converter first. Then, a DC-DC buck converter is used to explain the differential-mode and common-mode in power converter.

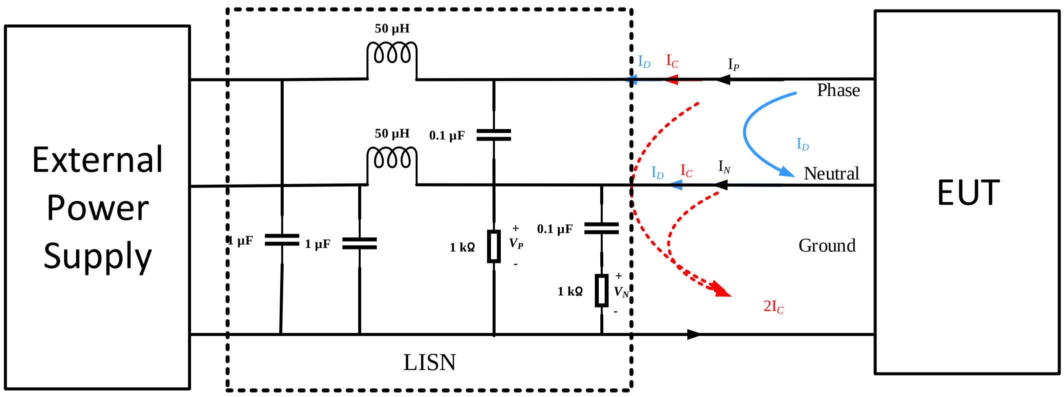

Figure 1.2 Equivalent circuit on conducted emissions measurement.

Figure. 1.2 shows a equivalent circuit on measuring conducted emissions from the equipment under test (EUT). To verify compliance with regulatory limits, emissions are to be measured with a line impedance stabilization network between the EUT and the power supply. The LISN is inserted at the measurement point between the EMI source and the power source to block electromagnetic emissions that are not due to the product under testing, in order to ensure that only emissions from the EUT are measured. Thus, the EMI measurement is repeatability and comparability.

The noise currents are decomposed into common-mode and differential-mode currents. Differential mode currents flow between neutral and phase conductors whereas common mode currents flow through the phase and neutral conductors, and take ground wire as the return path. Measured phase and neutral noise currents can be rewritten as follows:

$$I_P = I_C + I_D \tag{1.1}$$

$$I_N = I_C - I_D \tag{1.2}$$

Solving thees gives

$$I_D = \frac{1}{2}\left(I_P - I_N\right) \tag{1.3}$$

$$I_C = \frac{1}{2}\left(I_P + I_N\right) \tag{1.4}$$

The measured voltages are

$$V_P = 50(I_C + I_D) \tag{1.5}$$

$$V_N = 50(I_C - I_D) \tag{1.6}$$

Figure 1.3shows a representation of DM and CM current paths in synchronous buck converter. Two Y-capacitors are connected from positive and negative supply lines to GND conveniently complete the CM current propagation path [2].

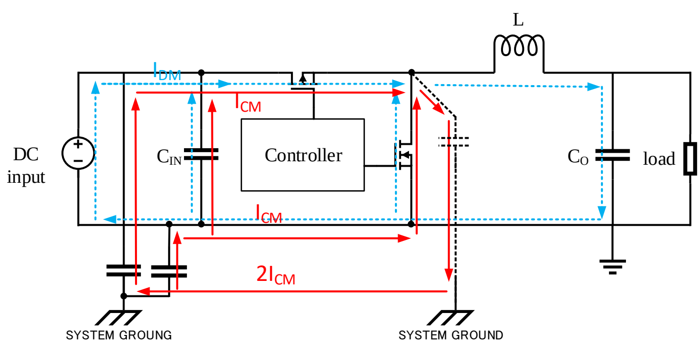

Figure 1.3 Noise propagation of DC-DC buck converter.

Understanding the sources and propagation paths for both differential-mode (DM) and common-mode (CM) conducted emissions noise components enables further insight into

DC/DC regulator conducted EMI behavior. DM noise current I_DM is due to intrinsic switching action and flows in opposite directions in the positive and return power lines. DM noise generally flows in a small loop area, with a close and compact return path. On the other hand, CM noise current, I_CM, flows in the system GND wire and returns via both power lines. The CM noise is mainly due to the high dv/dt at the switch node (SW) causing a displacement current that couples to the GND system through the parasitic capacitance associated with the MOSFET case, heatsink and switch node trace. Besides, the coupling capacitance associated with long cabling from a converter ' s input or output may present a CM noise path.

1.2 Literature Review

Power electronics products utilizing fast-switching semiconductors generate electromagnetic interference (EMI) noise. In order to ensure that the designed products meet EMC standard requirements, EMI filters are widely used. EMI filter applications and EMI problem analysis have been studied extensively to better handle noise generated by power converters [3–11].

To provide a design guide for attenuating switching ripple noise and maintaining adequate stability of buck converters, a secondary LC filter was proposed in [3]. The fundamental EM1 source mechanisms was studied in detail [4]. Two sources of the common-mode current of a PCB connected to an attached cable are described, which were differential-mode voltage and differential-mode current. In [5, 6], the approach to improve switching power devices EMI performance was proposed. EMI specifics of synchronous DC-DC buck converter were studied in [7], the mechanism of EMI generation of buck converter was explained. For better EMI filter attenuation, the mix-mode problem was addressed in [8]. Mix-mode (MM) noise is in addition to the differential-mode (DM) and common-mode (CM) noise conventionally associated with offline power converters. The intricate phenomenon of mix-mode was explained and the filter design guidelines were based on the mix-mode problem with balancing or canceling in [9–11].

However, EMI still poses many challenges to power electronic engineers, even though there are many known ways of lowering noise in the system. The later the engineer attempts to reduce noise the more costly the task becomes. Earlier in the design stage, noise can be filtered or contained using a variety of techniques. Layout, device selection, or filtering are only a few of the options that can reduce noise and can easily be changed earlier in the design process. If EMI is still a problem in the production phase of the product the only option an engineer has is to increase the size of the EMI filter. This will have the consequence of increased costs and a longer design cycle time. Thus, with a reliable model that accurately predicts EMI in a system the reduction of noise may be optimized for size, weight, reliability, and cost. To address this issue, a number of efforts have been made related to modelling and characterization of the EMI noise emissions of a particular device or system. These efforts are in the field of power electronics. [12–57]

Figure 1.4 summarizes how the conducted EMI modeling methods are classified [12].

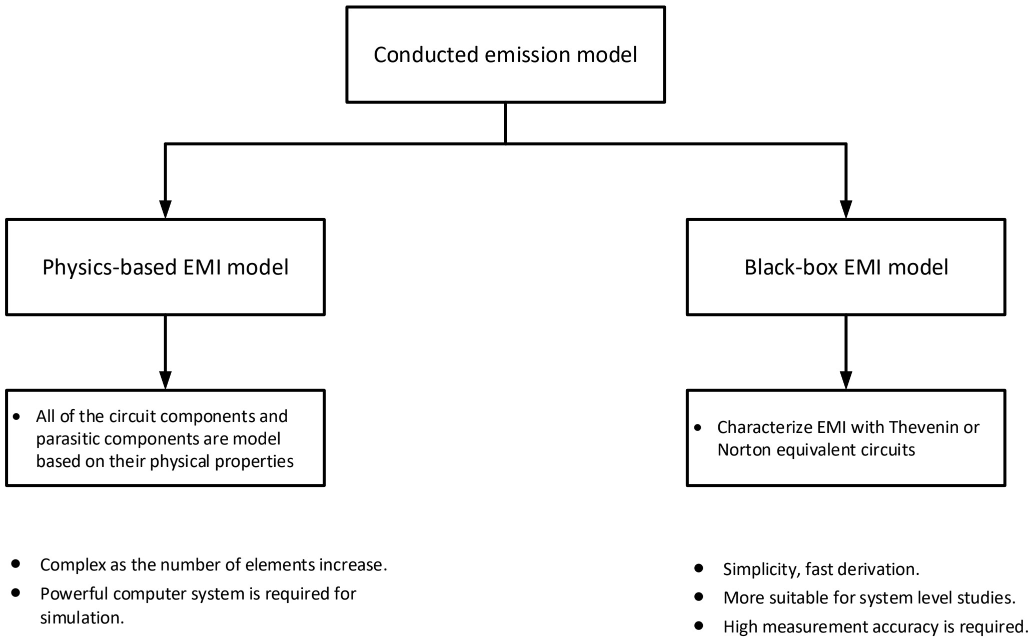

Figure 1.4 Comparison between physics-based and black-box EMI model.

The modeling of EMI can generally be broken down into two categories:

- Physical-based detail modeling [13–24].
- Behavioral modeling [25–57].

The detailed lumped circuit modeling approach is based on the physics of the circuit. It is a classical way to model the EMI from an electronic circuit.A detailed model can incorporate many aspects of a system model, including active switching devices, discrete passives, interconnections, and control circuitry. In most cases, these detailed models are created for use in time-domain circuit simulations. Model complexity and accuracy vary widely. The ultimate goal is to reduce complexity without sacrificing accuracy. Models of devices can range from an ideal switch, to an ideal switch with parasitic passives, to a complete physics-based analytical model that captures the entire electron transfer process in silicon. The complete model of an active device includes non-linear and higher order switching characteristics as well as static characteristics. The modeling technique relies on powerful computer systems to calculate large amounts and solve a large number of formulas or matrices. The PCB traces and wires are calculated using passive RLC equivalents. PCBs are typically extracted by electromagnetic numerical software, and the components are analyzed within 2-D or 3-D environments, usually within a co-simulation. The time depends on the complexity of the model.

In [13] the partial element equivalent circuit (PEEC) method approach is extended d for more flexible application in full-wave solvers. A full-bridge inverter conducted EM1 emissions are predicted in [14] with physics-based device modeling and time-domain reflectometry (TDR) for parasitics characterization, and then developed in [15]. In [16] the parasitic components and noise path of a AC motor drive are identified and measured with the TDR method, and developed in [18]. In [17] a frequency domain model with a large number of passive series connected networks was used to model long cables and no appreciable increase in the simulation times. With the reliable simulation result, the EMI filter selection based on the EMI model is proposed in [19]. The calculation of filter values for aircraft applications can be carried out by the proposed approach. A power converter model was built through a 3-D quasi-static finite element (3-D FE) approach. The prediction shows very good accuracy. However, since many factors related to the physics of semiconductors should be considered, the total work will increase with more actual semiconductor devices. The 3-D electromagnetic modeling approach for EMI filter design was proposed in [21]. The influence on conducted EMI of heat sink in SiC JFET Inverters was examined in [22]. The parasitic extraction method followed the previous studies [18]. Another some developed buck converter EMI model studies are describe in time-domain and compared with measurement result [23, 24]. Although the accuracy is good compared with measurement, the time for analyzing and building a model is dependent upon the complexity of the converter. In terms of cost and time, it is more effective to consider EMI issues at the design stage that would minimize post-processing solutions, including additional mitigation components, and testing time and cost. An EMC-integrated design requires comprehensive system modeling capable of predicting EMI emissions.

For this problem, a black-box EMI model, also known as a behavioral model or equivalent model, was recently proposed for faster and simpler EMI prediction. A black-box EMI model models power converters using multi-port networks with independent sources. It is then used to predict noise currents in CM and DM based on the derived equivalent circuit. A set of measurements can then be made in order to obtain predetermined parameters once the equivalent network has been determined. CM and DM noises can be separately or together modeled based on mixed mode noises. Experimental measurements are primarily used to identify model parameters (impedances and sources). Behavioral modeling is an appropriate method for system-level studies. On the other hand, the detailed modeling approach considers the features of the circuit elements.

An equivalent circuit is initially proposed in [25]. The conducted noise spectrum is straightforward computed in the frequency domain with an equivalent circuit. The prediction results were compared with time-domian prediction result with high accuracy. Calculation speed is much faster than the time-domain model method. In [26], the EMI characteristics is model by a a linear model with noise impedance and noise source. DM noise and CM noise is predicted by simplified EMI model. With the consideration above, [27] proposed a Modular Terminal Behavioral (MTB) model. The CM and DM emissions was predicted together, this modeling approach can also take into account mixed mode emissions. An IGBT phase leg is modeled by a three terminal Norton model, a multi-port impedance network replaces the propagation path, and the size of the impedance matrix is dependent on the number of phase legs. This model is future developed to a general model in [28] and [29]. The model is applied the insertion loss method proposed in [31]. A kind of EMI filter called "shunt impedance" to insert to to filter the conducted emission was used to catch up the behavior of the DC-DC converter interference. The noise impedance and noise impedance can be solved by a numerical matrix with several times measurements. In [28], the black-box EMI model was firstly developed to be a general model, the basic structure is determined with three noise impedance and two noise source.

Since the structure was well determined, and the parameters identification process were set to be standard, the other researchers were therefore focused on the prediction accuracy, fast Fourier transform process, application on inverter [30] or system model [34–36], etc. In addition to the whole EMI model, the studies on noise source impedance identification were also described in [32, 33]. The studies improved the noise impedance identification accuracy, especially the phase of noise impedance. The noise impedance phase is signification for EMI filter design. However, using only an equivalent circuit model does not provide any information on the EMI propagation and the precise sources position. A hybrid model with equivalent model and 3-D geometry model is proposed in [37]. The nonlinear semiconductor switches were replaced by behavioral voltages sources. The coupling path is simulated by 3-D EMI software. With the proposed model, a geometry view and the noise value can be examined visually. There were also studies on noise parameter identification process like [39] and non-symmetrical system level converter EMI prediction [38]. These studied developed the black-box EMI model to many novelty directions, but the basic structure did not change lot from the study in [28].

The application of black-box model is not only limited within conducted emission. Several studies have applied the equivalent circuit model to predict the radiation emission from power converters[53–55]. Moreover, the filter design based on black-box model were also described in [56, 57].

However, there are several unanswered questions in the existing study. The power converter is working under a time-variant condition, random noise is existing [58]. This problem was firstly discussed in [45], the limitations of black-box EMI model are described. The insufficient attenuation value by shunt impedance will lead numerically ill-conditioned matrix. Thus the parameter identification will be affected a lot. This problem has been discussed in [29]. Another problem is the switching fluctuation effect during the EMI measurement. In [47, 48], a methodology considering the time-varying nature of power devices for black-box model is proposed. The proposed methodology relies on the robust and elegant theory of periodically switched linear systems, providing the user with a tool for the generation of frequency-domain augmented linear time-invariant equivalents. Besides, in studied [49] the stochastic behavior of DC-DC converter has been considered during parameter identification. The averaged spectrum amplitude in higher frequency is small than maximized magnitude. Based existing studies, it can be found that the power converter switching fluctuation affects measurement accuracy. The methods require high accurate parameter identification, which is challenging particularly at high frequencies. This problem is the also the main problem in this thesis. Besides, it should be noted that the black-box model can only accommodate one type of operation condition for a power converter. Each operating point will require a repeated measurement setup once the load value, input port voltage changes. This thesis also proposed an approach to solve this deficiency.

1.3 Motivation and Objective

This thesis intends to assist in expanding a the noise-source equivalent circuit model that can be used as a general method for engineers to determine the most appropriate modeling method for the given application. According to the literature review, the noise-source equivalent circuit model provide high accuracy over a wide range of frequencies along with the convenience of simulations. Besides, he noise-source equivalent circuit model offers the well promise for the design and analysis of EMI filters and system level EMI. It is easy to simulate this class of models due to their simple topology

The purpose of this thesis is to extend the knowledge gained from our previous equivalent circuit model, and predict the realistic noise spectra in good accuracy. Model prediction results at lower frequencies are fairly accurate, but at higher frequencies, the errors are large [43]. There is a switching fluctuation effect in the measurement process that is responsible for this phenomenon. Due to switching fluctuations, portions of higher frequency noise are removed during measurement. To remove switching fluctuation effects, a method called waveform decomposition is proposed. This approach predicts the "ideal" noise spectrum of a DC-DC buck converter. Nevertheless, switching fluctuation effects should be considered in order to predict realistic noise spectra. Inherent switching fluctuation is found to have the same performance with frequency modulation technique, so noise reduction can be achieved. The noise reduction caused by switching fluctuation is obtained by an experimental method considering this consideration. Therefore, the realistic noise spectrum can be obtained by combining the "ideal" noise spectrum with noise reduction.

The proposed model and approach have also been shown to work well for a commercial buck converter. However, more work needs to be done to validate its generality for other types of converters.

The literature review also pointed out that all models of converters are based on the input side of the converter, i.e., no consideration is given to the load. EMI modeling should take into account noise at the output port and the load effect. The EMI model should be able to handle a wide range of load conditions.

In light of the limitations and unexplored directions mentioned above, the following goals have been identified for this dissertation:

(1) For improving noise-source parameter identification accuracy, an approach will be proposed to avoid the inherent switching fluctuations of DC-DC converters.

(2) In order to determine the realistic noise spectrum, the DC-DC converter switching fluctuation and its impact on the EMI spectrum will be examined.

(3) The proposed approach will be validated for converters with a boost type converter and a GaN-based buck converter.

(4) A load-variable equivalent circuit model will be developed to accommodate any changes in the value of the load.

1.4 Outline of The Thesis

In this study, an EMI model of DC-DC converter using noise-source equivalent-circuit model for optimal filter design is proposed.

Firstly, an approach called waveform decomposition method to remove the effect of switching fluctuation is proposed. By using the proposed waveform decomposition method, the parameter identification accuracy is well improved at higher frequencies. Besides, the inherent jitter behaves similar to the frequency modulation technique and reduces the noise amplitude at higher frequencies. On the basis of the hypothesis that the inherent jitter has similar effect to the frequency modulation technique, the reduction through the experimental approach using the spectrum caused by switching fluctuation is estimated. To obtain the actual noise spectrum in reality, the actual noise spectrum is obtained by the "ideal" spectrum using the waveform decomposition method considering the switching fluctuation effect. By accounting for switching fluctuation, the predicted noise spectrum agrees with the measured noise spectrum with 1024 times averaging. Moreover, it is discussed that the proposed model is applicable to different types of DC-DC converters using the buck and boost types converters as an example. Finally, a load-variable equivalent circuit model focused on normal mode noise from DC-DC converter with various load values is discussed.

In summary, this thesis focuses on the equivalent-circuit EMI models for conducted emissions from DC-DC converters and its wide applicable range. This thesis is organized as follows. Chapter 2 introduces the proposed noise source model and the waveform decomposition method for accuracy improvement. Chapter 3 explains the noise reduction caused by the switching fluctuation and evaluates the noise reduction due to switching fluctuation. Chapter 4 treats general applications of the proposed model using a boost type converter and a GaN-based buck converter as an example. Chapter 5 describes the extension of the model to load-variable application. Chapter 5, describes the load-variable equivalent circuit model.

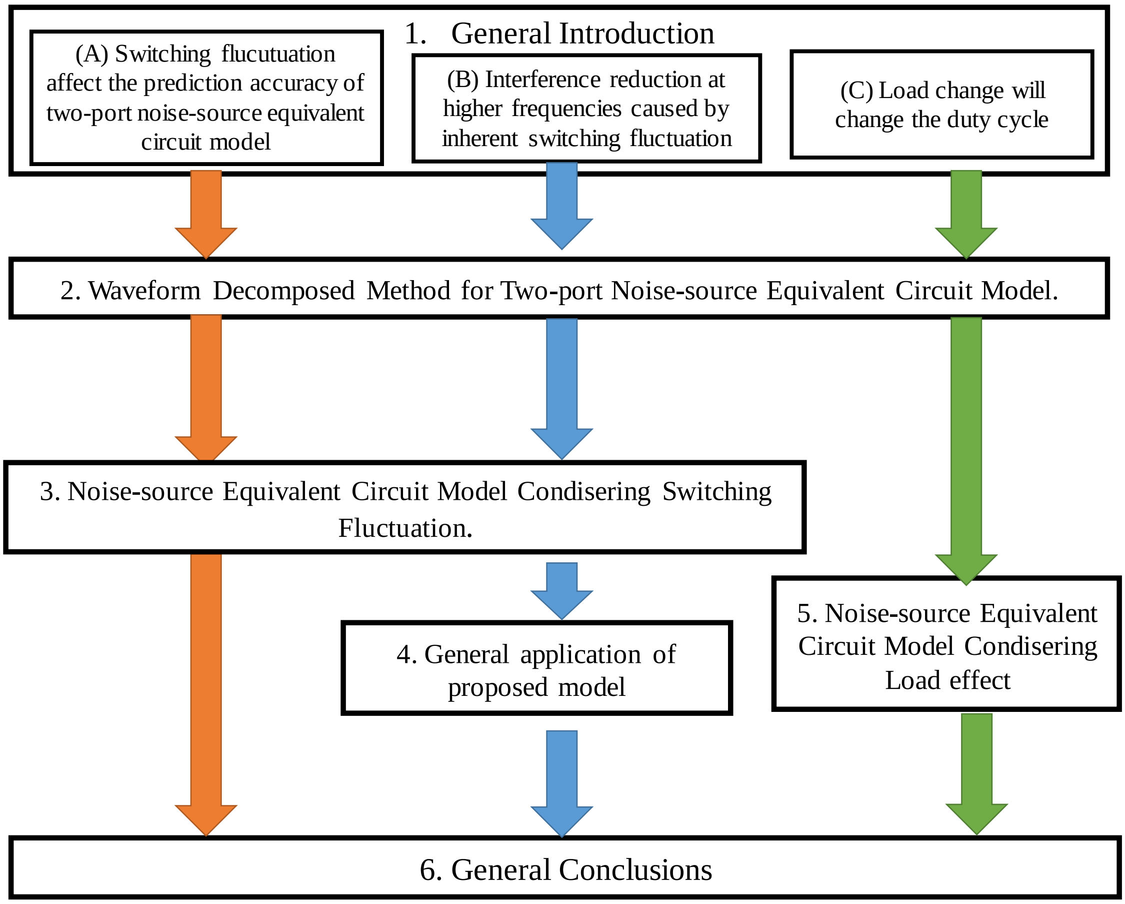

Figure 1.5 Chapter flows of this thesis.

Chapter 2

Waveform Decomposed Method for Two-port Noise-source Equivalent Circuit Model

2.1 Introduction

High-speed switching of power converters is associated with electromagnetic interference issues. In order to provide the most effective solutions, EMI modeling can be used to study and control EMI emissions.

It has become increasingly important to model electromagnetic interference (EMI) caused by power supply switching in recent years. With the partial element equivalent circuit (PEEC) method [13], parasitic elements of the entire propagation path can be obtained using commercial software, from which it is possible to obtain a complete set of parasitic elements. In contrast, the cost of this method increases significantly for complex components and systems. The second approach involves representing the EMI characteristics by using a Norton or Thevenin equivalent circuit with noise impedance and noise sources. The prediction process is relatively simple when the details of the electronics are unknown.

There have been many studies on EMI prediction based on the black-box method for DC-DC converter. Liu *et al.* proposed an EMI model called the modular-terminal-behavioral (MTB) model [27]. In another approach, the insulated-gate bipolar transistor (IGBT) phase leg conducted emission was modeled by a Norton equivalent noise emission model. Baisden and Bishnoi *et al.* developed the general terminal modeling (GTM) method as an extension of the MTB model for wider applications such as converter and DC-motor drive noise prediction [28–30]. Both the prediction accuracy and frequency range were improved in the GTM model by applying the insertion loss method proposed by Zhang *et al.* [31]. Shunt impedance was used to identify the noise impedance of the noise source and to determine the boost converter noise parameters. A system-level model was also developed based on this type of model in[35, 36, 38].

The black-box EMI model is considered to be a useful tool for predicting EMI at the system level. An approach to identifying noise parameters has been studied in [39]. In consideration of the physical meaning of converters, Zhang *et al.* developed a model of a four-port network for mixed-mode noise [40]. Fig. 2.1. illustrates a DC-DC converter with a load placed above the system ground. The GTM model is constructed by focusing on the blue box in Fig. 2.1, which yields the model shown in Fig. 2.2a. As a fixed load is applied to the GTM model, it can predict both the normal-mode (NM) noise as well as the common-mode (CM) noise, but it is unable to address the load dependence of the noise.

Accordingly, to address the load dependence, the red box in Fig. 2.1 can be modeled by removing the load. The black-box noise source model was first proposed to focus only on the NM noise [42]. It was then modified as shown in Fig. 2.2b [43] to improve the prediction accuracy by more than 20 dB. Thus, conducted noise can be predicted up to 200 MHz at both the input and output ports. Afterwards, the load effect was examined [44]. As long as a semiconductor device mounted on a printed circuit board (PCB) is well-grounded, we can focus only on differential-mode noise (DM).

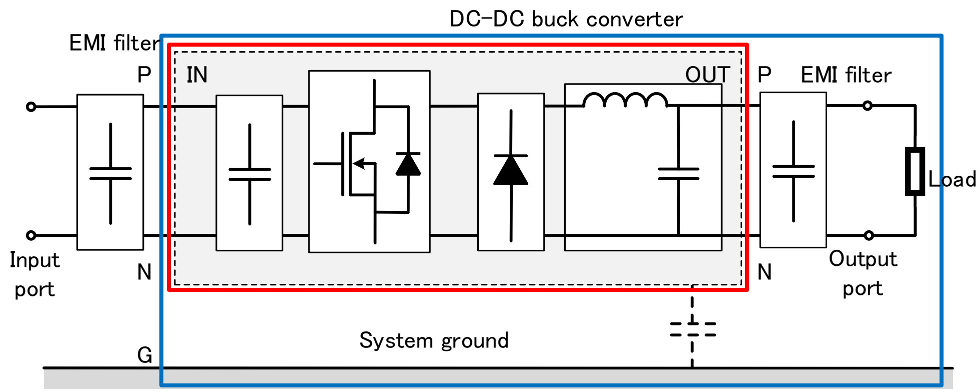

Figure 2.1 DC-DC converter with a load placed above the system ground.

However, the behavior modeling method has the disadvantage that the EMI from a DC-DC converter is not time-invariant due to its fluctuating switching frequency. There have been several studies that have addressed the time-variant behavior of DC-DC converters [45–50, 59]. Using the above technique requires maintaining the converter's operating conditions as time-invariant as possible by some means, such as maintaining the input voltage and load at fixed values and measuring the noise using an averaging mode. Rebholz *et al.* showed that small jitter could be eliminated through time-domain averaging of 10-200 signals, but the result was limited to periodic noise sources [45]. Sanchez *et al.* proposed a model to predict nonstationary and impulsive interferences from a switching power supply [46]. An enhanced Norton model has been developed by Trinchero *et al.* which incorporates the periodic time-varying activity of switching to predict DM

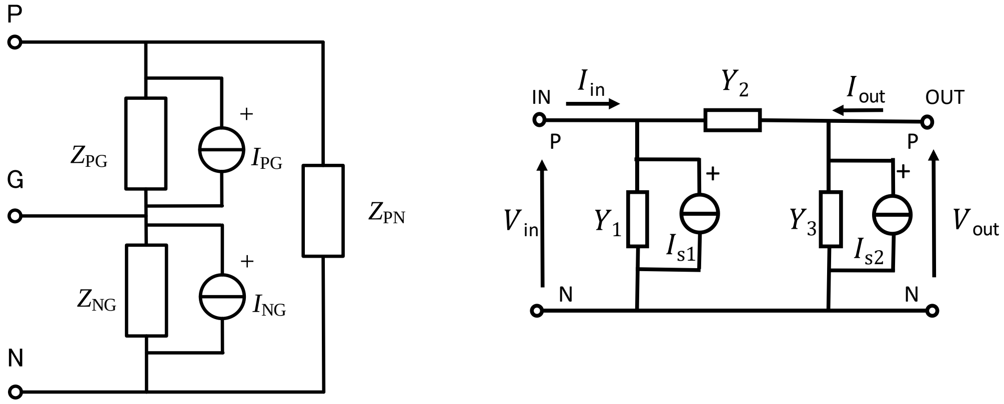

(a) Load included (b) Load excluded

Figure 2.2 Two-port noise source models including and excluding the load.

noise.The frequency range and accuracy were limited with the Fourier expansions of the admittance matrix [47, 48].

In order to characterize the noise signal characteristics of a DC-DC converter, Shen *et al.* considered the stochastic behavior of the converter and proposed the use of a custom PCB. The results of both the averaged spectrum and the maximum spectrum from the converter were predicted [49]. In their analysis, they found that the maximum EMI spectrum was 10 dB greater than the averaged spectrum at frequencies above 10 MHz, because intentional random modulation or oscillator instability reduced the peak level of the EMI spectrum.

In the studies discussed above, averaging measurements was used to eliminate random noise due to switching fluctuation. It should be noted that the use of an averaging mode reduces the high-frequency spectrum, resulting in a difference between the prediction and the actual measurement.

In order to ensure the accuracy of black-box models, we need to ensure measurement reliability. Therefore a method was developed for decomposing a measured time-domain noise signal without fluctuation into ripple noise and turn-on and turn-off spike noises in order to avoid accuracy degradation during parameter identification [60]. By using the waveform decomposition method, the undesired averaging effect in time-domain measurements can be avoided and the actual (peak) noise level can be predicted. With this waveform decomposition method for peak detection, it is possible to predict noise spectra without switching fluctuation within a 3-dB prediction error up to 200 MHz.

2.2 Two-port Noise-source Equivalent Circuit Model

2.2.1 Model Definition

Figure 2.3. shows a model based on a Norton equivalent circuit that includes three noise admittances and two noise current sources. By separating the load from the model, a two-port model can be used to study noise-source equivalent circuit parameters for different loads. In contrast to load-dependent models, this model is limited to DM noise prediction, since it does not take into account the ground wire, i.e., the system ground. As a general rule, CM noise is generated by the grounding of the system and the surrounding metals, which is not considered in this model. In practice, on-board measurement can minimize the mode conversion between common and differential modes. The model only focuses on the DM noise of input-port noise $\dot{V}_{\mathrm{in}}$ and output-port noise $\dot{V}_{\mathrm{out}}$.

In [43], the circuit equations with the five model parameters ($\dot{Y}_1, \dot{Y}_2, \dot{Y}_3, \dot{I}_{\mathrm{s1}}, \dot{I}_{\mathrm{s2}}$), were derived from the noise model shown in Fig. 2.3 on the basis of Kirchhoff's current law and expressed as follows:

$$\begin{bmatrix} \dot{I}_{\mathrm{in}} \\ \dot{I}_{\mathrm{out}} \end{bmatrix} = \begin{bmatrix} \dot{V}_{\mathrm{in}} & \dot{V}_{\mathrm{in}} - \dot{V}_{\mathrm{out}} & 0 & -1 & 0 \\ 0 & -\dot{V}_{\mathrm{in}} - \dot{V}_{\mathrm{out}} & \dot{V}_{\mathrm{out}} & 0 & -1 \end{bmatrix} \begin{bmatrix} \dot{Y}_1 \\ \dot{Y}_2 \\ \dot{Y}_3 \\ \dot{I}_{\mathrm{s1}} \\ \dot{I}_{\mathrm{s2}} \end{bmatrix}. \tag{2.1}$$

To identify the model parameter, the input port current $\dot{I}_{\mathrm{in}}$ and output port current $\dot{I}_{\mathrm{out}}$ as well as $\dot{V}_{\mathrm{in}}$ and $\dot{V}_{\mathrm{out}}$ are required under different conditions: normal condition with no filter and attenuated condition with a capacitor, as shown in red in Fig. 2.3 The capacitor filter is used because it will affect neither the input dc voltage nor the duty cycle of the DC-DC converter.

For the normal condition, $\dot{I}_{\mathrm{in}}$ and $\dot{I}_{\mathrm{out}}$ are calculated using the following equations:

$$\dot{I}_{\mathrm{in}} = -\dot{V}_{\mathrm{in}}/Z_{\mathrm{IN}}, \tag{2.2}$$

$$\dot{I}_{\mathrm{out}} = -\dot{V}_{\mathrm{out}}/R_{\mathrm{load}}, \tag{2.3}$$

where Z_{IN} denotes the impedance of our handmade artificial mains network circuit. The photo is shown in Fig. 2.4. The circuit diagram and impedance magnitude are shown in Fig. 2.5 and Fig. 2.6.

Attenuated conditions are achieved using capacitor filters with equal capacitance inserted into the DC-DC converter's input and output ports. Then measure the filtered input-port noise $\dot{V}'_{\mathrm{in}}$ and output-port noise $\dot{V}'_{\mathrm{out}}$, and calculate input-port and output-port current by:

$$\dot{I}'_{\mathrm{in}} = -\dot{V}'_{\mathrm{in}}/(Z_{\mathrm{IN}} \parallel Z_{\mathrm{cin}}), \tag{2.4}$$

$$\dot{I}'_{\mathrm{out}} = -\dot{V}'_{\mathrm{out}}/(R_{\mathrm{load}} \parallel Z_{\mathrm{cout}}), \tag{2.5}$$

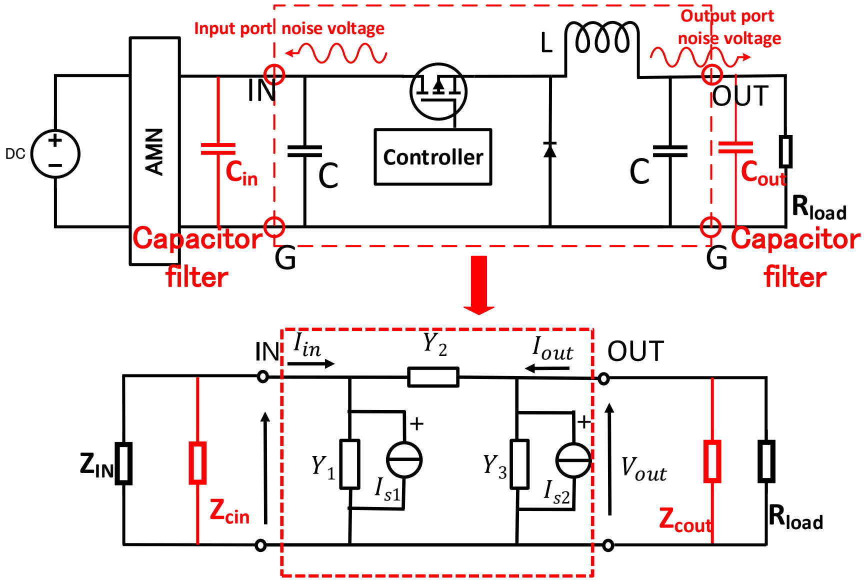

Figure 2.3 Two-port noise source model structure.

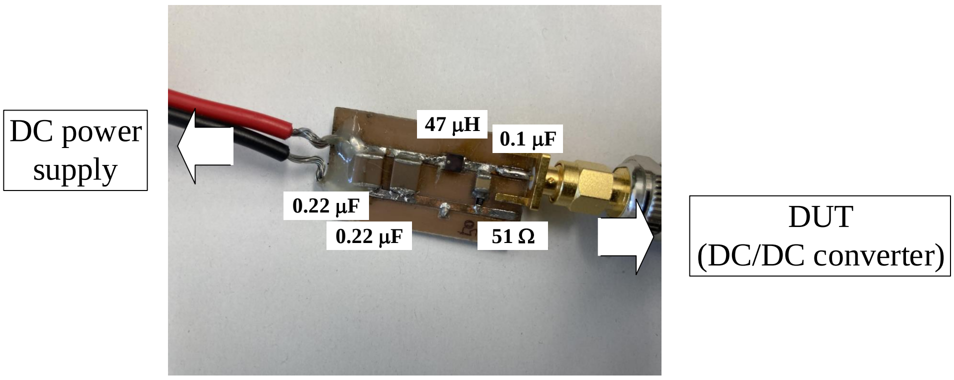

Figure 2.4 Picture of homemade LISN.

where Z_{cin} and Z_{cout} are respectively the impedances of the filter inserted in the input and output-ports including ESL and ESR. The measurement process and filter information are presented in the next section.

To solve (2.1), it is necessary to obtain noise signals under at least three different conditions. The noise signals must be obtained under at least three different conditions. In order to obtain attenuated noise signals, the capacitances at the input and output ports can be changed in order to filter the conducted noise. Each measurement yields a pair of equations. Measurement three times results in an overdetermined system of equations. In order to find a set of solutions to an overdetermined system, the ordinary least squares method is applied.

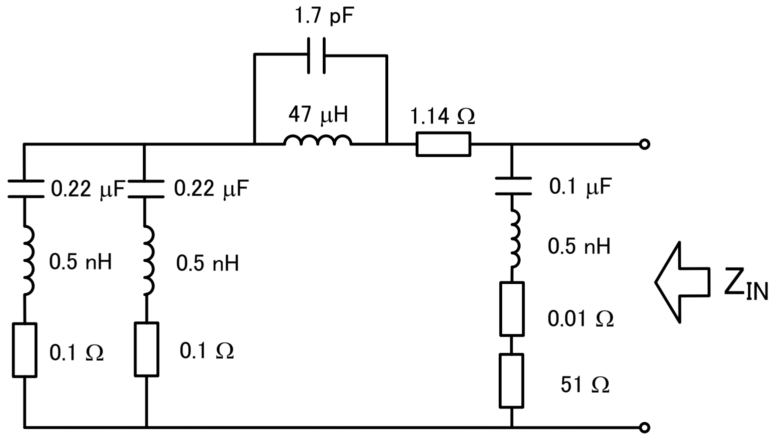

Figure 2.5 Circuit diagram of homemade LISN.

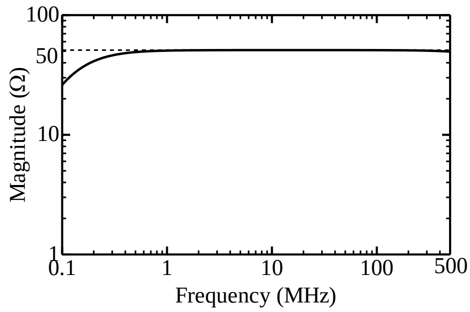

Figure 2.6 Impedance of homemade LISN.

2.2.2 Linear Time-invariant System for Modeling

This model utilizes a linearly equivalent circuit to approximate non-linearly time-varying noise from power electronics. In order to keep the converter linear for modeling, AMN also called LISN is used to block interference from the power supply. Keep the load fixed so that the converter operates under stable conditions. As for the converter's inherent switching fluctuation, the conducted emission has been averaged over 1024 times. However, the measurement result is affected by the switching fluctuation effect. In this thesis, we applied the waveform decomposition method to avoid the switching fluctuation effect.

2.2.3 Switching Fluctuation Effect on Emission Measurement

The prediction accuracy of this model is highly correlated to oscilloscope measurement. For this thesis, a DC-DC buck converter (Rohm, BD9G341EFJ-EVK-101) with a 10-Ω load was used for evaluation. The input voltage was 18 V, and the output voltage was 5 V. Two passive 10:1 probes (KEYSIGHT N2894A with 10-MΩ input resistance and 9.5-pF input capacitance) were used for measuring the input and output noise, while another one was used for measuring the reference signal, as shown in Fig. 2.7. As a reference signal, the signal at the switching node of the DC-DC converter was used. The switching frequency was 200 kHz. An application of the trigger was made to the switching-node voltage, with a trigger level of 9 V, which is half the maximum switching-node voltage of 18 V.

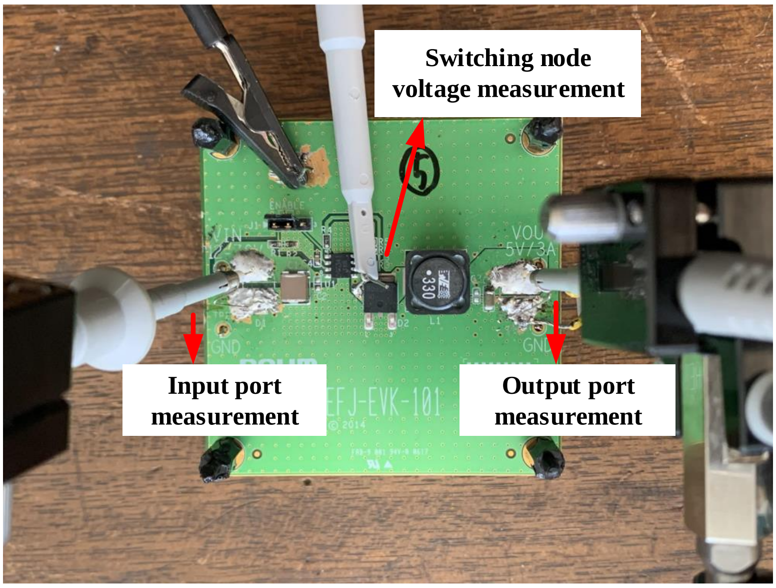

Figure 2.7 Measurement setting on DC-DC converter board.

Noise measurement is time-variant as a result of switching fluctuation, which makes the time-invariant black-box model (EMI) inapplicable. Generally, noise measurements are conducted using the averaging mode to eliminate switching fluctuations, but this leads to a second problem.

Accordingly, the measured noise signals were compared with and without averaging in both the time domain and the frequency domain of the input port. Although a power converter is a nonlinear, time-variant network, the noise-source equivalent circuit model is assumed to be a linear time-invariant (LIT) circuit when the conducted noise of the DC-DC converter approximated to be linear. While averaging can improve measurement accuracy, the oscilloscope averaging mode eliminates random noise and approximates time-invariant measurements. Furthermore, with the averaging acquisition mode, conducted noise at higher frequencies is significantly reduced.

Here, we took the input time-domain signal as an example. We set the oscilloscope (Keysight DSOS104A) to AC voltage measurement with a rising trigger slope. Figure 2.8 shows the time-domain signal and the frequency-domain spectrum averaged over 1024 times when the trigger was set to the time-zero position. Figure 2.9 shows the measured result without averaging and the frequency-domain spectrum after application of a fast Fourier transform (FFT). The random noise in the frequency-domain spectrum was approximately 40 dB, but parts of the averaged noise signal were removed by averaging. An approximately 10 dB reduction is observed in the range of 10 to 200 MHz. Consequently, even though averaging improves measurement accuracy at lower frequencies, the noise signal degrades at higher frequencies due to the DC-DC converter's actual noise.

This results in a trade-off between averaging the measurements and measuring the actual noise. It is possible to measure an interference signal with a high signal-to-noise ratio (SNR) by using the averaging mode. However, the amplitude of the high-frequency noise will be smaller than that of the actual noise. In contrast, a stochastic interference signal obtained without averaging has a low SNR and cannot be analyzed with a linear approach. As a result, it is important to maintain SNR without compromising EMI measurements.

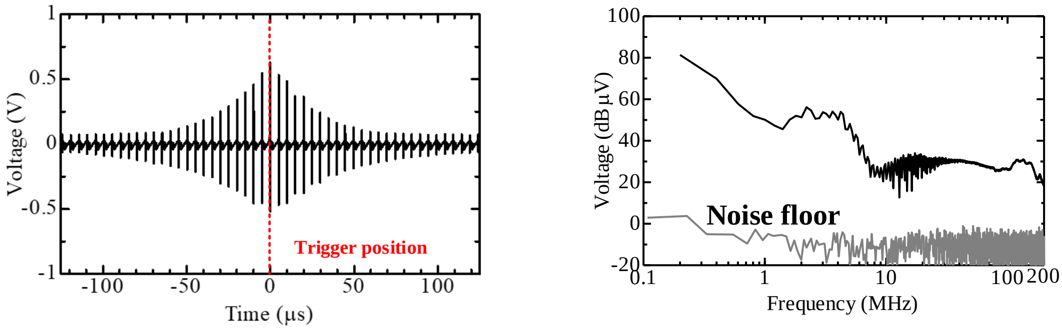

Figure 2.8 Noise signal averaged 1024 times.

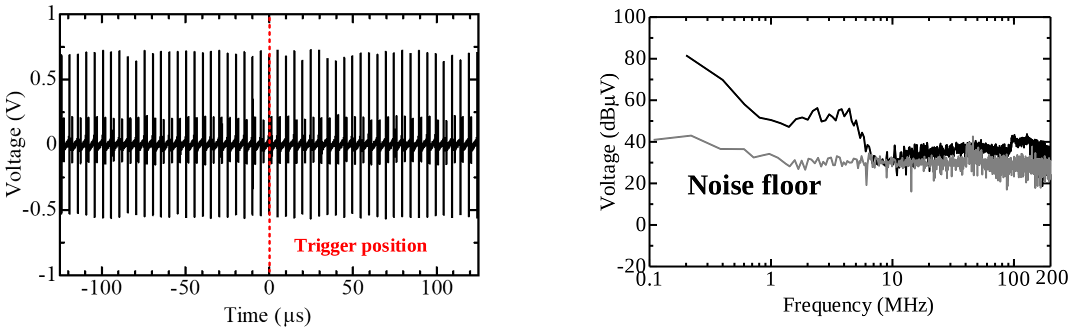

Figure 2.9 Noise signal without averaging.

The next step was to investigate untriggered and triggered spike noise signals. Here, the switching node signal was used as a reference, and the trigger edge was rising. Figure 2.10 shows 50 samples of zoomed 2.10a turn-on and 2.10b turn-off spike noise signals without averaging. The results indicate that there is no switching fluctuation in the triggered turn-on spike noise signal, but there is fluctuation in the turn-off spike noise signal.

Therefore, only triggered spikes and ripple noise (i.e., noise below 10 MHz) meet the accuracy requirements. That is, because the averaging mode only keeps the periodic noise signal, much of the turn-off noise in Fig. 2.10b is removed, which makes the prediction

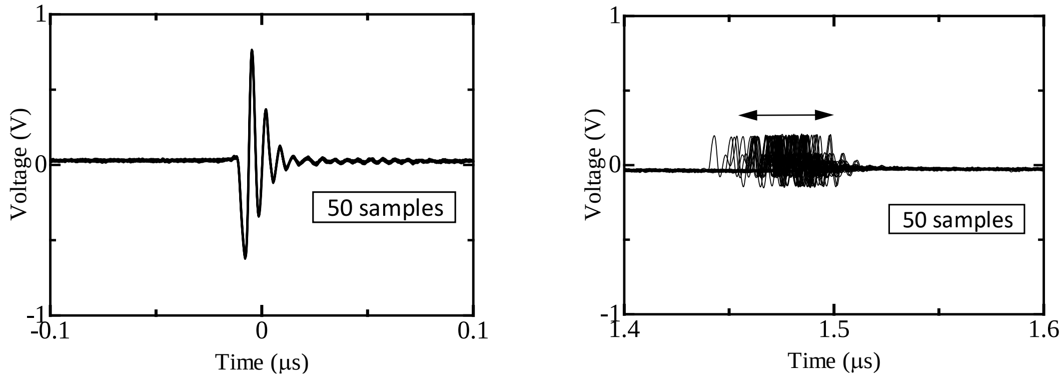

(a) Triggered turn-on noise

(b) Untriggered turn-off noise

Figure 2.10 Spike noise with and without triggering.

inaccurate. Because averaging improves measurement accuracy only for the triggered signal and degrades measurement accuracy for the untriggered signal, identifying the noise parameter will be more accurate if the noise signal is decomposed and only the triggered noise signal is acquired.

The basic idea for waveform decomposition is to extract the ripple noise and spike noise to avoid the switching fluctuation influence. The general process to extract the decomposed noise signal will be introduced in 2.3.

2.3 Waveform Decomposition Method

2.3.1 Decompose Noise Signal to Keep Measurement Accuracy

This method divides the time-domain signal into three parts and builds a noise model for each part, as shown in Fig. 2.11. In this DC-DC converter, the time-domain noise signal is composed of ripple noise (below 10 MHz), turn-on spike noise, and turn-off spike noise (10-200 MHz). By using this method, it is possible to predict the peak noise amplitude without fluctuation.

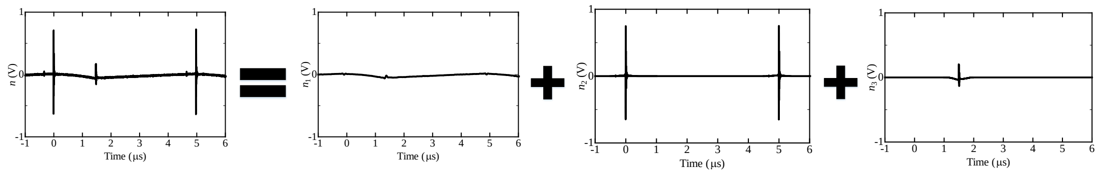

Figure 2.11 Schematic of waveform decomposition method.

Figure 2.12 illustrates the process of the waveform decomposition method, and Table 2.1 lists the measurement conditions. For the three decomposed noise components of the time-domain signal—that is, the ripple noise $n_1(t)$, the turn-on spike noise $n_2(t)$, and the turn-off spike noise $n_3(t)$—the following equation holds:

$$n(t) = n_1(t) + n_2(t) + n_3(t) \ . \tag{2.6}$$

The time-domain signal expressed by (2.6) can then be transformed into a frequency spectrum:

$$N(f) = N_1(f) + N_2(f) + N_3(f) \ , \tag{2.7}$$

$$N_i(f) = \mathrm{FFT}[n_i(t)] \quad (i = 1, 2, 3). \tag{2.8}$$

Due to the decomposition of the noise signal into three components, the noise models for prediction are also divided into three categories. In order to account for each port, six noise prediction models must be developed [60, 61].

Table 2.1 Measurement conditions.

	Condition 1	Condition 2
Sampling rate	1 Gs/s	10 Gs/s
Measurement time	250 µs	1 µs
Averaging times	1024	1024

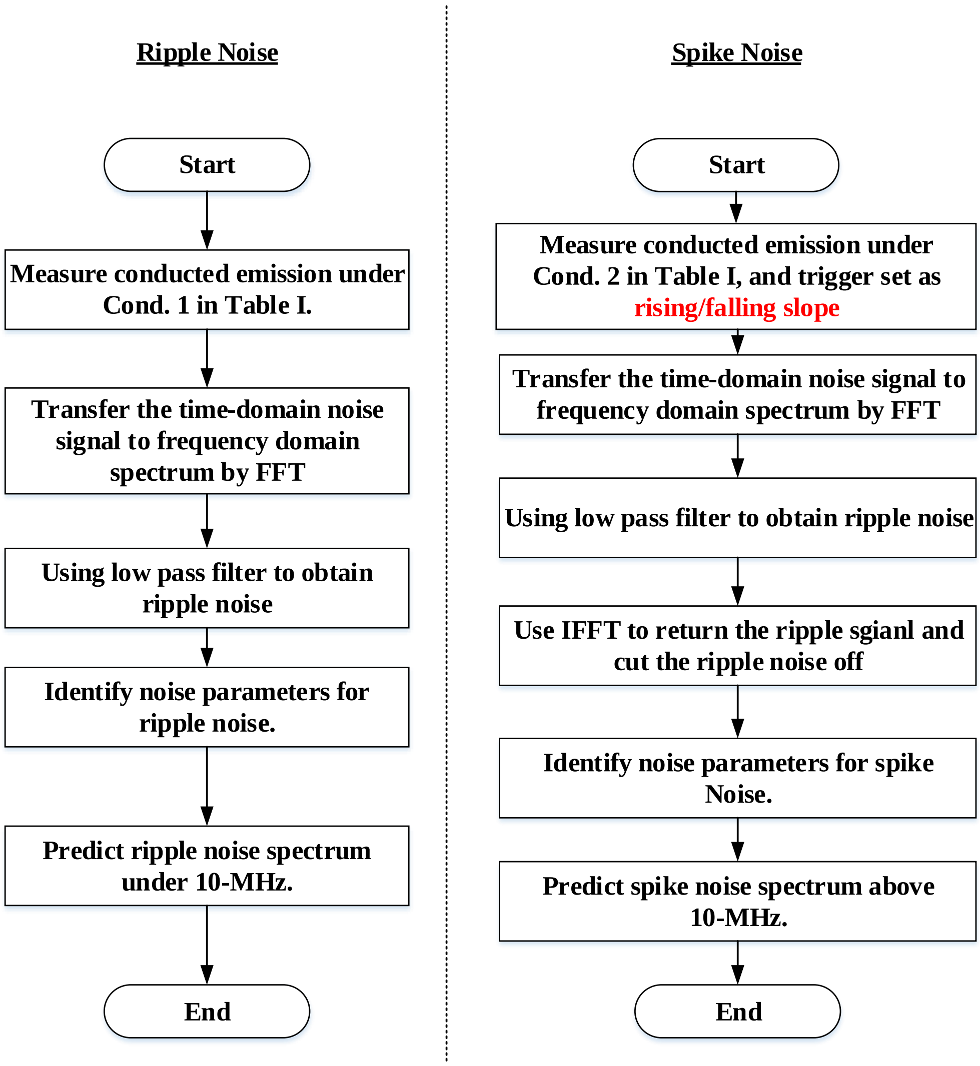

Figure 2.12 Prediction process.

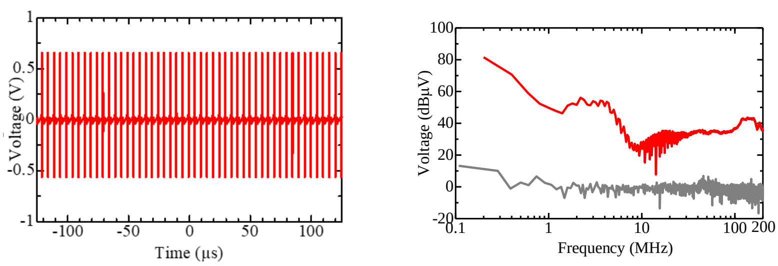

Figure 2.13 Ideal noise spectrum.

The process described above can be used to obtain a single spike noise waveform with high S/N ratio. However, due to its short time-length and poor frequency resolution, it is challenging to convert the time-domain signal into a frequency-domain signal with a complete spectrum. The single turn-on spike noise waveform is duplicated for 50 times and composited with ripple noise for an ideal noise signal. The signal and spectrum are shown in Fig. 2.13.

2.3.2 Experiment Setup and Interference Prediction Flow

In the measurement setup shown in Fig. 2.14, and the real measurement setting picture shown in Fig. 2.15 a handmade artificial mains network of which the circuit diagram and impedance with frequency are shown in Fig. 2.6. was used to block the noise from the DC power supply (KENWOOD PW18-1.8AQ $\pm$ 18V/1.8A).

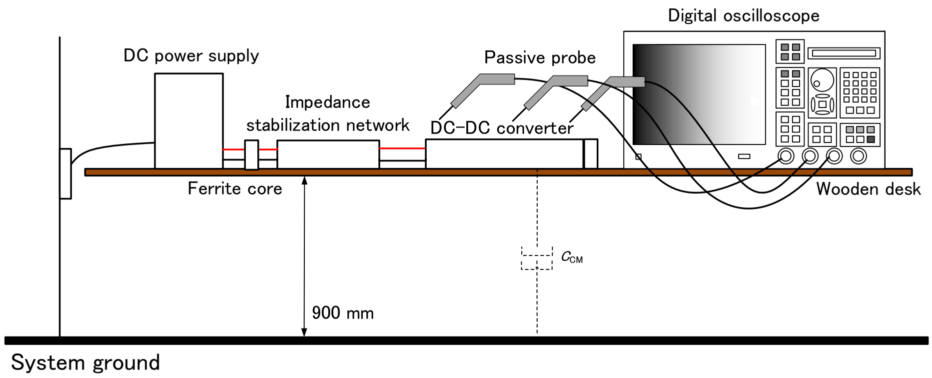

Figure 2.14 Measurement setup.

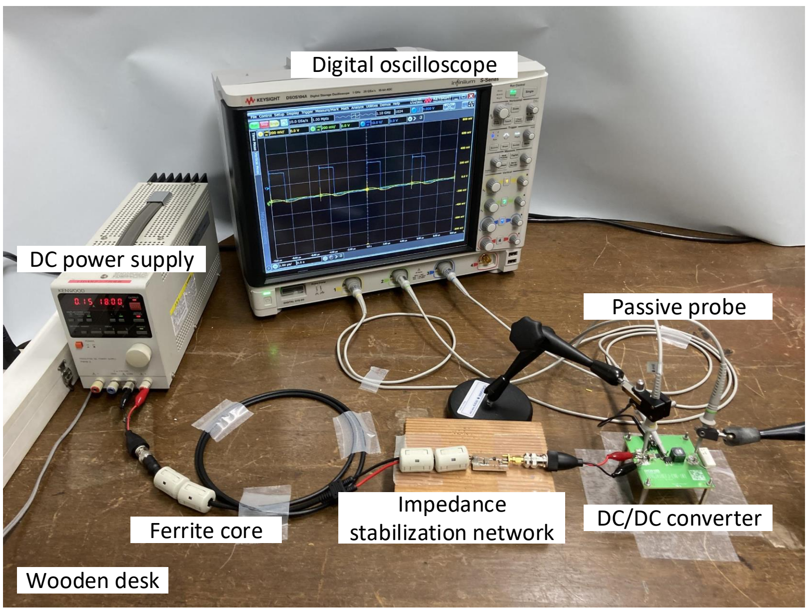

Figure 2.15 Setting of the test bench.

Table 2.2 shows the equipment used for measurement. An oscilloscope (Keysight DSOS104A with 1 GHz bandwidth, 20 GSa/s) with three high-impedance passive 10:1 probes (KEYSIGHT N2894A 700 MHz with 10-MΩ input resistance and 9.5-pF input capacitance) was used for measurement: one for measuring the triggered signal from the switching node of the DC-DC converter, and two for measuring the input and output port noise. A 10-MHz low-pass filter built into the matlab function *designfilt*. was used to obtain the waveform via the waveform decomposition method. The sampling rate was 1 GS/s, and the measurement time was 250 µs, averaged 1024 times. The turn-on and turn-off spike noise were measured by setting the trigger to the rising and falling slopes, respectively, of the reference signal. For obtaining enough points in a short period of time, the sampling rate was 10 GS/s, and the measurement time was 1 s, averaged over 1024 times. Furthermore, the noise floor was measured at 200 mV/div, the same setting as the ripple noise and spike noise measurements.

For each decomposed noise spectrum, noise parameters were identified. For parameter identification, 4.7-μF filter capacitors (GRM31CR71A475KA01) with 5-mΩ ESR and 0.5-nH ESL were soldered in parallel at each converter port. The table 2.3shows the filter condition and the prediction case.

The filter cases for parameter identification were "not applicable" (N/A), 9.4 µF (two capacitors in parallel), and 19.8 µF (four capacitors in parallel). The conduction emission measured in the 4.7-µF filter case was used for evaluation. For each decomposed noise spectrum (low-frequency ripple noise and high-frequency spike noise), noise prediction was performed.

Table 2.2 Table for equipment used for measurement.

Equipment	Type
DC power supply	KENWOOD PW18-1.8AQ ± 18V/1.8A
Oscilloscope	Keysight DSOS104
High-impedance passive probe	KEYSIGHT N2894A 700 MHz 10:1
DC/DC converter (DUT)	ROHM BD9G341AEFJ-EVK-101
EMI filter	Murata GRM31CR71A475KA01

Table 2.3 Filter case for parameter identification and prediction case.

	$C_{in}(\mu F)$	$C_{out}(\mu F)$
Filter case for parameter identification	N/A	N/A
	9.4	9.4
	18.8	18.8
Filter case for result evaluation	4.7	4.7

The noise signals were measured in above filter cases and decomposed to ripple noise, turn-on spike noise, and turn-off spike noise. Then transfer to frequency-domain spectrum shown in :.

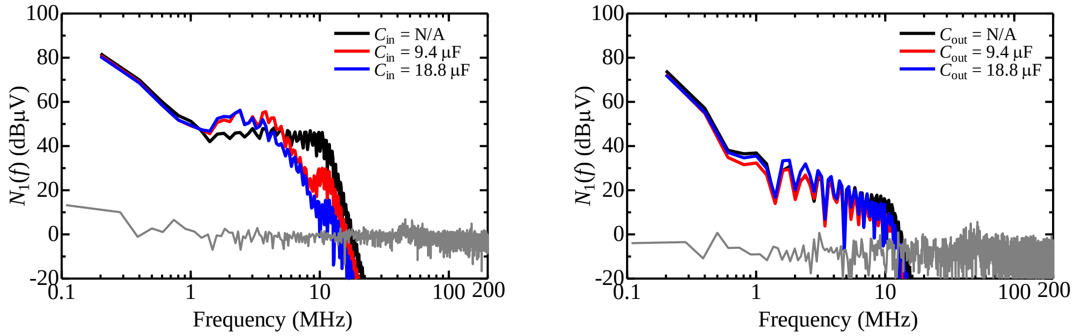

(a) Input-port ripple noise spectrum for parameter identification

(b) Output-port ripple noise spectrum for parameter identification

Figure 2.16 Ripple noise spectrum for parameter identification.

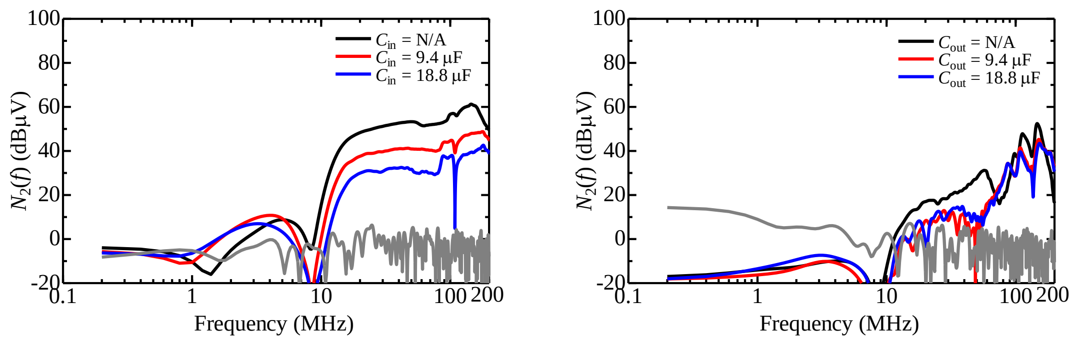

(a) Input-port turn-on spike noise spectrum for parameter identification

(b) Output-port turn-on spike noise spectrum for parameter identification

Figure 2.17 Turn-on spike noise spectrum for parameter identification.

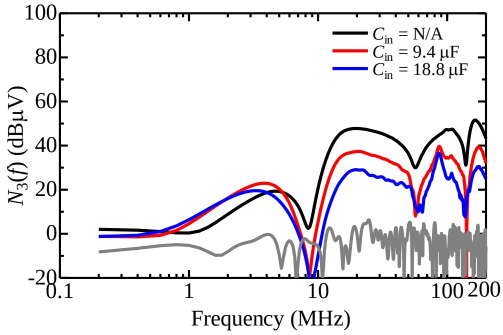

(a) Input-port turn-off spike noise spectrum for parameter identification

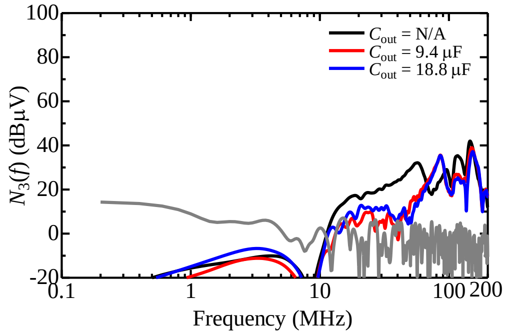

(b) Output-port turn-off spike noise spectrum for parameter identification

Figure 2.18 Turn-ff spike noise spectrum for parameter identification.

2.4 Result Evaluation

Below are the results of parameter identification. The magnitudes of ripple noise, turn-off spike noise, and turn-on spike noise are shown in red, blue, and green, respectively. The ripple noise and spike noise were recomposed via (2.7).

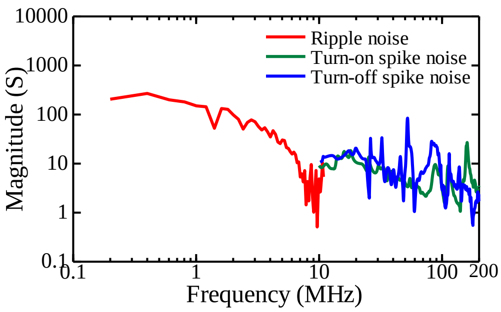

(a) Y1 Magnitude

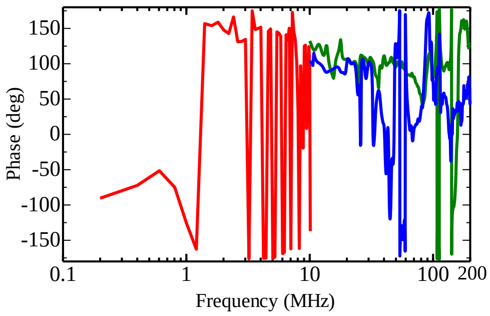

(b) Y1 Phase

Figure 2.19 Input port impedance Y1.

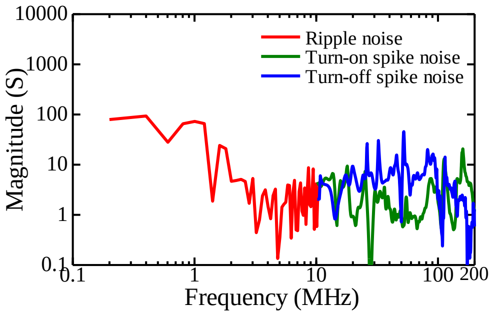

(a) Y2 Magnitude

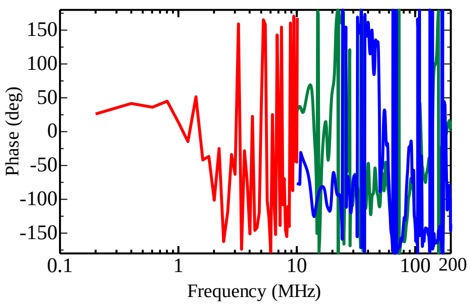

(b) Y2 Phase

Figure 2.20 Isolation impedance Y2.

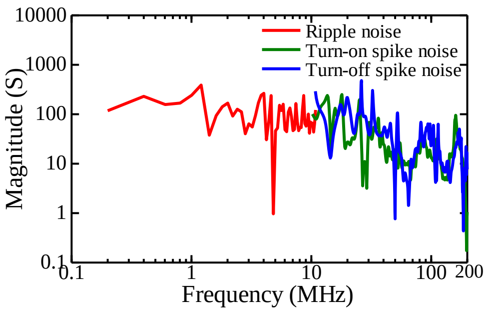

(a) Y3 Magnitude

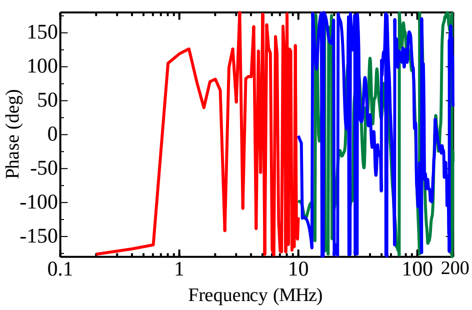

(b) Y3 Phase

Figure 2.21 Output port impedance Y3.

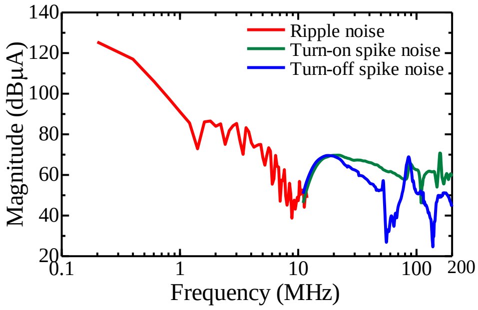

(a) Input port current source Is1

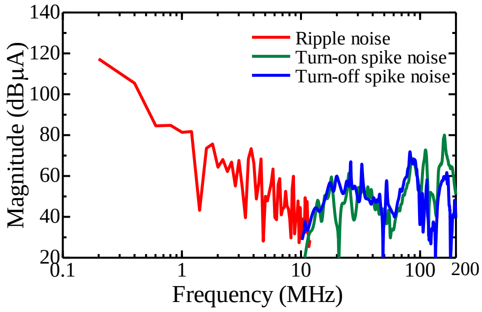

(b) Input port current source Is2

Figure 2.22 Identified noise current source magnitude.

As shown in the Figure 2.23 and 2.24, noise spectra are compared between prediction and measurement results for the input and output ports, respectively. Each of these figures shows the ripple noise spectrum, the turn-on spike noise spectrum, and the turn-off spike noise spectrum. As can be seen from the figures, the prediction difference was within 3 dB in the range up to 200 MHz. Between 10 and 200 MHz, the turn-off spike noise was overwhelmed by the turn-on spike noise. The prediction in both input-port and output-port error are shown in Fig. 2.25.

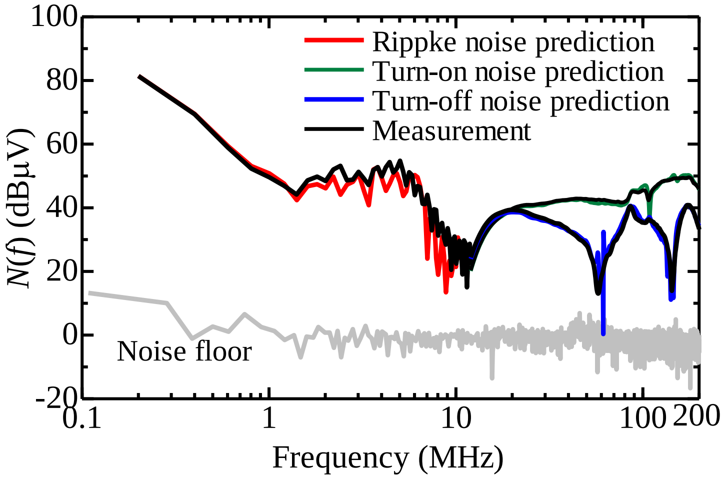

Figure 2.23 Input port noise voltage prediction.

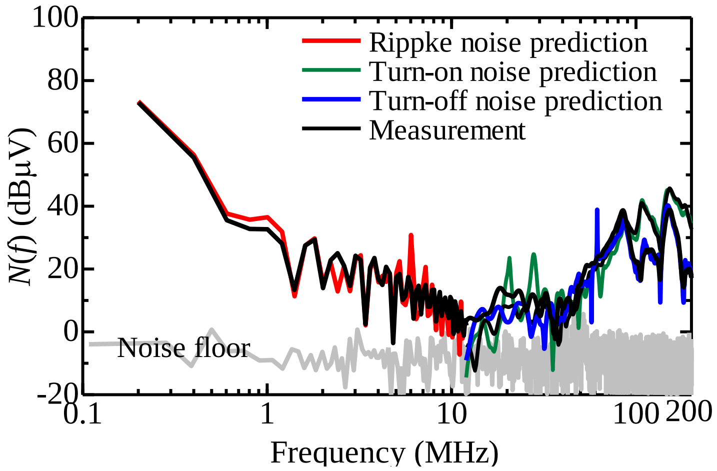

Figure 2.24 Output port noise voltage prediction.

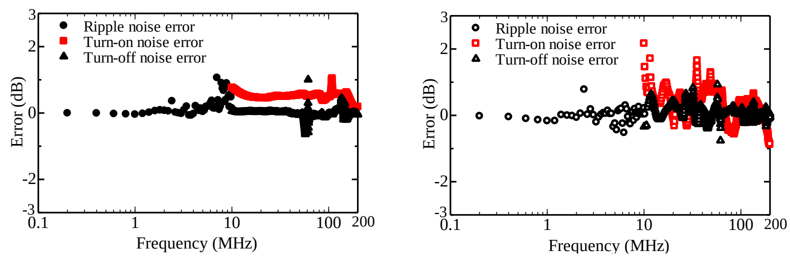

(a) Input port prediction error (b) Output port prediction error

Figure 2.25 Prediction error with waveform decomposition method.

2.5 Conclusion

This Chapter proposes a method of decomposing the whole time-domain noise signal waveform into ripple noise, turn-on spike noise, and turn-off spike noise. It was possible to eliminate the switching fluctuation effect during parameter identification for the equivalent noise source model by using this method. Based on the method's prediction, the peak amplitude was closely related to the prediction result, and the error was within 3 dB up to 200 MHz. However, the prediction result applying waveform decomposition method is an ideal spectrum, which can not obtain by actual measurement. The effect of switching fluctuation should be considered. In next chapter, the effect of switching fluctuation will be investigated and considered in actual conducted emission prediction.

Chapter 3

Noise-source Equivalent Circuit Model Considering Switching Fluctuation

3.1 Introduction

The measurement results are crucial for black-box noise prediction since it is based on measurement. The Fig. 3.1 describe the switching fluctuation of DC-DC converter. A DC-DC converter's switching fluctuation affects not only the accuracy of the noise source model but also the noise spectrum [49]. DC-DC converter switching fluctuation is attributed to a number of factors, including nonlinearity of the sawtooth slope of the analog pulse-width modulation (PWM) controller, ground noise coupling between the power and control stages, inadequate PWM resolution in the digital controller, and the selection and placement of components.

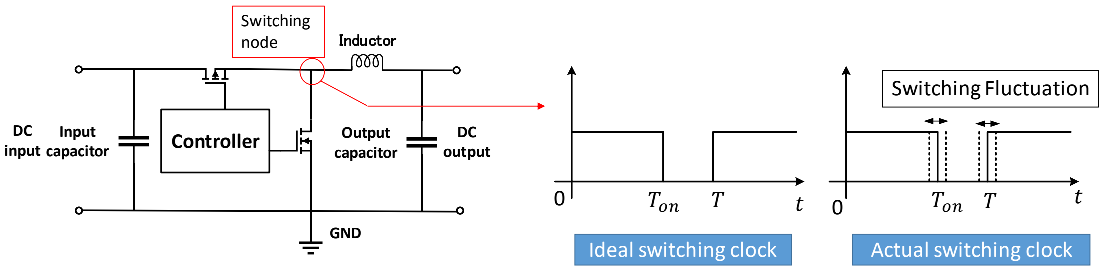

Figure 3.1 Ideal switching signal and actual switching signal.

As a result of the converter's inherent jitter, the peak of the conducted noise is several decibels higher than the averaged noise. The idea here comes from the frequency modulation technique [62–64] based on Carson's rule [65]. Peak amplitudes are produced under conditions of no fluctuation, whereas average amplitudes are produced under conditions of fluctuation. The fluctuation spreads the peak spectrum to the sideband without affecting the total power of the noise. By using the frequency modulation technique, a method is proposed in [61], for predicting the peak magnitude of the noise and determining its reduction.

In [61], it is assumed that the inherent jitter in a DC-DC converter has the same effect as the frequency modulation technique normally used in digital circuits to reduce EMI at higher frequencies. To spread the energy to harmonics, the frequency modulation technique introduces controlled jitter in the time-domain switching signal. Using the technique, it was possible to estimate the noise reduction caused by the DC-DC converter's inherent jitter effect and predict the averaged emissions from the converter.

The jitter distribution caused by frequency modulation differs from the inherent jitter of DC-DC converters. Although the predicted spectrum agreed to some extent with the measured spectrum, the technique was not deemed suitable to evaluate the inherent jitter effect because the switching fluctuation distribution in a DC-DC converter differs from that introduced by frequency modulation, which is caused by the difference between random and deterministic jitter. Consequently, a trigger-source measurement method is proposed to assess noise reduction.

In summary, inherent jitter behaves similarly to frequency modulation and reduces the noise amplitude at higher frequencies. Based on the hypothesis that inherent jitter has the same effect as the frequency modulation technique, the reduction is achieved using an experimental approach that uses the spectrum caused by switching fluctuation. In order to get the actual noise spectrum, it is also necessary to get the "ideal" noise spectrum without any fluctuation. The "ideal" spectrum by using the waveform decomposition method was presented in the last Chapter. Finally, the "ideal" noise spectrum is subtracted by noise reduction to obtain the actual noise spectrum.

3.2 Effect of Switching Fluctuation on Spike Noise

First, the principle of frequency modulation is described in this section. Secondly, we correlated the inherent switching fluctuation with the frequency modulation technique. Due to both inherent switching fluctuation and the frequency modulation signal introduced in the DC-DC converter, noise is reduced at higher frequencies.

3.2.1 Frequency Modulation Principle

A diagram illustrating frequency modulation is shown in the Fig. 3.2. A time-domain periodic, square waveform and corresponding frequency-domain spectrum are shown in Fig. 3.2a and Fig. 3.2b. In the case of modulated square waves, each harmonic is spread over a certain frequency range, resulting in a reduction of EMI peaks.

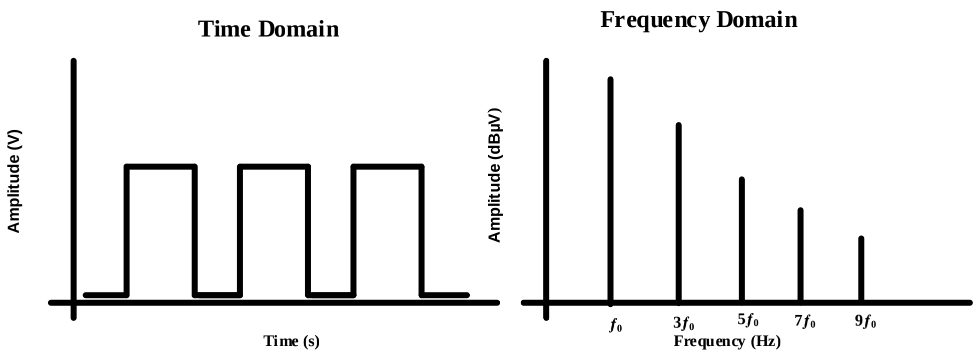

(a) Ideal switching signal

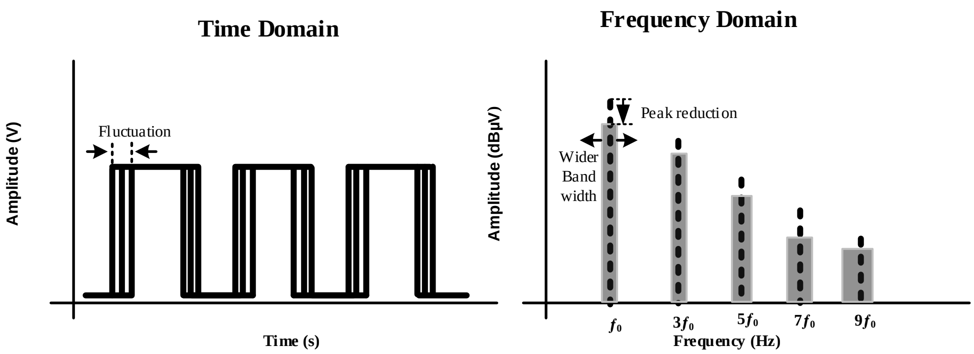

(b) Frequency-modulated switching signal

Figure 3.2 Time and frequency domains for an ideal signal and a signal with switching fluctuation.

It consists of the introduction of controllable jitter into the time-domain switching signal in order to avoid perfect periodic behavior, thereby spreading out the power of each harmonic component over a wider bandwidth. The spreaded bandwidth depends on the jitter characteristics introduced.

A serious sinus wave modulated by a kind of modulation profile can be used to examine the effect of frequency modulation on each harmonic. The sinus signal is used here as an example of the principle of frequency modulation. A simple sinusoidal signal $x(t)$ is modulated by a specific modulation profile.

$$x(t) = A_0 \cos(2\pi f_c t), \tag{3.1}$$

The modulated signal is:

$$\widetilde{x}(t) = A_0 \cos(\omega_0 t + \theta(t)) \tag{3.2}$$

where

A_0 is the amplitude of the original signal without modulation;

f_c is the center frequency. $\theta(t)$ is a time-dependent phase angle, according to

$$\theta(t) = \int_t^o k_\omega \cdot v_m(\tau) \cdot d\tau \tag{3.3}$$

where

k_ω is the factor controlling the peak of frequency deviation; $v_m(\tau)$ is a periodic unitary amplitude function of frequency f_m. $v_m(\tau)$ gives the frequency modulation profile, which can be a random value or a deterministic value.

The total power of this signal is $1/2A^2$ and it is approximately spread in the Carson ' s bandwidth $[f_c - \Delta f, f_c + \Delta f]$. Δf is the frequency deviation.

As the total signal power does not change, the power spectral density (PSD) (dBm/Hz) is used to calculate noise reduction quickly.

The PSD of unmodulated signal $S(f)$, the total power is equal to $1/2A^2$. The modulated signal PSD is $\widetilde{S}(f)= \int_{f-\triangle f}^{f+\triangle f} \widetilde{S}(f)\ df$, we assume the energy is spreaded fairly evenly in Δf. Then we have the total power in Carson ' s bandwidth:

$$\frac{1}{2}A^2 = \int_{f-\triangle f}^{f+\triangle f} \widetilde{S}(f)\ df \tag{3.4}$$

For quick examination we approximately treat the spreaded spectrum is rectangular:

$$\widetilde{S}(f)\frac{2\triangle f}{f_m} = \frac{1}{2}A^2 \tag{3.5}$$

The attenuation value A_{dB} is approximately to be:

$$A_{dB} = 10log(\frac{S(f)}{\widetilde{S}(f)}) = 10log(\frac{2\triangle f}{f_m}) \tag{3.6}$$

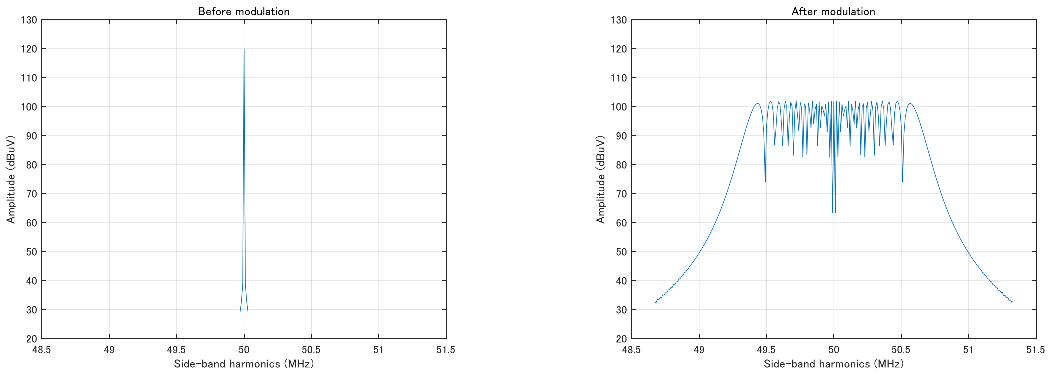

(a) Before frequency modulation (b) After frequency modulation

Figure 3.3 Frequency modulation simulation in frequency domain.

Figure 3.3 illustrates an example calculated in Matlab. This experiment involved modulating a 50 MHz sinusoidal wave with a 10 kHz triangular wave. According to the figure, the effect of frequency modulation is reduced by about 12 dB at 50 MHz.

When taking into account a more complex periodic signal in DC-DC converter, it is equivalent to apply 3.6 to each signal harmonic, with the only difference that the n time harmonic is spread within a bandwidth of amplitude $2n\Delta f$.

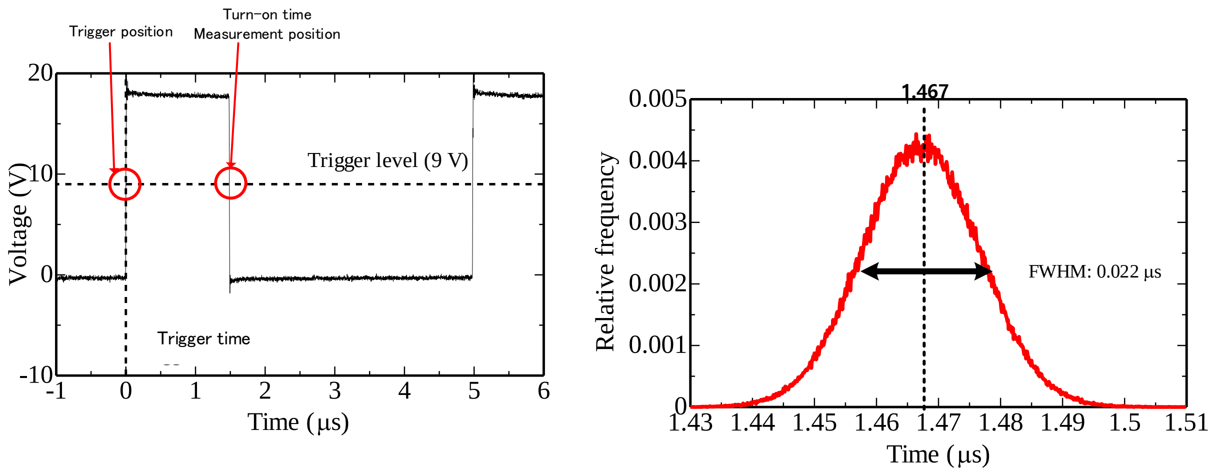

(a) Distribution measurement position (b) Switching fluctuation distribution

Figure 3.4 Switching fluctuation measurement results.

3.2.2 The Distribution of DC-DC Converter Inherent Switching Fluctuation

Similarly to the frequency modulation technique, DC-DC converters are characterized by inherent fluctuations that spread the noise power spectrum. Despite the fact that

that technique is generally used to reduce EMI, Carson's rule can provide insight into how switching fluctuations affect the noise spectrum. By introducing controlled jitter into a time-domain signal, frequency modulation compensates for the converter's non-periodic behavior, spreading harmonic power over a wider bandwidth. There is a direct relationship between the bandwidth and the characteristics of jitter introduced.

Figure 3.4a shows the trigger source measurement positions in the time-domain switching signal from the switching node, and Fig. 3.4b shows an oscilloscope histogram of the jitter distribution at the indicated measurement position in 3.4a. The results indicate that the switching fluctuation can be considered to have a normal distribution. The full width at half maximum (FWHM) is 22 ns; therefore, the standard deviation σ is calculated as 9.34 ns, because FWMH $= 2\sqrt{2}\sigma$.

Since the measured result can be viewed as total jitter, it can be split into random jitter (i.e., random distribution) and deterministic jitter (i.e., deterministic distribution). Therefore, based on the central limit theorem in probability, total jitter tends to follow a Gaussian distribution.

3.3 EMI Reduction Calculation Caused by Switching Fluctuation

In view of the fact that the spike noise signal is caused by a high dv/dt switching clock, the peak spike noise results from the ideal switching condition without fluctuation. The ideal turn-on time is approximately 1.467 seconds, which is the mean of the normal distribution shown in Fig. 3.4b. In addition, the actual spectrum is spread by the inherent switching fluctuation. Thus, there is a variation in the actual turn-on time, which follows a normal distribution.

In light of the above consideration, noise reduction can be achieved by comparing actual switching signals (with fluctuation), Fig. 3.5 with ideal switching waveforms (without fluctuation) Fig. 3.6. An oscilloscope was used to measure the actual switching signal in order to obtain a waveform with fluctuation, as shown in Fig. 3.7a. In the first step, 100 periods of the switching signal were measured at a sampling rate of 1 GS/s. It was the switching node that was measured shown in Fig. 3.1. The turn-on time varied, and the time deviation distribution followed that shown in Fig. 3.4b. From the measured waveform, a one-period switching signal was extracted, which had a turn-on time of approximately 1.467 seconds, and the waveform was then duplicated 100 times to obtain a waveform without fluctuation. As a result, we obtained a waveform like that shown in Fig. 3.7b.

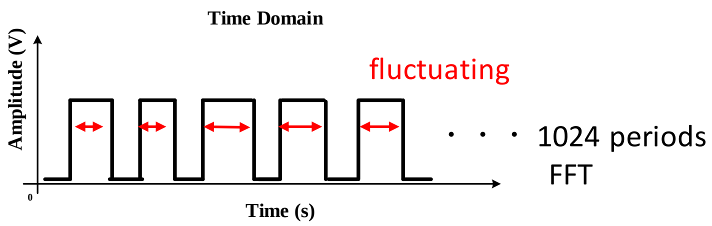

Figure 3.5 Actual switching node signal (measured).

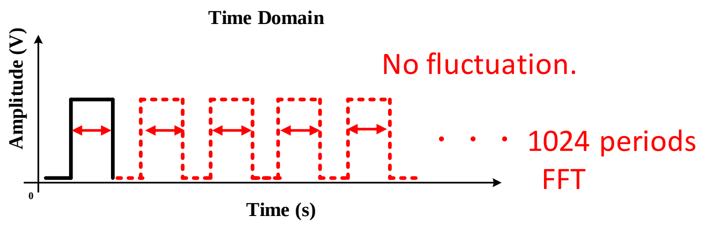

Figure 3.6 Ideal switching node signal (duplicate from one switching signal).

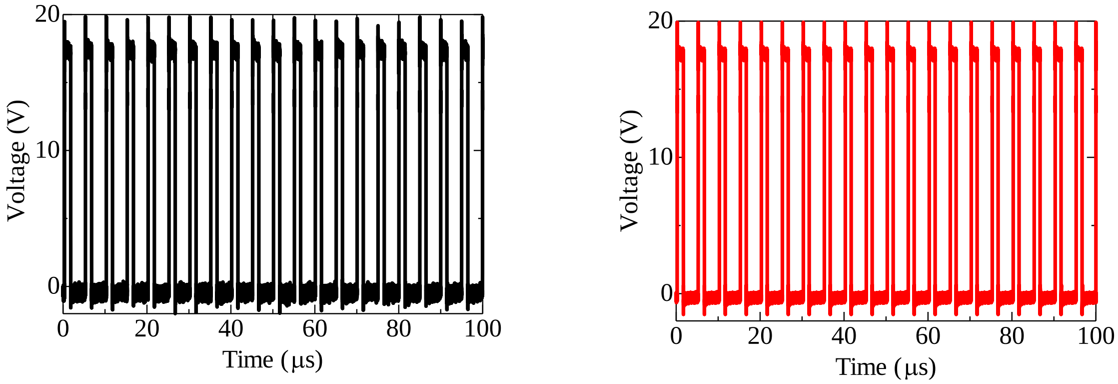

(a) Switching signal with fluctuation

(b) Switching signal duplicated from one period without fluctuation

Figure 3.7 Switching signal waveforms.

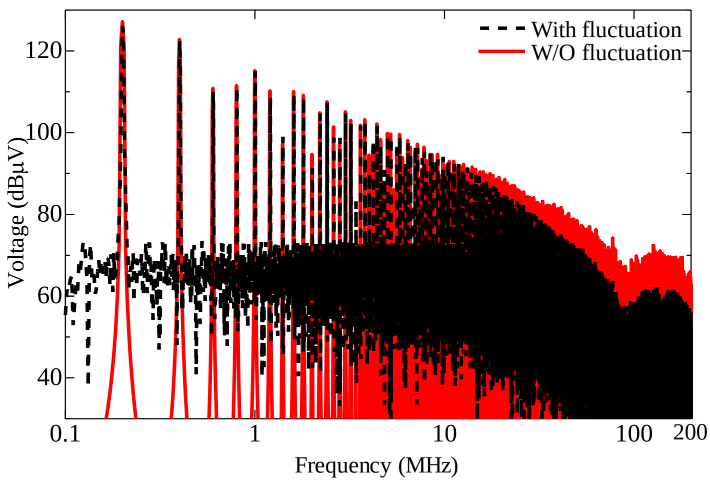

Figure 3.8 Spectrum comparison (100 periods).

Figure 3.8 shows the FFT result obtained in MATLAB. From 10 to 200 MHz, the switching signal with time deviation spectrum has a lower amplitude than the switching signal without time deviation. There is a positive correlation between the difference and frequency. In the spike noise frequency range, the duration of the switching signal is the primary factor that influences the spectrum amplitude. In a sufficiently long waveform, the spectrum eventually converges to its amplitude, whereas a short duration is incapable of containing the reduction due to fluctuation. Figure 3.9 shows the envelope spectra for different durations, which indicate that the envelope converges at about 1000 periods of the switching waveforms. By using 1024 switching periods, which is the same as the

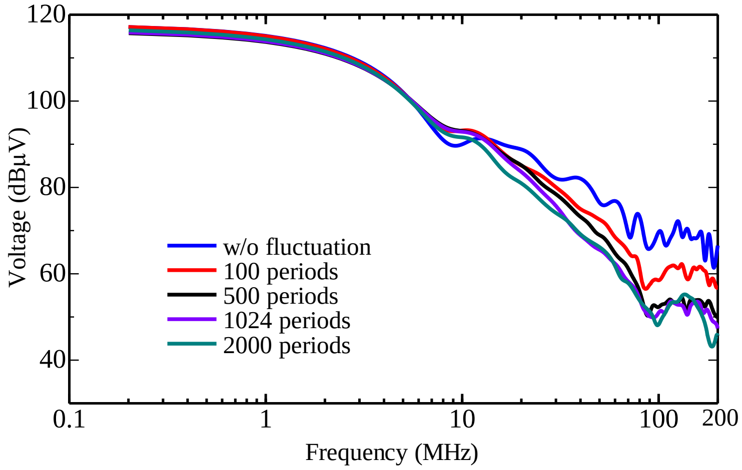

Figure 3.9 Envelope spectra for different numbers of switching periods.

oscilloscope's averaging without fluctuation, noise reduction can be calculated from the differences between the switching signal spectra with fluctuation. The calculated result is shown in Fig. 3.10, and as a result, the noise spectrum is reduced above 10 MHz, which corresponds to the spike noise range. Consequently, ripple noise is not affected by switching fluctuation.

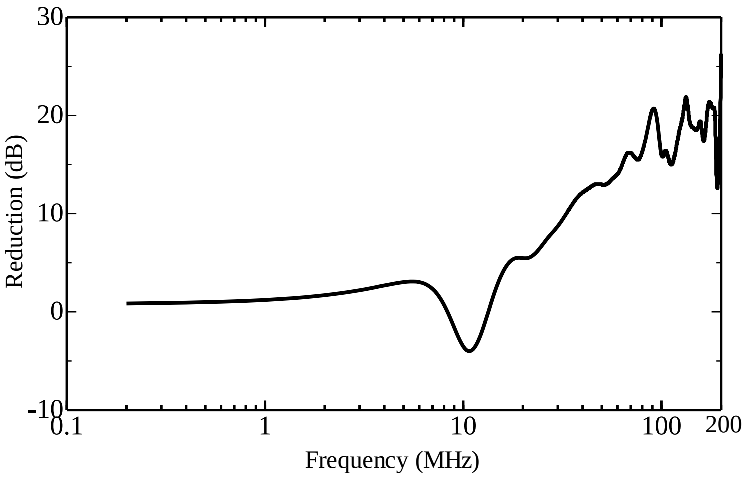

Figure 3.10 Noise signal reduction due to switching fluctuation.

3.4 Averaged Emission Spectra Prediction Result

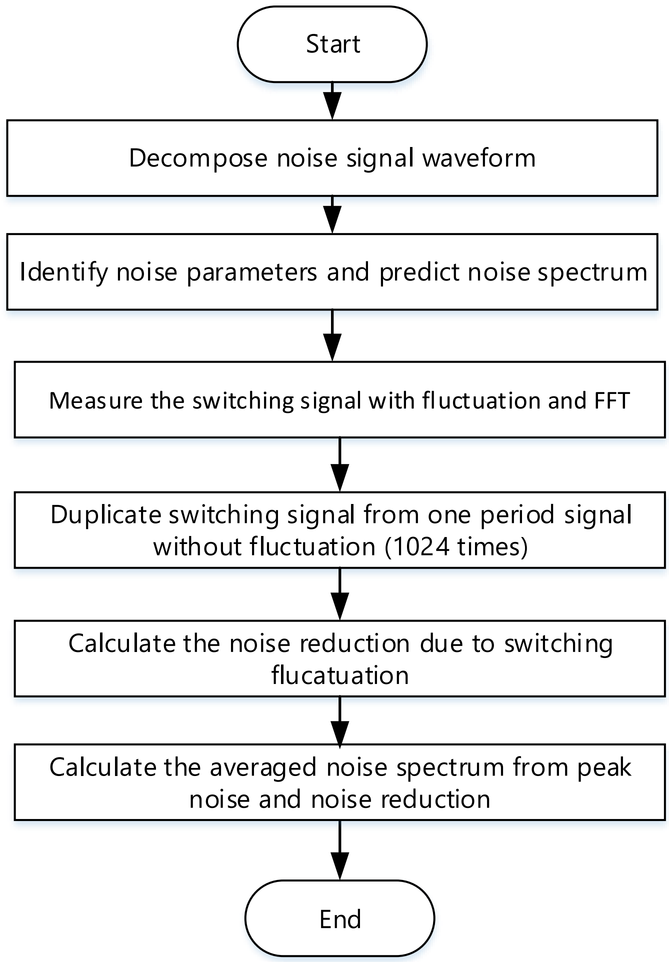

Figure 3.11 The flowchart to periodic input port averaged spectrum.

In Chapter 2, the prediction results indicated the spectrum of a decomposed signal without switching fluctuations. Although the prediction results were close to the peak detected spectrum, our goal is to predict the averaged spectrum derived from measurement.

Because ripple noise is not affected by switching action, the reduction process is only applicable to switching noise (i.e., spike noise). In addition, the prediction results indicated that the turn-off spike noise is smaller than the turn-on spike noise. The results for the turn-on spike noise are presented here in the absence of results for the turn-off spike noise, since the spectrum of the turn-on spike dominates that of the turn-off spike during measurement.

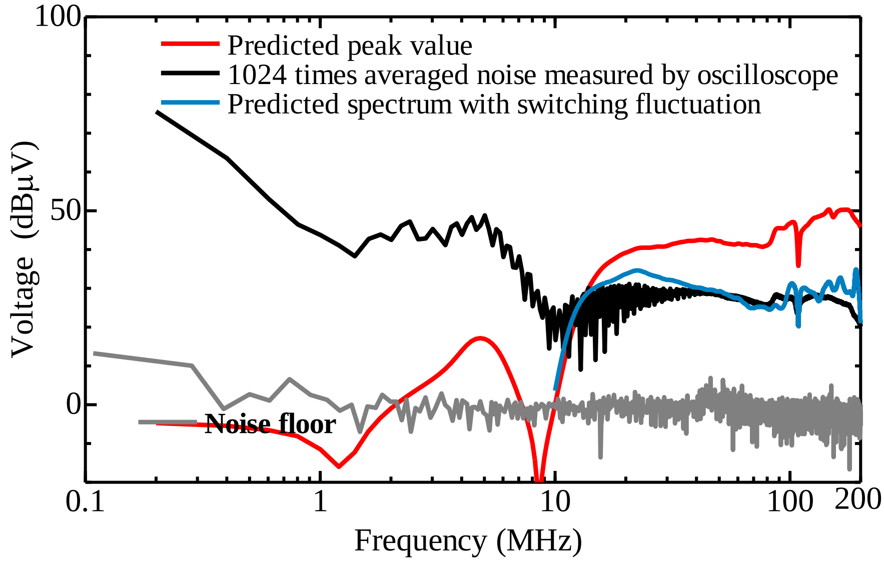

Figure 3.12 Noise prediction accounting for switching fluctuation of input port noise.

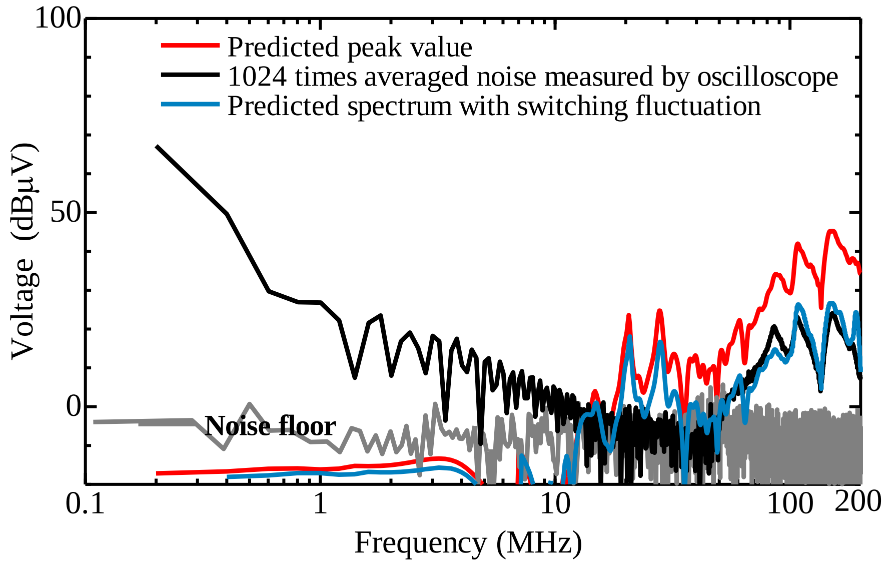

Figure 3.13 Noise prediction accounting for switching fluctuation of output port noise.

By subtracting the reduction from the peak detected noise predicted using waveform decomposition method without switching fluctuation, one can obtain an averaged noise spectrum based on the hypothesis that noise reduction at higher frequencies is caused by switching fluctuation.

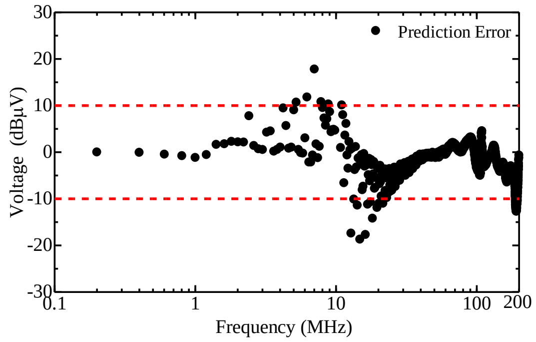

(a) Input port prediction error of buck converter

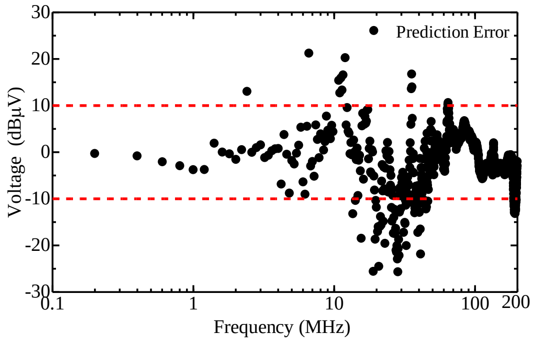

(b) Output port prediction error of buck converter

Figure 3.14 Prediction error of GaN-based buck converter.

The turn-on spike noise spectrum above 10 MHz was thus predicted by subtracting the reduction shown in Fig. 3.10. Figure 3.12 ,and Fig. 3.13 show the predicted spectrum in blue, compared to measured spectrum in red, with the peak spectrum in black. There is good agreement between the measured and predicted spectra. The prediction error are shown in Fig. 3.14a and Fig. 3.14b. For input port prediction, the results show that most of prediction are in 10 dB. For output port prediction, the prediction from 20 MHz to 40 MHz is not good. The reason for this large error is the S/N ratio of output port noise (20 MHz - 40 MHz) is pretty low, which will affect prediction accuracy.

3.5 Conclusion

The purpose of this chapter is to predict the averaged noise from a DC-DC converter. So far, the hypothesis has been proposed that the inherent jitter caused by switching fluctuation of the DC-DC converter reduces the noise amplitude at higher frequencies, and it has been verified using semi-empirical methods. During time-domain measurement, the black-box model was combined with the waveform decomposition method to eliminate switching fluctuations.

The influence of switching fluctuations on noise during converter operation is examined. In an ideal switching clock, the fluctuation was assumed to be a frequency modulation that spreads the noise spectrum. By using the ideal switching waveform and the actual switching waveform, the reduction in spike noise power was calculated. Finally, the noise actual spectrum is predicted with ideal noise spectrum and the obtained noise reduction in good accuracy.

Chapter 4

General Application on The Other Type DC-DC Converter

4.1 Introduction

It has been demonstrated in the previous chapter that waveform decomposition and experimental analysis can be used to evaluate the noise reduction caused by switch fluctuation. It is applicable to a buck converter. There is still a need to investigate whether the method can be applied to other types of converter. To demonstrate the applicability of the method to other types of converters, two converters will be modeled using the proposed method.

For the evaluation of two other DC-DC converters, two other manufacturers' converters were used since the approach presented in Chapters 2 and 3 is not independent of the type of DC-DC converter. The first converter is a boost DC-DC converter, and the second is a GaN buck DC-DC converter shown in Fig. 4.2 [66–68].

Table 4.1 List of DC-DC converters treated in this study.

Type	Buck converter	Boost converter	Buck converter
Transistor materials	Si	Si	GaN
Maker	Rohm	Analog devices	EPC
Part No.	BD9G341AEFJ-EVK-10	DC2186A-A	EPC916
Input port voltage	18 V	9 V	18 V
Output port voltage	5 V	12 V	5 V
Switching frequency	200 kHz	1.5 MHz	2 MHz

4.2 Conducted Emission Properties from Different Type Converter

In DC-DC buck converters, the input port noise is typically greater than the output port noise. In contrast, the output port noise in boost converters is normally greater than the input port noise. To illustrate this phenomenon, the following figure illustrates the input and output port noise measured by an oscilloscope in Fig. 4.1, and Fig. 4.2. According to the figure in time-domain, the triggered noise signal in the output port is approximately 180 mV, while the triggered noise signal in the input port is approximately 15 mV, the signals were transferred to the frequency domain. Noise at each frequency of the output port is greater than that at the input port.

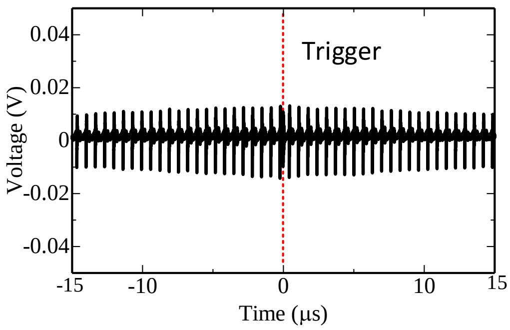

(a) Boost converter averaged input-port noise signal

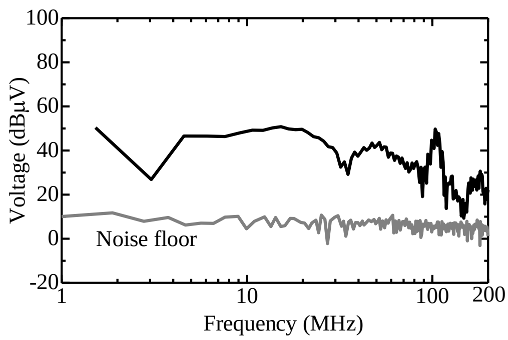

(b) Boost converter averaged input-port noise spectrum

Figure 4.1 Boost converter input-port noise.

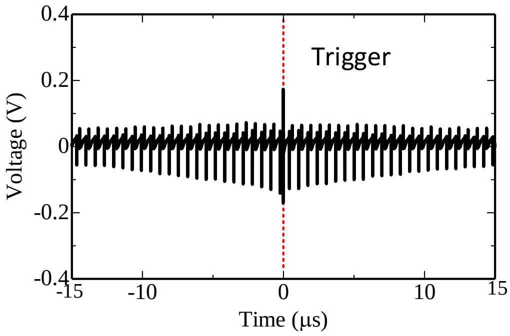

(a) Boost converter averaged output-port noise signal

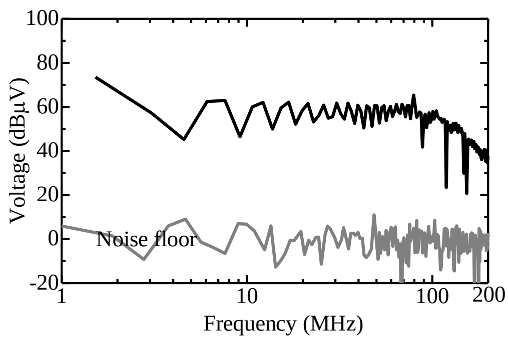

(b) Boost converter averaged input-port noise spectrum

Figure 4.2 Boost converter output-port noise.

In Fig. 4.3, the noise path of when switch turn-on and turn-off is shown. As can be seen from the figure, when the boost converter switch is turned off, the noise path is larger and has a higher di/dt value. Therefore, the output-port and turn-off noise will be larger in boost converters. Furthermore, this phenomenon emphasizes the importance of a two-port noise model. Based on the proposed model, both ports can be predicted at the same time, and the filter design can be designed simultaneously.

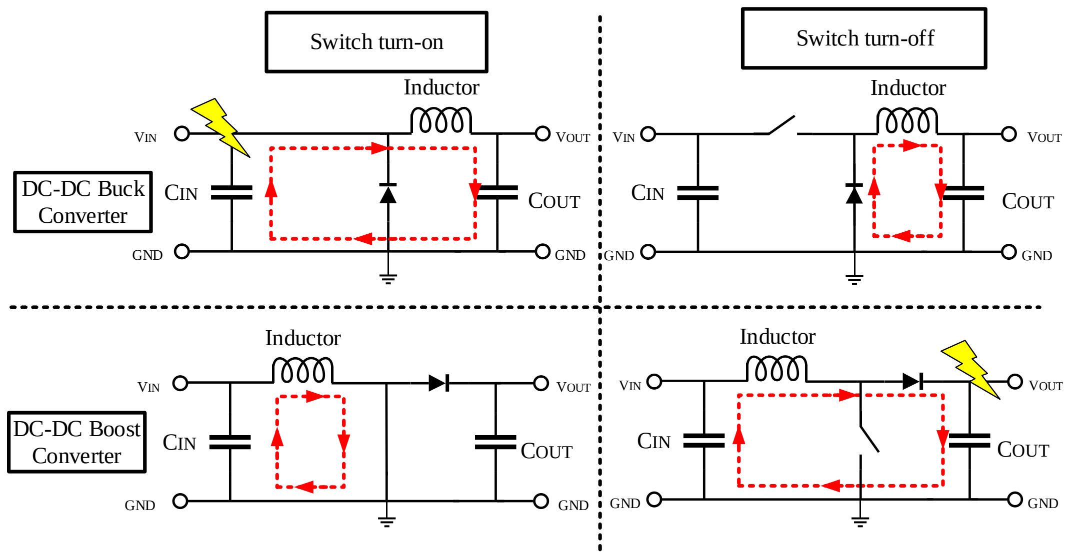

Figure 4.3 Conducted emission properties between buck type and boost type converter.

4.3 General Application Flow and Practical Examples

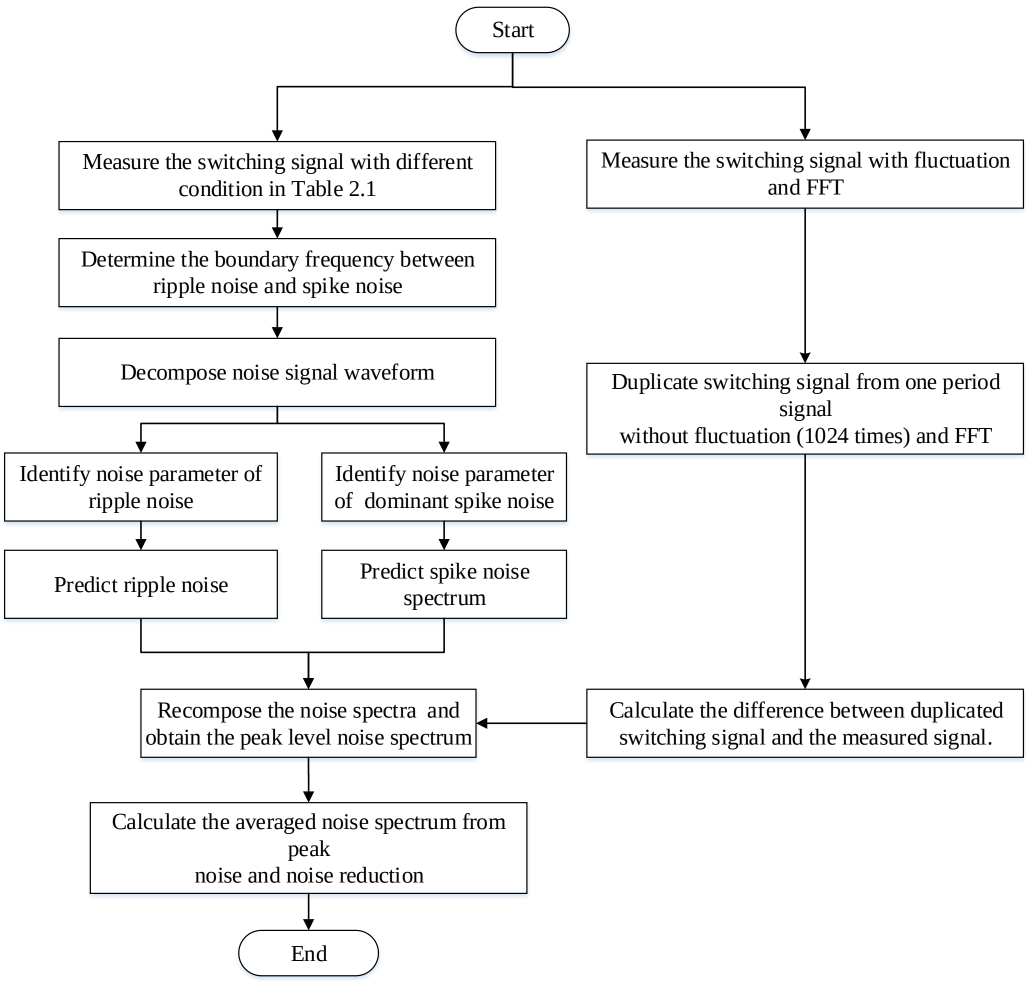

Figure 4.4 The flowchart for general application for predicting the conducted emission from DC-DC converter.

The purpose of this section was to conclude the general application of the equivalent circuit model. Figure 4.4 illustrates the flowchart for predicting the conducted emission from a DC-DC converter. It consists of two parts, one of which is the waveform decomposition part, and the other is the noise reduction evaluation.

It has been estimated that the boundary frequency between ripple noise and spike noise is 20 to 50 times the switching frequency of the converter. The ripple noise is dominated below the boundary frequency, whereas the spike noise is dominated above the boundary frequency. Since spike noise only consists of a short period of time, the resolution of the

FFT is inadequate. During the spike noise FFT process, zero-padding is used. Besides, the one period spike noise is duplicated for several times for high frequency resolution. The EMI measurement condition and result verified condition are shown in Table 4.2.

Table 4.2 Measurement conditions for different type of DC-DC converter.

Type of converter	**Load (Ω)**	**Filter capacitance values for parameter identification (μF)**	**Filter capacitance value for prediction(μF)**
BD9G341AEFJ-EVK-10	10	N/A, 9.4, 18.8	4.7
DC2186A-A	30	N/A, 2, 4	1
EPC916	10	N/A, 9.4, 18.8	4.7

4.3.1 DC-DC Boost Converter

A DC-DC boost converter (Analog Devices, DC2186A-A) with a 30-Ω load was used for evaluation. The input voltage was 9 V, and the output voltage was 12 V. The switching frequency was 1.5 MHz. The measurement view is shown in Fig.4.5. The noise properties of a boost converter differ from those of a buck converter. In a boost converter, the turn-off noise is greater than the turn-on noise. Thus, we predicted the boost converter turn-off noise accounting for switching fluctuation.

The experiment and prediction processes are identical to those for the buck converter, except for the filter capacitor value and the low-pass filter stopband which are built in Matlab. As the switching frequency of the boost converter is 1.5 MHz higher than that of the buck converter we used, the ripple noise frequency range is increased, and a smaller capacitor value is used to filter the switching harmonics. For parameter identification, a 1-μF filter capacitor (GRM42-6F105Z25) with a 0.14-m Ω ESR and a 1.55-nH ESL was soldered in parallel at each converter port. It is found that the ripple noise range is 20 times that of the switching frequency, and the low-pass filter stopband is 30 MHz.

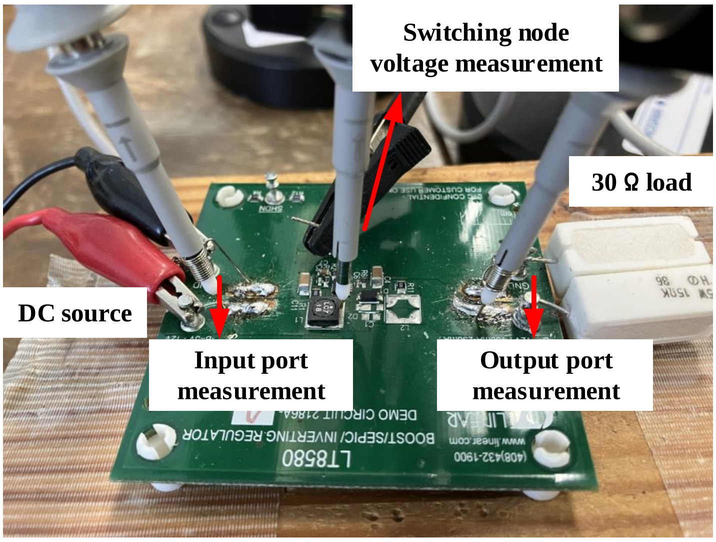

Figure 4.5 DC-DC boost converter measurement view.

The decomposed time-domain signal and frequency domain signal are shown in ripple noise in black, Fig. 4.6, turn-on spike noise in red Fig. 4.18, and turn-off spike noise in blue Fig. 4.8. The spike noise signal time length is 0.67 μs. The ripple noise spectrum, and the spike noise spectrum are filter by the 1-μF capacitor. Then, identify the parameters of the noise source and predict the noise spectrum. The prediction results will be presented in the next section. In this case, the result is the ideal prediction without switching fluctuation. Next step is the obtain the noise reduction caused by switching fluctuation

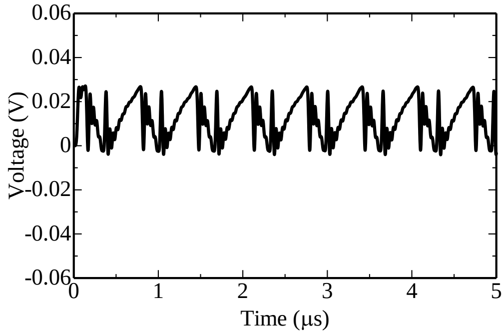

(a) Boost converter ripple noise signal

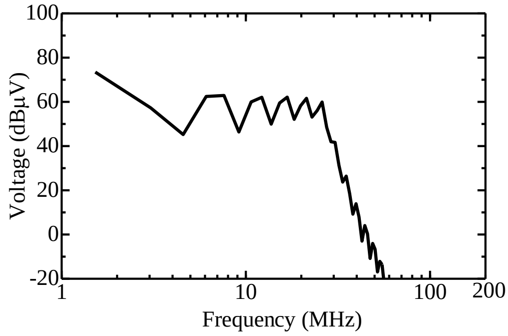

(b) Boost converter ripple noise spectrum

Figure 4.6 Boost converter ripple noise.

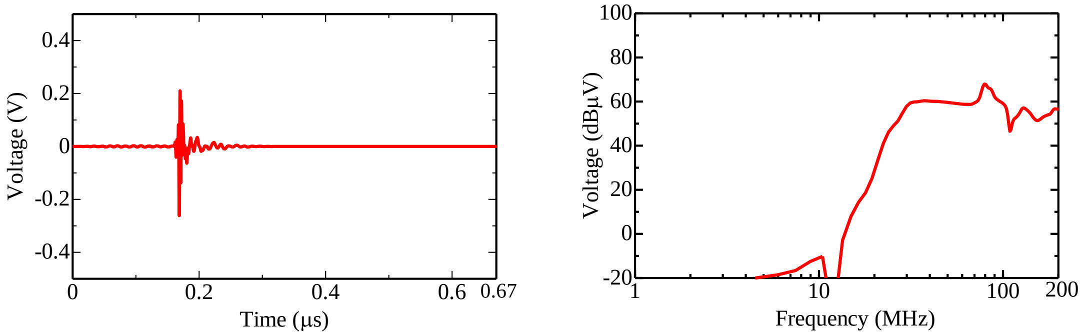

(a) Decomposed boost converter turn-on spike noise signal

(b) Decomposed boost converter turn-on spike noise spectrum

Figure 4.7 Boost converter turn-on spike noise.

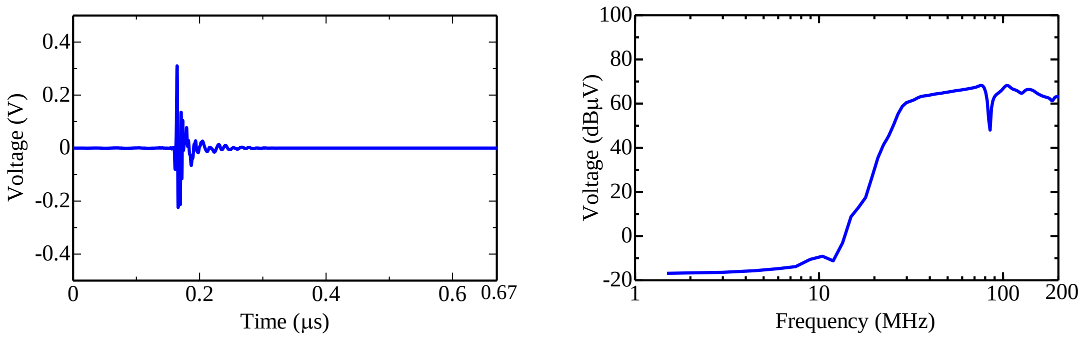

(a) Decomposed boost converter turn-off spike noise signal

(b) Decomposed boost converter turn-off spike noise spectrum

Figure 4.8 Boost converter turn-off spike noise.

The same process is used for obtaining the noise reduction caused by switching fluctuations as described in Chapter 3. The actual switching signal is measured by an oscilloscope, which is shown in Fig. 4.9a, while the ideal switching signal without switching fluctuation is shown in Fig. 4.9b. As shown in Fig. 4.10. There is a difference between an ideal and an actual signal. Based on the results in Chapter 3, the switching signal periods were set to 1024 since the reduction is found to be convergent after 500 periods. The obtain noise reduction is shown in Fig. 4.11.

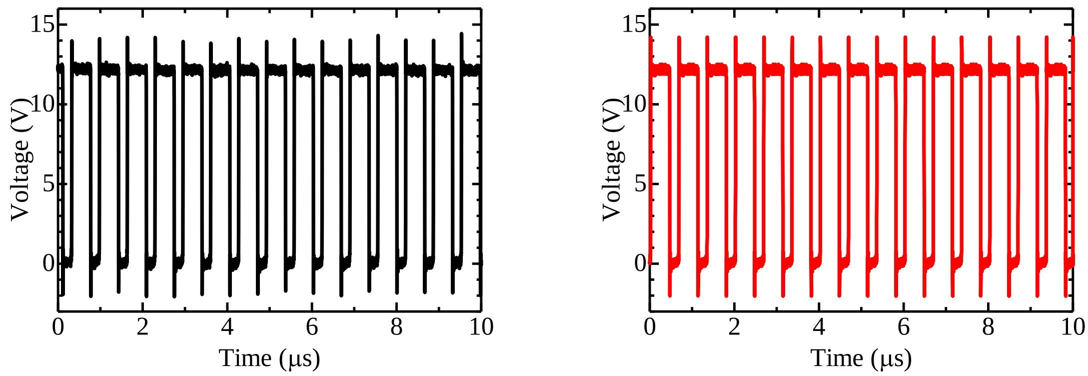

(a) Switching signal with fluctuation

(b) Switching signal duplicated from one period without fluctuation

Figure 4.9 Switching signal waveforms.

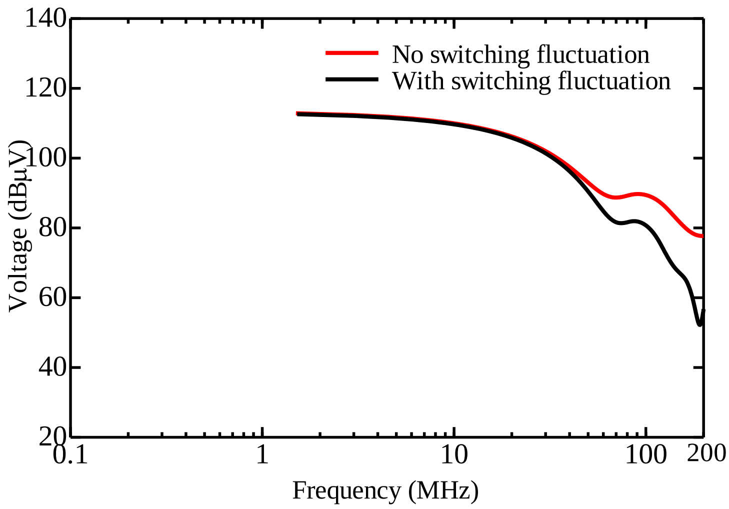

Figure 4.10 The switching fluctuation effect on switching signal of boost converter.

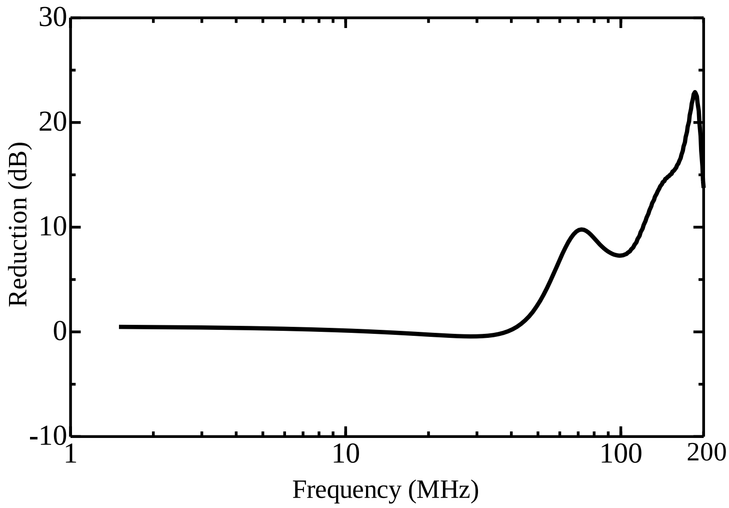

Figure 4.11 Noise reduction caused by fluctuation in boost converter.

4.3.2 GaN Based DC-DC Buck Converter

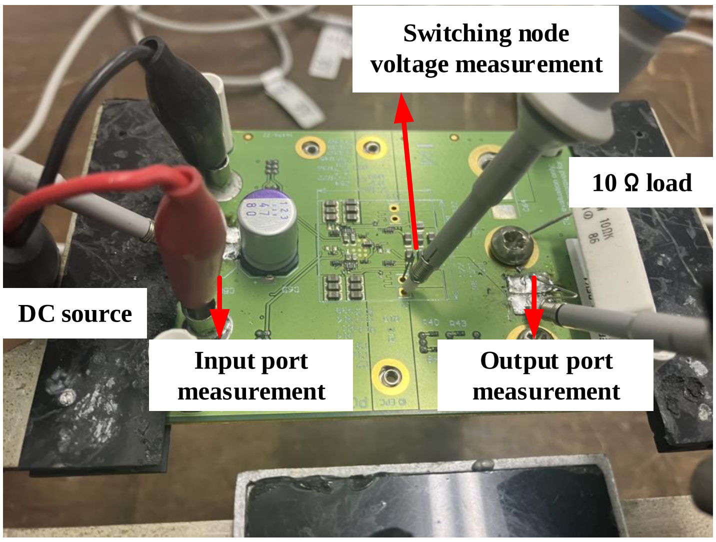

Figure 4.12 GaN-based DC-DC buck converter measurement view.

GaN power devices have been developed as the high performance power devices of the next generation. However, the faster switching action and the higher switching frequency will result in more EMC issues. The switching frequency was 2 MHz. The measurement view is shown in Fig.4.12.

The GaN based converter (EPC9160) with a 10-Ω load was used for evaluation. The input voltage was 18 V, and the output voltage was 5 V, which is same voltage condition with the converter in Chapter 2 and Chapter 3. The same process is applied for obtaining the ideal identified parameter and reducing noise caused by switching fluctuations. The noise reduction caused by switching fluctuation is shown in Fig. 4.14.

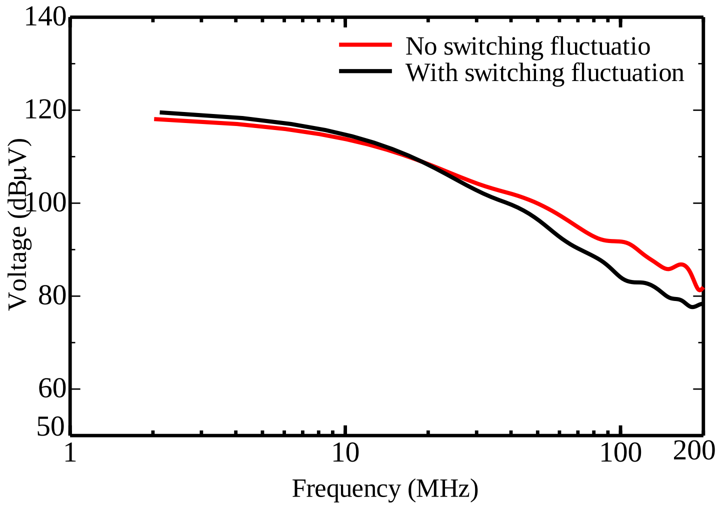

Figure 4.13 The switching fluctuation effect on switching signal of GaN-baased converter.

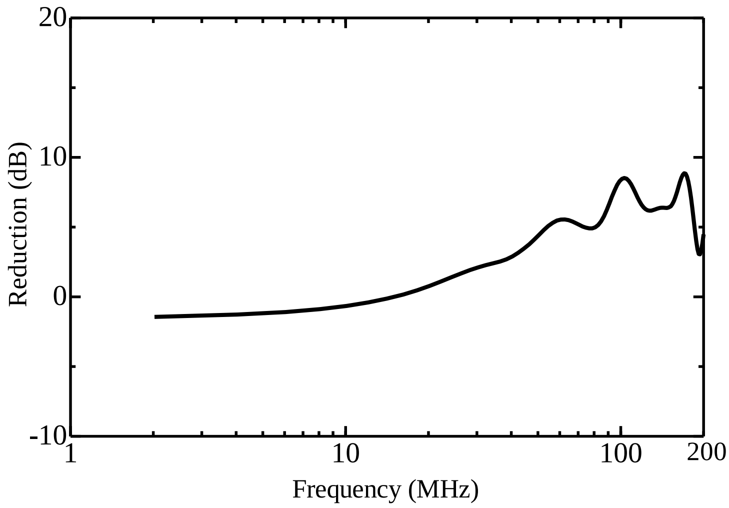

Figure 4.14 Noise reduction caused by fluctuation in GaN-based buck converter.

4.4 Result Evaluation

The results of the evaluation of the boost converter and the GaN buck converter have been conducted separately. They both include the result of applying the waveform decomposition method and the realistic prediction results.

4.4.1 The Prediction Result of DC-DC Boost Converter

First is the boost type converter prediction result. The high accuracy parameters can be obtained by applying waveform decomposition and parameter identification. Figure 4.15 is the comparison of the input port prediction result with the measured spectrum. In boost converter condition, the turn-on spike noise will be overwhelmed by the turn-off spike noise; therefore, only the turn-off spike noise is recomposed with ripple noise.Prediction is shown by the red dot line, and measurement is shown by the black line. As a comparison target, both converter ports with 1-μF capacitor filter conditions are used The output port prediction is shown in Fig. 4.16. Good accurate result are shown in both port. Based on the prediction result, it can be confirmed that waveform decomposition is a valid method.

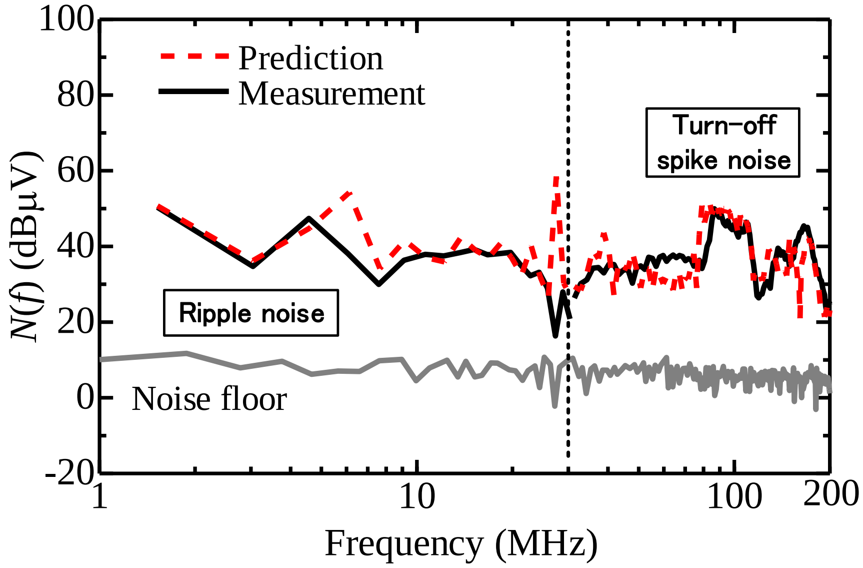

Figure 4.15 DC-DC boost converter input-port noise.

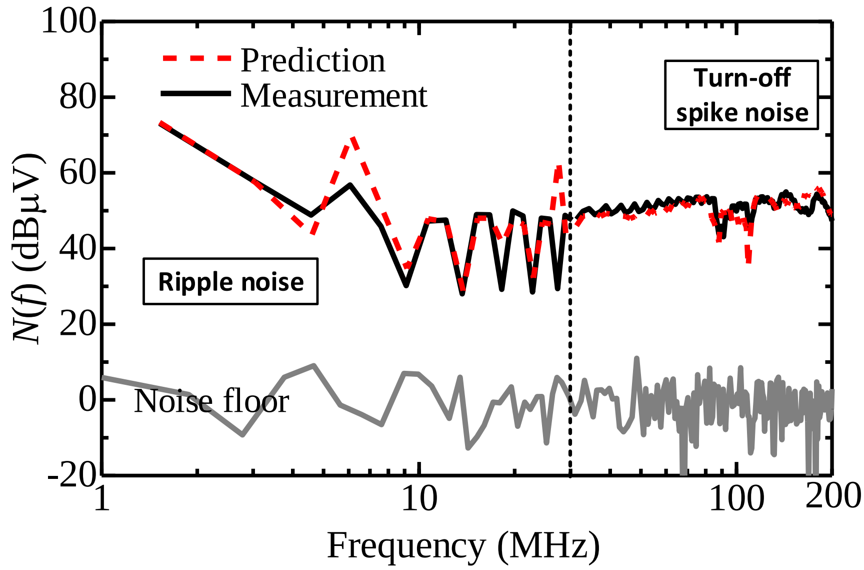

Figure 4.16 DC-DC boost converter output-port noise.

The averaged spectra prediction are shown in Fig. 4.17 and Fig. 4.18. As a result of combining the noise reduction with the ideal peak detected noise, the blue line represents the predicted averaged spectrum. It appears that both the input port noise and the output port noise in higher frequencies are of good accuracy, as indicated in the measurement results in black. The prediction error are shown in Fig. 4.19a and Fig. 4.19b. Most error are in 10 dB up to 200 MHz.

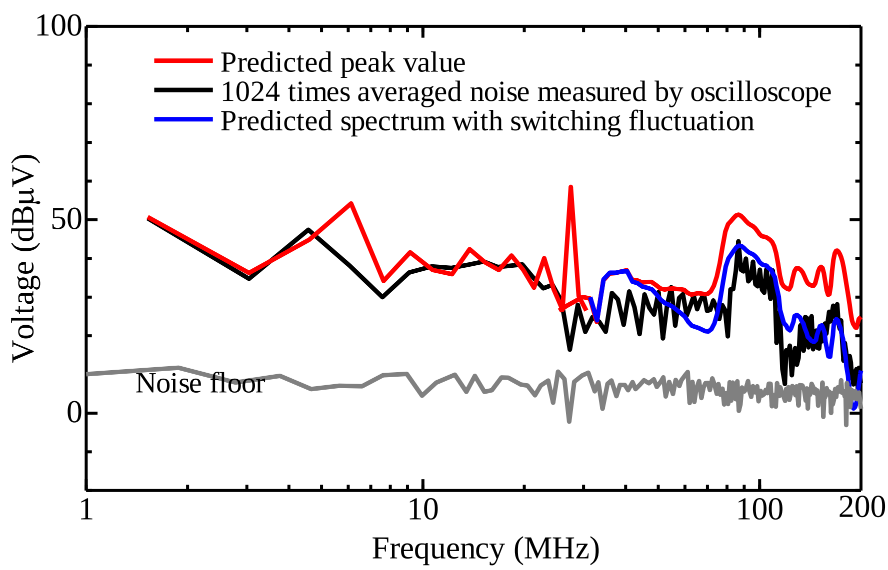

Figure 4.17 DC-DC boost converter averaged input-port noise.

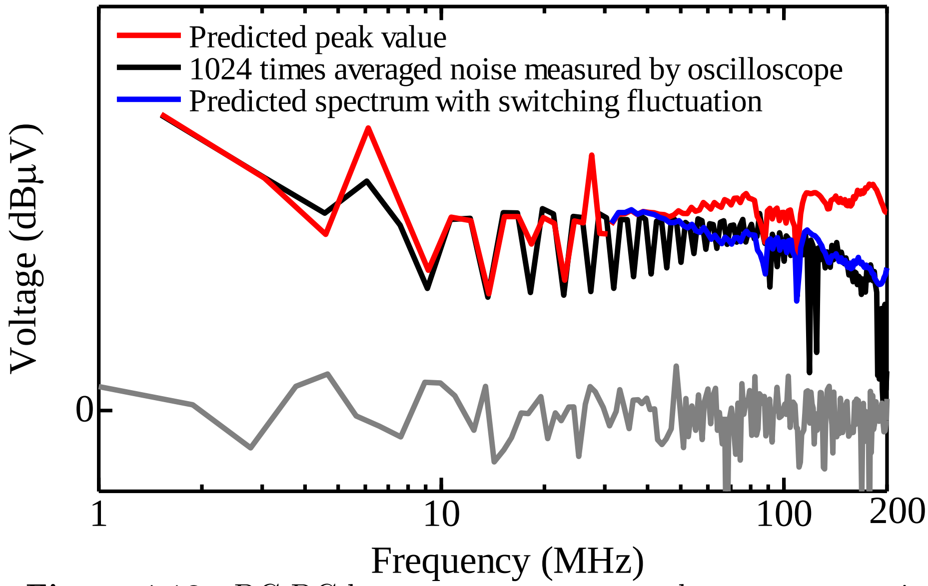

Figure 4.18 DC-DC boost converter averaged output-port noise.

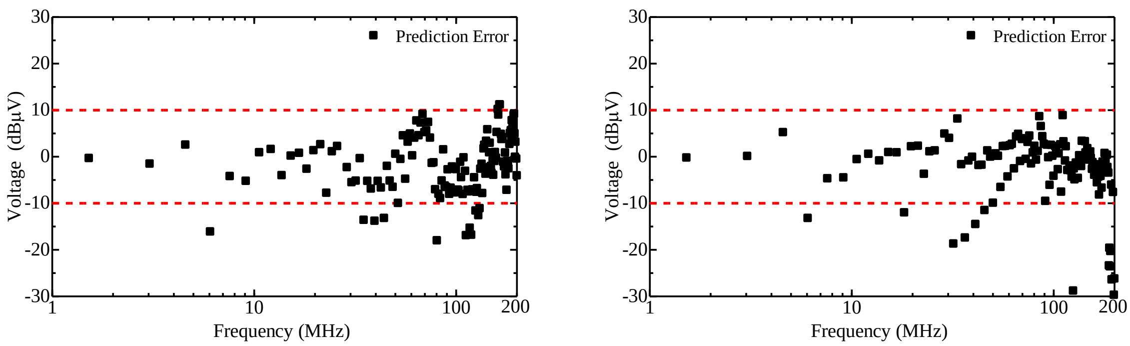

(a) Input port prediction error of boost converter.

(b) Output port prediction error of boost converter.

Figure 4.19 Prediction error of boost converter.

4.4.2 The Prediction Result of GaN Based DC-DC Buck Converter

Same process is applied to GaN-based buck converter. There are only several differences on ripple-spike noise frequency boundary. Since the GaN-based switching frequency is 2 MHz, the ripple-spike noise frequency boundary is 20 times of switching frequency, which is 40 MHz. The low-pass filter stopband is set to be 40 MHz. bFor parameter identification, a 4.7-μF filter capacitor with a 0.18-m$/Omega$ ESR and a 1.84-nH ESL was soldered in parallel at each converter port. Both converter ports with a 4.7-μF capacitor filter are used as comparison targets

The ideal spectrum prediction results are shown in Fig. 4.20 and Fig. 4.21.

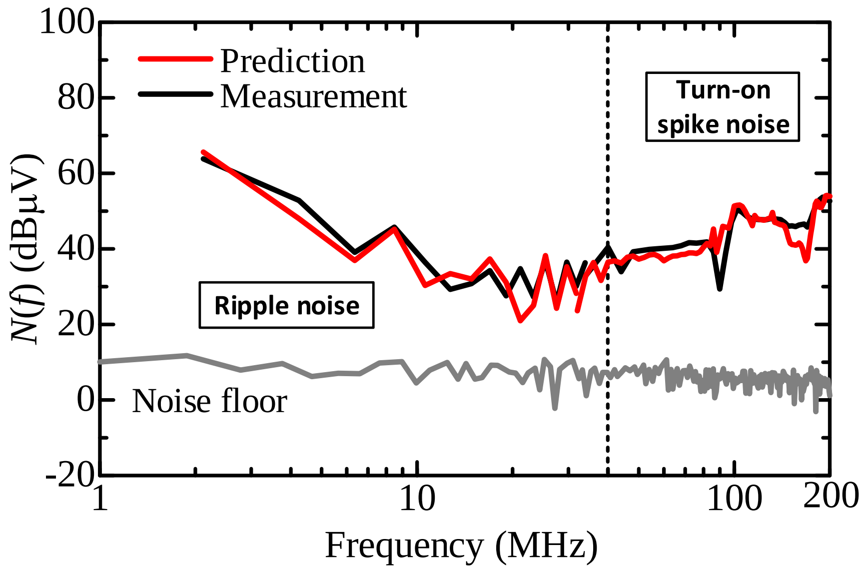

Figure 4.20 GaN-based DC-DC buck converter input-port noise.

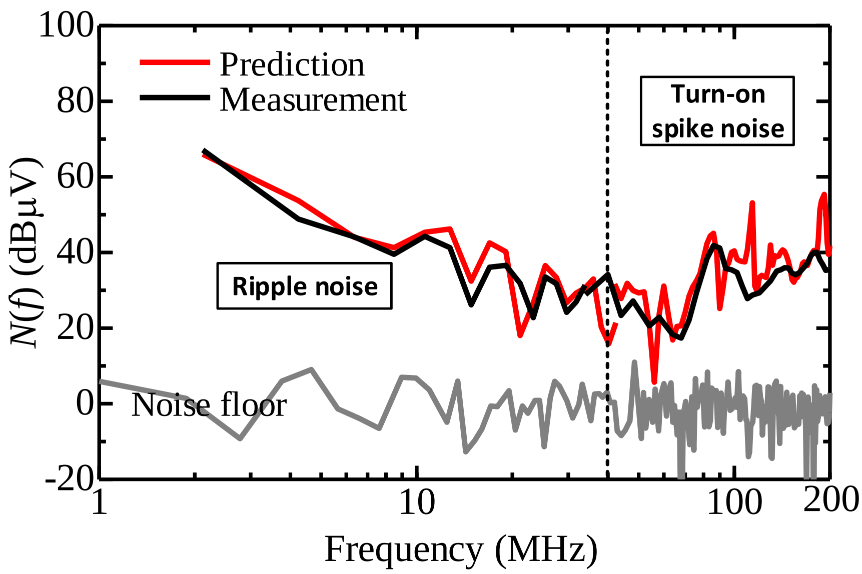

Figure 4.21 GaN-based DC-DC buck converter output-port noise.

The averaged spectrum prediction results are shown in Fig. 4.22 and Fig. 4.23. The green line is the predicted spectrum. The prediction error are shown in Fig. 4.24a and Fig. 4.24b. Most error are in 10 dB up to 200 MHz.

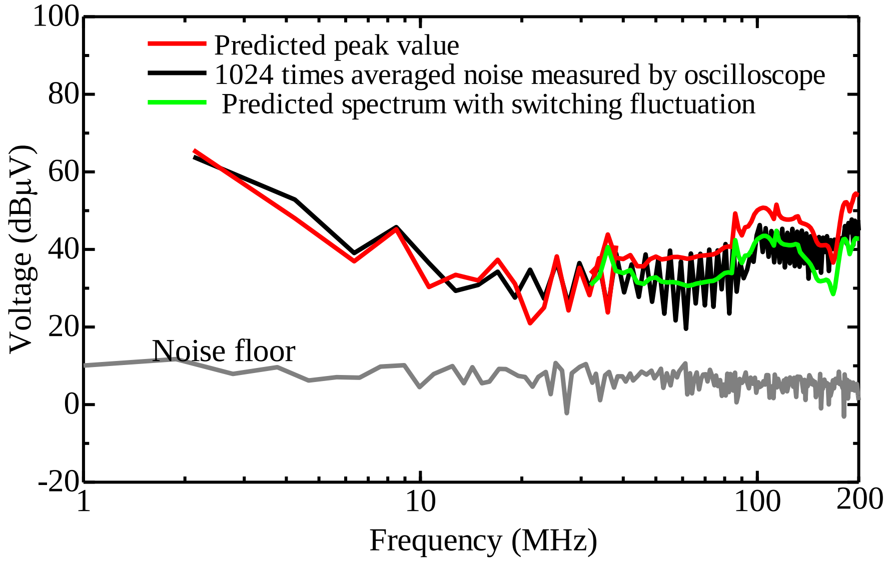

Figure 4.22 GaN-based DC-DC buck converter averaged spectrum prediction.

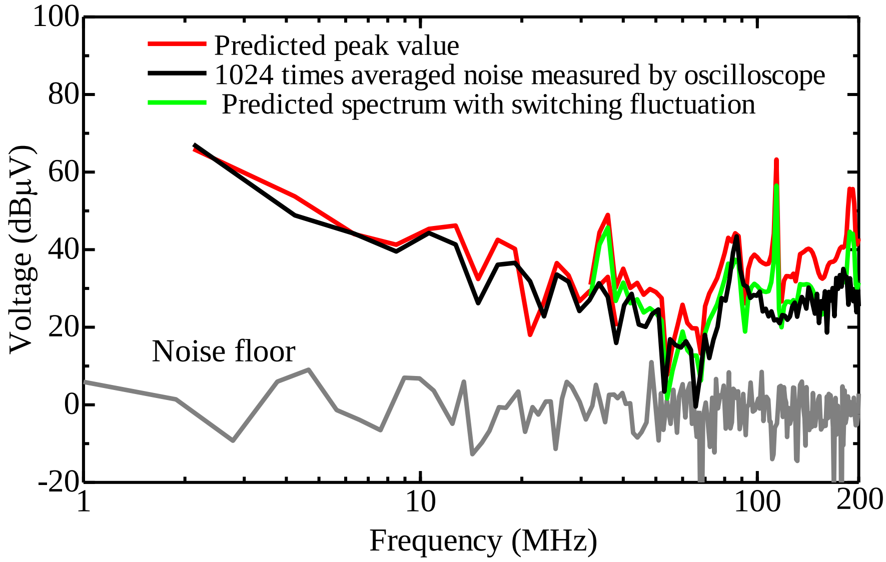

Figure 4.23 GaN-based DC-DC buck converter averaged spectrum prediction.

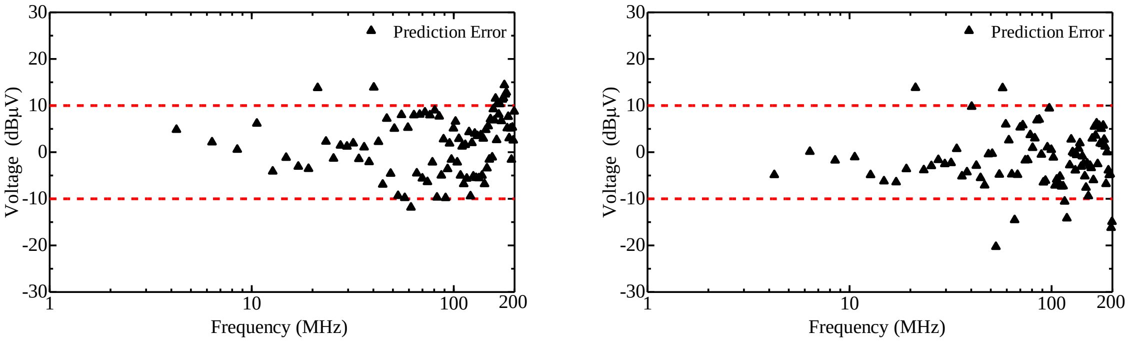

(a) Input port prediction error of GaN-based buck converter

(b) Output port prediction error of GaN-based buck converter

Figure 4.24 Prediction error of GaN-based buck converter.

4.5 Conclusion

The general application of the proposed approach described in Chapters 2 and 3 is tested in this chapter. A boost DC-DC converter and GaN-based DC-DC converters are used as examples for testing the application. Based on the results, the prediction with a capacitor filter condition matches the measured results.The results demonstrate that this technique can be used to develop models of a wide variety of DC-DC converters with a high degree of accuracy, compactness, and linearity.

In both the input and output ports, switching fluctuation reduces noise at high frequency. There are two important points need to to consider for general applications: determine the ripple-spike boundary in frequency domain, and choose an appropriate filter. Right now, ripple-spike boundary determination is an experimentally based method with some experience. To select the appropriate filter, it is necessary to take into consideration the switching frequency, the noise spectrum amplitude, and the attenuation value. They are also considered to be the future direction of this model.

Chapter 5

Load Variable Noise-source Equivalent Circuit Model

5.1 Introduction

Emissions from electronic devices are predicted using the black-box model. For complex circuits and system-level interference, this type of model predicts EMI without looking at device details. For describing the behavior of EMI, the model usually consists of one or more pairs of Norton/Thevenin equivalent circuits [27–29]. The Modular Terminal Behavioral (MTB) model for characterizing switching module conducted emission was originally proposed in [27], and it has since been expanded into a generalized terminal model [28, 29]. The converter load is included and fixed in the terminal model, so the effect of the converter load on conducted emissions cannot be considered.

Several studies have examined the load effect on conducted emissions [69, 70]. According to [69], the conducted emissions from a SiC-based boost converter increased with the load current when operated under different conditions. This indicates that the load is not independent of the converter's EMI, which must be considered in the EMI modeling process. In [70], suggested that the switching condition depends on load and conducted tests with various loads. In their study, they discovered that when the output load increased, the fundamental switching frequency and its harmonics were shifted to a higher frequency range as a result of changes in the internal operation conditions.

Since the load affects the conducted emissions, the black-box model should be able to guide the filter design under a variety of load conditions. A generic black-box model, however, can only be adapted to a specific load condition. This led to the conclusion that a black-box model that excludes load is required.

A load-excluded two-port equivalent circuit model was proposed, and a preliminary study of the effect of load on the equivalent noise parameters was conducted [31]. Several different loads were used to identify the noise parameters, and it was determined that the internal impedances were independent of the load change, while the noise current source was dependent on the load change. Using noise current sources estimated from two different loads, a linear interpolation method was also applied to predict the noise spectrum at an unknown load. Despite this, we were unable to clarify the effect of load on noise parameters as switching fluctuations affected noise parameter identification in higher frequencies. As discussed in Chapter 2, the waveform decomposition method is used in this chapter to identify the model parameters precisely, along with a cubic spline interpolation method that is more accurate than linear interpolation.

5.2 Load Effect on DC-DC Converter Duty cycle

We utilize a DC-DC buck converter (ROHM, BD9G341EFJ-EVK- 101) operating at the switching frequency 200 kHz for the model evaluation. The noise signal is measured in the time domain and converted into frequency spectra by fast Fourier transform (FFT) using MATLAB. The time-domain measurement can catch the noise magnitude and phase information at the same time, which is essential for black-box EMI modeling. An oscilloscope (Keysight DSOS104A) with three high-impedance passive 10:1 probes (KEYSIGHT N2894A, 700 MHz) with 1 M Ω input resistance and 9.5 pF input capacitance were used for measurement: one to measure the triggered signal from the switching node of the DC-DC converter, and two to measure the input and output port signals. The input voltage was 18 V, and the output voltage was 5 V. The trigger was applied to the switching-node voltage. The measurement setup is shown in Fig. 5.1, where two probes are used for port noise measurement and one is used for measuring the switching node signal as a trigger source.

The DC-DC converter is working in the CCM, since if it works in the discontinuous condition mode (DCM), the diode needs to be turned off one more time, creating a third circuit condition. Several loads are connected with the DC-DC converter, and the switching node voltage in Fig. 5.1, is observed with different loads. The measured results are shown in Fig.5.2. The turn-on time is shorter with a larger load because the higher load current affects the feedback control process. Many studies on black-box EMI have set the load to fixed for the time-invariant system and include it in the model, the parameterization process has to repeat many times if the conducted emission is dealing with several different load conditions.

Based on the measurement results, it appears that a converter with a light load generates more input port noise and requires a longer time to turn on. Input port and output port noise was measured with different loads and decomposed into ripple noise and turn-on spike noise. However, the output port noise does not change significantly. When there is a light load, the load current is high, and as the load current increases, so does the

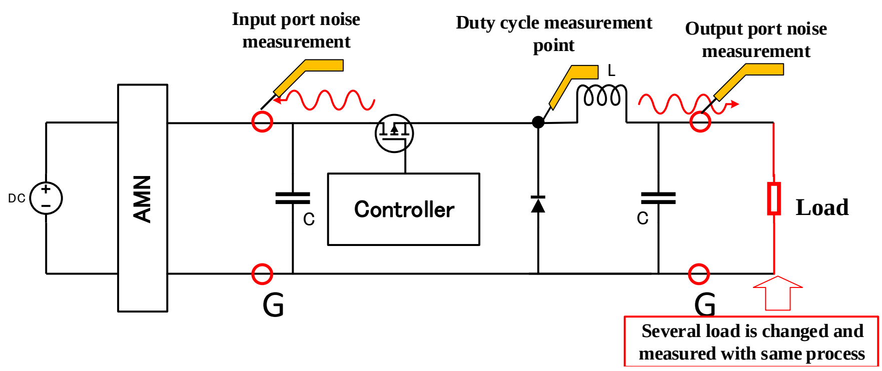

Figure 5.1 Measurement position.

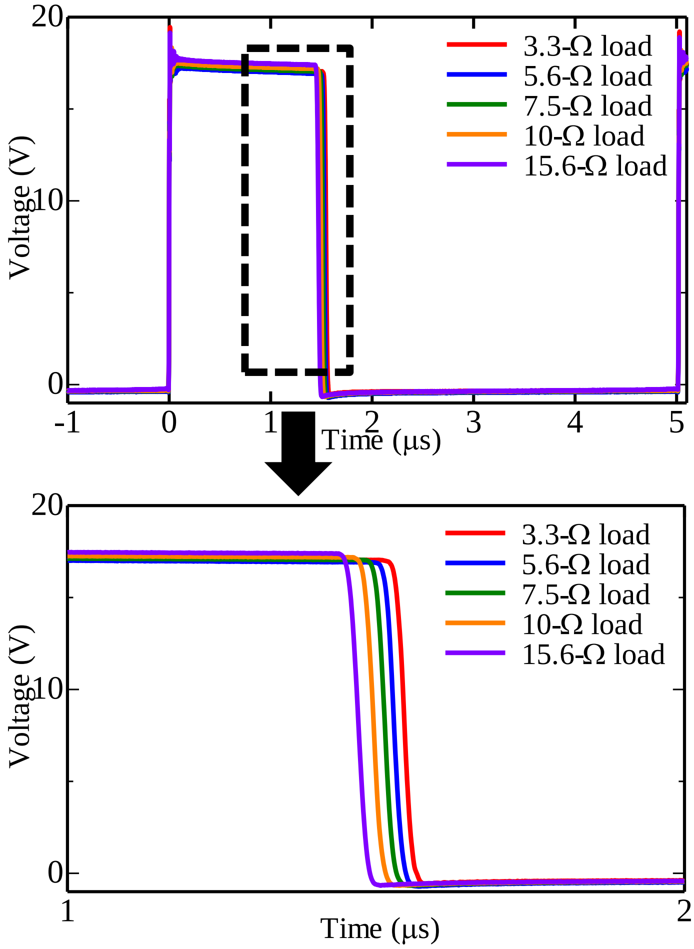

Figure 5.2 load effect on DC-DC converter duty cycle.

maximum recovery current and thus the disturbance levels, as mentioned in [71]. According to these measurement results, the noise amplitude correlates with different loads. As the magnitude of input port noise varies with the load value, this is of primary interest here.

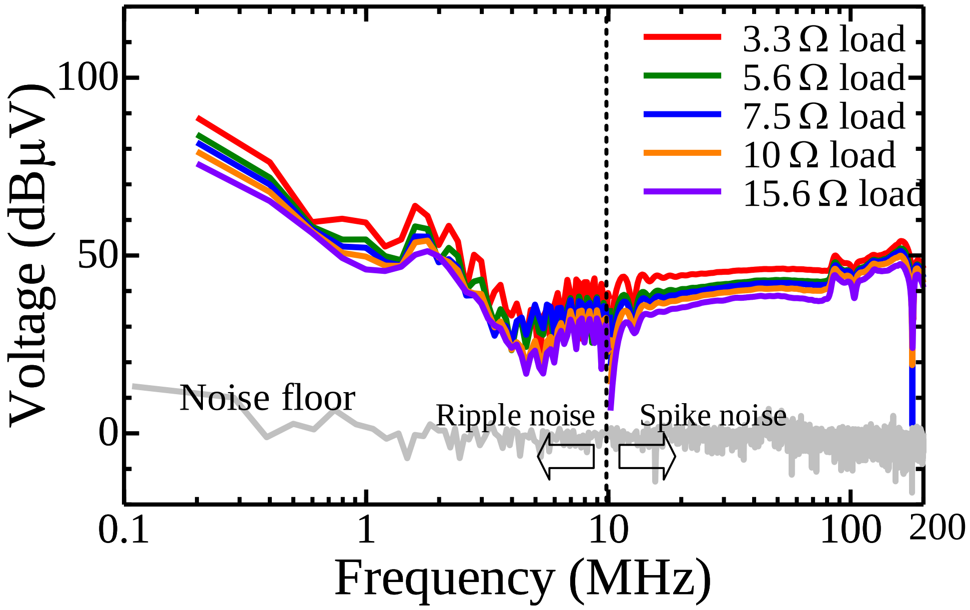

Figure 5.3 load effect on DC-DC converter input port noise Vin.

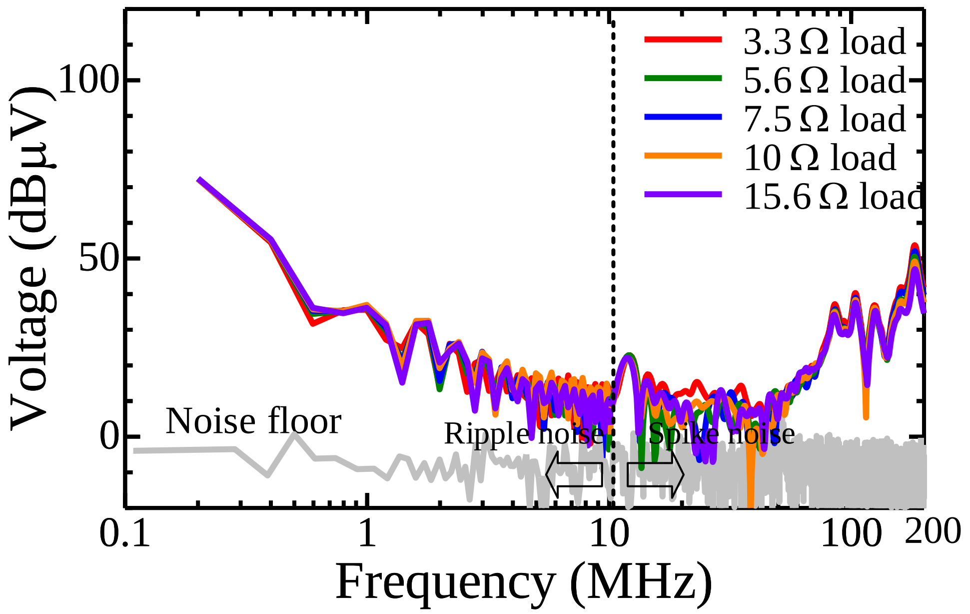

Figure 5.4 load effect on DC-DC converter output port noise Vout.

5.3 Identified Noise-source Parameter with Different Load

$$\begin{bmatrix} \dot{I}_{\text{in}} \\ \dot{I}_{\text{out}} \end{bmatrix} = \begin{bmatrix} \dot{V}_{\text{in}} & \dot{V}_{\text{in}} - \dot{V}_{\text{out}} & 0 & -1 & 0 \\ 0 & -\dot{V}_{\text{in}} - \dot{V}_{\text{out}} & \dot{V}_{\text{out}} & 0 & -1 \end{bmatrix} \begin{bmatrix} \dot{Y}_1 \\ \dot{Y}_2 \\ \dot{Y}_3 \\ \dot{I}_{\text{s1}} \\ \dot{I}_{\text{s2}} \end{bmatrix}. \tag{5.1}$$

The identified parameters are shown in below. To visualize the noise parameters across the entire frequency range, the ripple noise parameter is combined with the turn-on spike noise parameter in the same figure. Since the turn-on spike noise overwhelms the turn-off spike noise, the turn-off spike noise is ignored. Different colors indicate different noise behavior parameters under different load conditions. A total of five different load conditions were measured and parameterized in order to determine the conducted emissions. A parameter identification result can be divided into three categories: input port parameters I_{s1} and Y_1, output port parameters I_{s2} and Y_3, and isolation admittance Y_2. Considering that the noise parameter in the output port changes only minimally with load, the load will not affect the noise parameter.

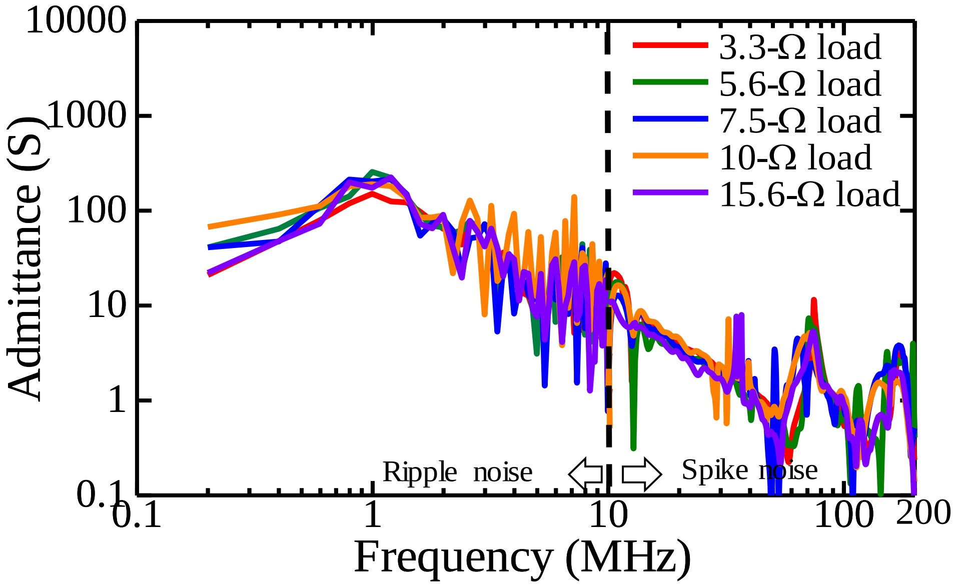

Figure 5.5 Identified input port noise admittance Y1.

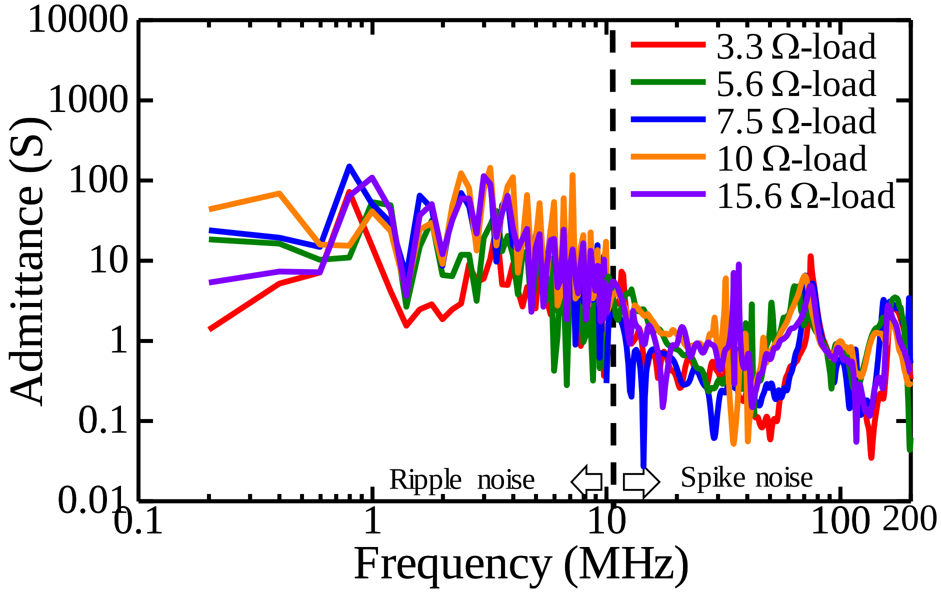

Figure 5.6 Identified isolation admittance Y2.

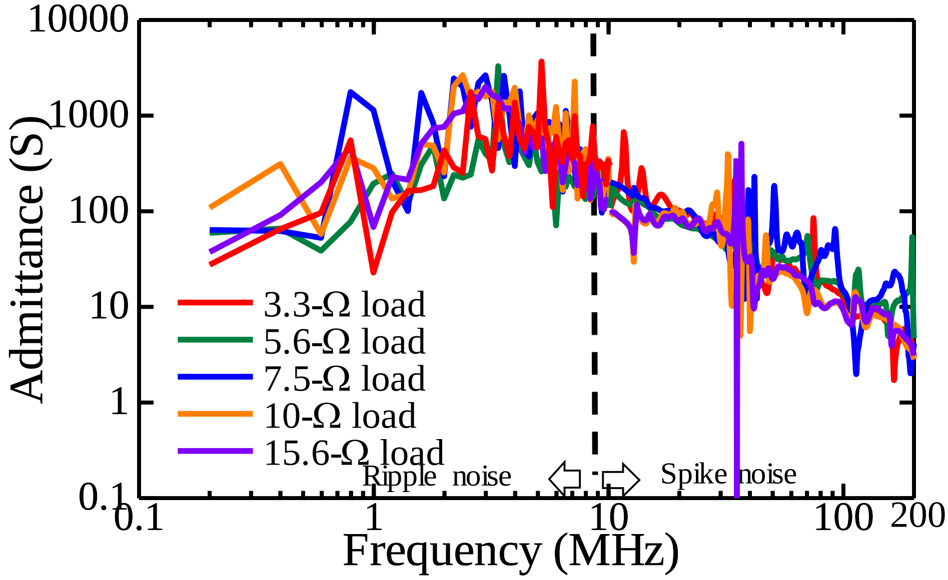

Figure 5.7 Identified output port noise admittance Y3.

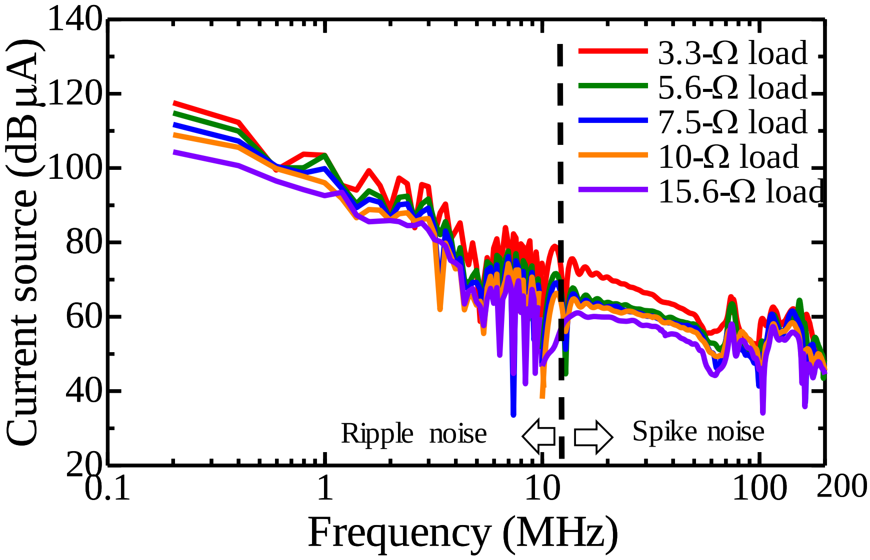

Figure 5.8 Identified input port noise current source Is1.

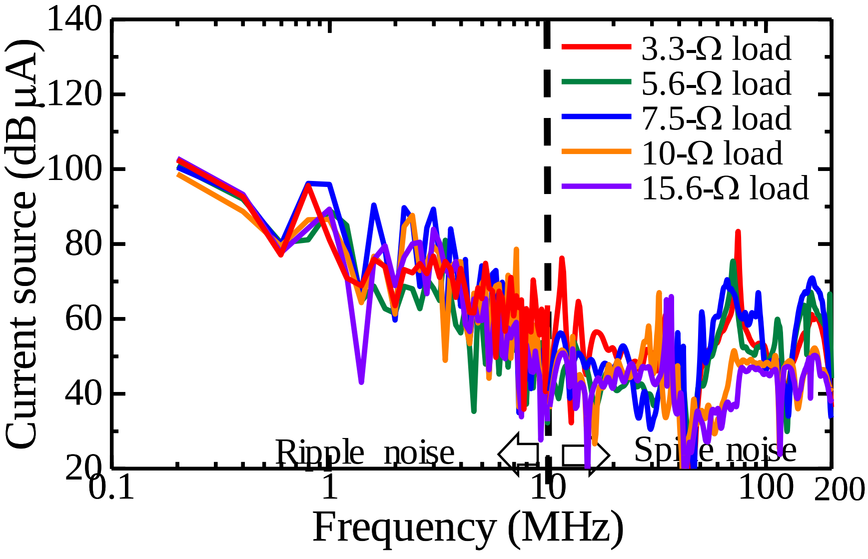

Figure 5.9 Identified output port noise current source Is2.

The input port parameters are shown in Fig.5.5 and 5.8. The noise current source magnitudes I_{s1} are following the load value, and the noise admittance magnitudes Y_1 are independent from load and show almost the same trend for each load. Errors occur at some frequencies because it is difficult to avoid errors in the least-squares method when solving (5.1), which is an overdetermined system.

Calculation errors tend to happen when fitting the results of unknown parameters. If the general trends of identified results are similar, we assume the noise admittance magnitudes Y_1 are fixed. That is because the noise path on board does not change with load value like the result shown in Fig.5.5.

The output port parameters I_{s2} and Y_3 are shown in Fig. 5.9. and 5.7.Although errors occur in several frequencies, the trends of the noise current and noise admittance are assumed to be the same. Even though errors occur at a variety of frequencies, the trends of the noise current and the noise admittance are assumed to be the same. Regarding the magnitude of noise admittance Y_2, a small load will result in a large noise current, which requires a greater isolation impedance. In this way, the smaller load value has smaller admittance magnitudes, resulting in a sufficient amount of isolation between the input and output ports. By calculating the input port current source I_{s1}, the input port noise voltage with an unknown load can be predicted.

5.4 Cubic Spline Interpolation Method for Load Variable Equivalent Circuit Model

5.4.1 Spline Cubic Interpolation Method

$$f(x) = \begin{cases} a_1x^3 + b_1x^2 + c_1x + d_1(x_1 \leqslant x \leqslant x_2) \\ a_2x^3 + b_2x^2 + c_2x + d_2(x_2 \leqslant x \leqslant x_3) \\ \cdots \\ a_3x^3 + b_3x^2 + c_3x + d_3(x_n \leqslant x \leqslant x_{n+1}) \end{cases} \tag{5.2}$$

It is necessary to state several equations in order to determine the $4n$ coefficients of all polynomials. Firstly, every polynomial passes through exactly two points. As a result, the equations for $2n$ are

$$\begin{cases} f_1(x_1) = y_1 \\ f_1(x_2) = y_2 \\ f_2(x_2) = y_3 \\ f_2(x_2) = y_3 \\ \cdots \\ f_n(x_n) = y_n \\ f_n(x_{n+1}) = y_{n+1} \end{cases} \tag{5.3}$$

Moreover, the first and second derivatives of all polynomials are identical at the points where they touch their adjacent polynomials:

$$\begin{cases} \frac{d}{dx}f_1(x) = \frac{d}{dx}f_2(x) \quad |_{x=x_2} \\ \frac{d}{dx}f_2(x) = \frac{d}{dx}f_3(x) \quad |_{x=x_3} \\ \cdots \\ \frac{d}{dx}f_{n-1}(x) = \frac{d}{dx}f_n(x) \quad |_{x=x_n} \end{cases} \tag{5.4}$$

For the second derivative, the same procedure is followed by stating:

$$\begin{cases} \frac{d^2}{dx^2}f_1(x) = \frac{d^2}{dx^2}f_2(x) \quad |_{x=x_2} \\ \frac{d^2}{dx^2}f_2(x) = \frac{d^2}{dx^2}f_3(x) \quad |_{x=x_3} \\ \cdots \\ \frac{d^2}{dx^2}f_{n-1}(x) = \frac{d^2}{dx^2}f_n(x) \quad |_{x=x_n} \end{cases} \tag{5.5}$$

In the boundary points of the interpolation function, a natural spline is defined as setting the second derivative of the first and last polynomials to zero:

$$\begin{cases} 6a_1x_1 + 2b_1 = 0 \\ 6a_nx_{n+1} + 2b_n = 0 \end{cases} \tag{5.6}$$

5.4.2 The Application of Spline Cubic Interpolation for Load-variable Model

The noise source magnitude I_{s1} with load variations for different frequencies is shown in Fig. 5.10 and 5.11. In order to make the results easier to visualize, separate them into two categories: noise sources with a higher magnitude (8 MHz - 80 MHz) and a lower magnitude (below 2 MHz). In Fig. 5.10 and 5.11, as the load value increases, the value of the identified noise source decreases. Therefore, taking into consideration the interpolation accuracy and simplicity of calculation, the natural cubic spline interpolation method is proposed to approximate the I_{s1} without the need for parameter identification as (5.1), $I_{s1}^{R_x}$ where the unknown current source with load value R_x.

$$I_{s1}^{R_x} = \begin{cases} a_1R_x^3 + b_1R_x^2 + c_1R_x + d_1(3.3 \leqslant R_x \leqslant 5.6) \\ a_2R_x^3 + b_2R_x^2 + c_2R_x + d_2(5.6 \leqslant R_x \leqslant 7.5) \\ a_3R_x^3 + b_3R_x^2 + c_3R_x + d_3(7.5 \leqslant R_x \leqslant 15.6) \end{cases} \tag{5.7}$$

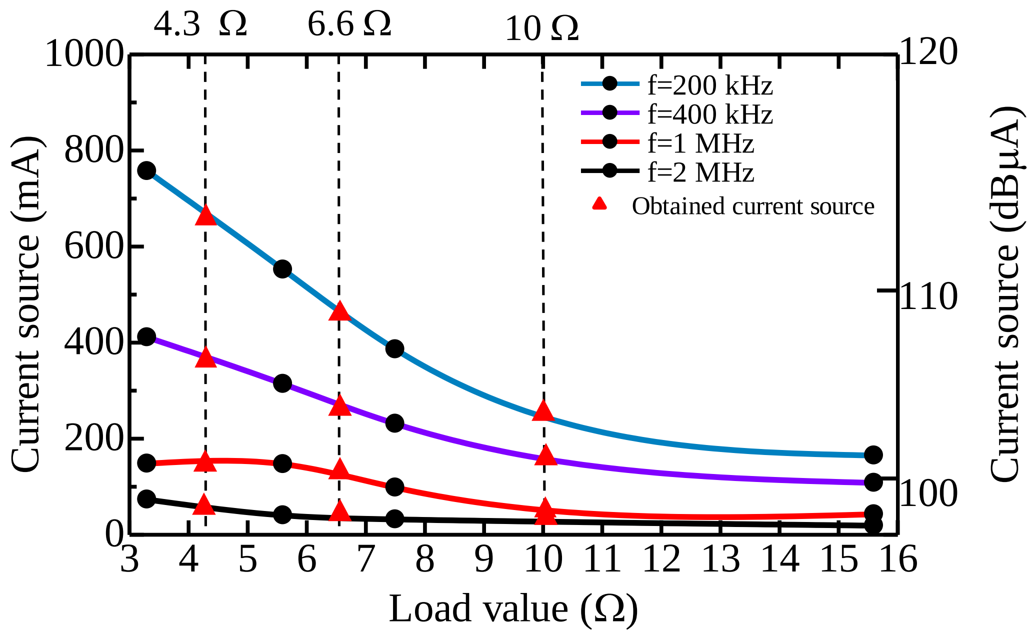

Figure 5.10 Current source value with load at given frequency (below 2 MHz).

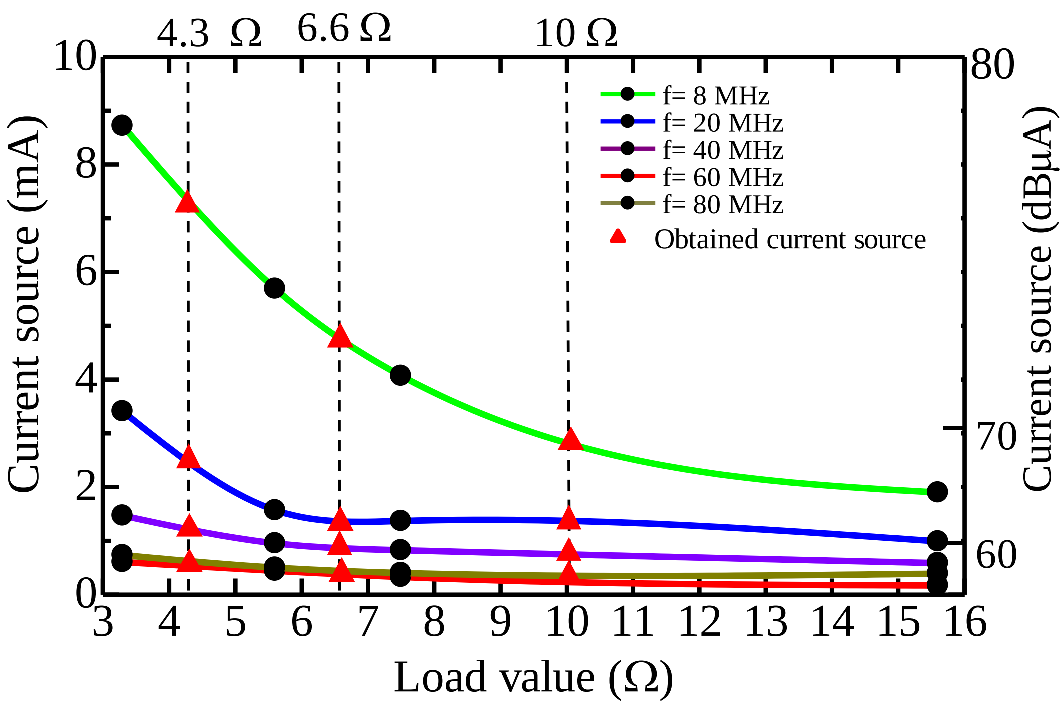

Figure 5.11 Current source value with load at given frequency (2 MHz-80 MHz).

5.5 Result Evaluation

The parameters with four different load values are shown in Fig. 5.10 and 5.11 for evaluation of the results: 3.3 Ω, 5.6 Ω, 7.5 Ω and 15.6 Ω, and noise current source with 10 Ω load is the prediction target. In this study, the noise parameters of four different loads were identified using the same process, the only difference was the load value.

The unknown current source $I_{s1}^{R_x=10\Omega}$ at each frequency is calculated by , and is shown in Fig. 5.12 The noise current source identified by (5.1) is the reference in black, and the orange curve shows the noise current source obtained from the cubic spline interpolation method. For input port voltage prediction, the noise impedances Y_1 and Y_3 are stable, and Y_2 should be enough for isolation, so the other parameters of 3.3 Ω load with larger isolation admittance is used. The input port voltage prediction result is shown in Fig. 5.13. As shown in the picture, the prediction and measurement are in good agreement as far as the accuracy is concerned.

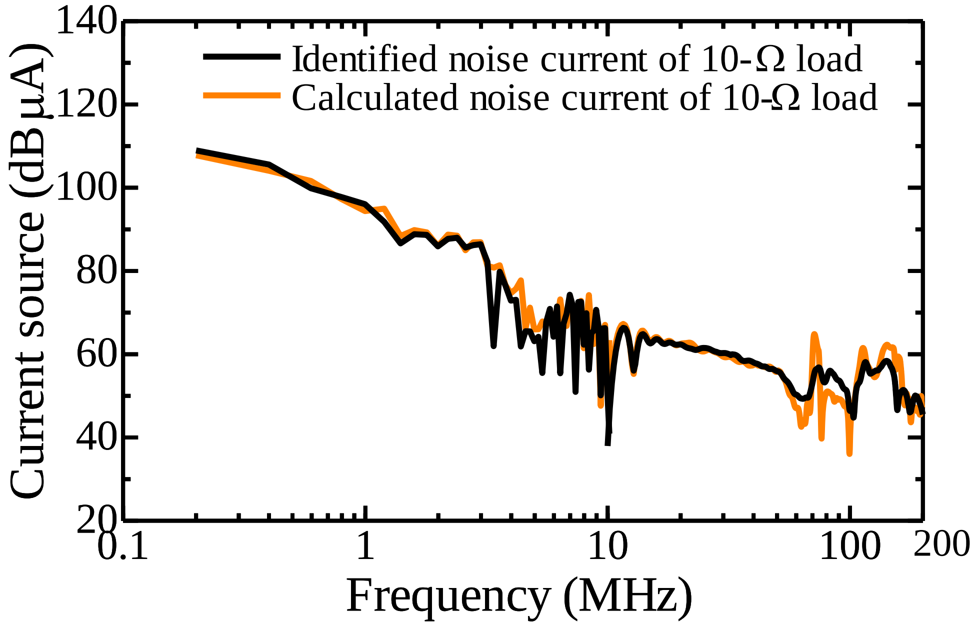

Figure 5.12 Predicted noise current source Is1

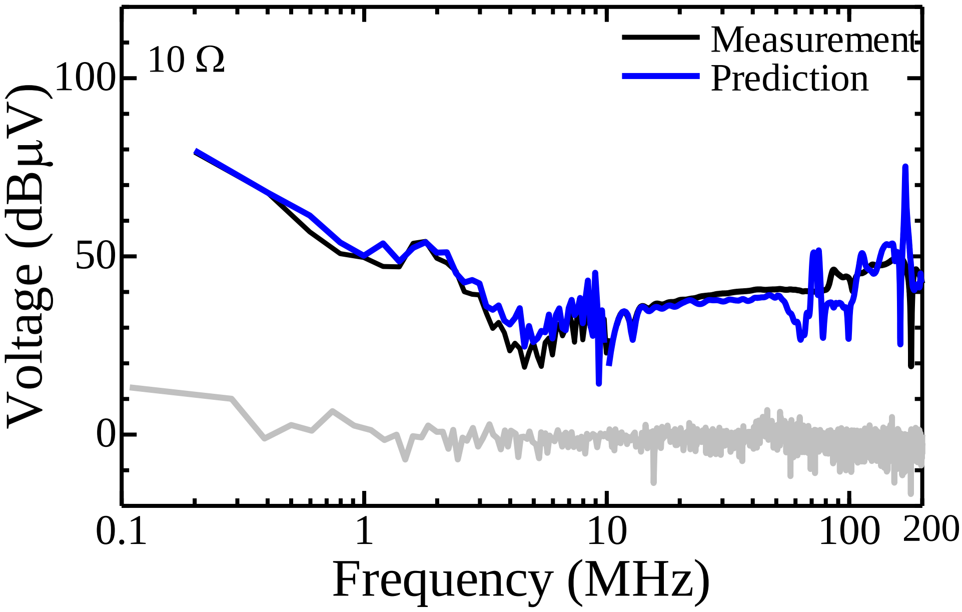

Figure 5.13 Predicted input port noise with 10 Ω load

In addition to the 10-Ω condition, the other load values such as 4.3 Ω and 6.6 Ω in different load ranges of (5.1) are calculated, and all the predictions showed good agreement with the measurements up to 80 MHz in the same way as 10 Ω though the figures are omitted due to space limitations. In the case of frequencies greater than 80 MHz, where the load is not affecting the input-port current source, assume that the deviation is caused by an accuracy degradation of the current source due to numerical interpolation under the rank-deficient problem. The proposed approach is therefore valid as long as the current source at the input port varies with load.

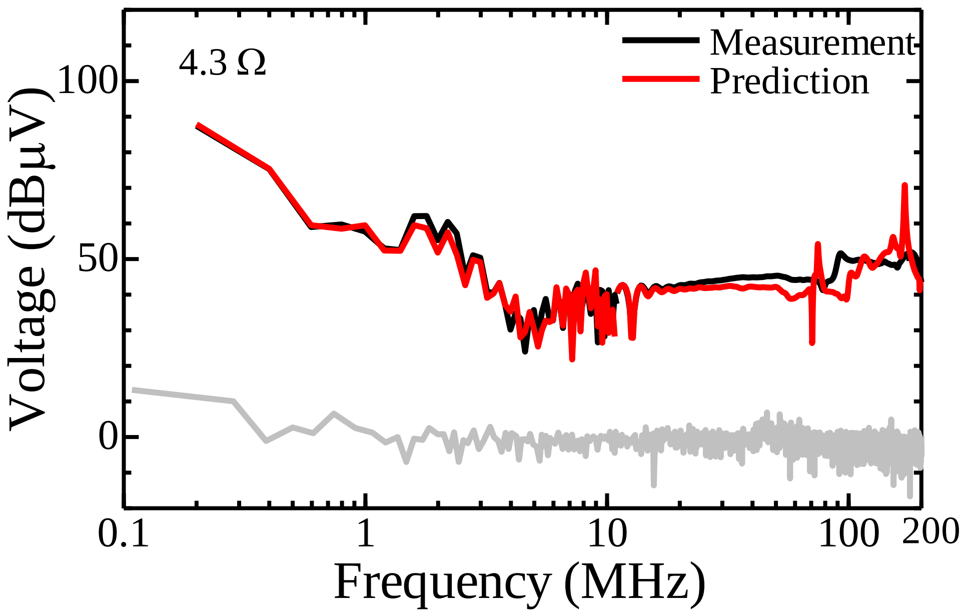

Figure 5.14 Predicted input port noise with 4.3 Ω load.

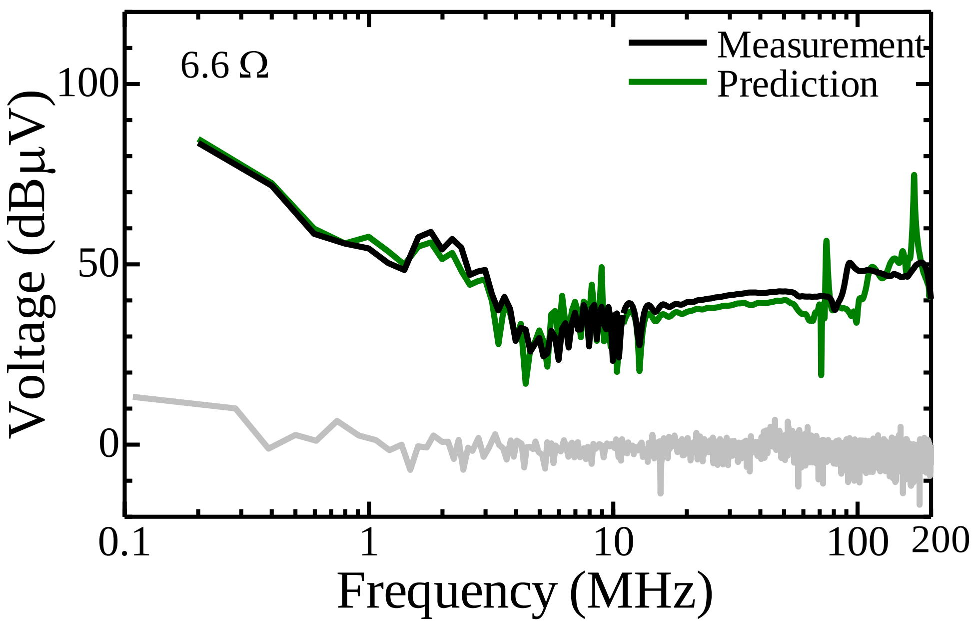

Figure 5.15 Predicted input port noise with 6.6 Ω load.

5.6 Conclusion

A black-box equivalent circuit model is generally used to predict electromagnetic interference (EMI) from DC-DC converters in order to assist in filter design. The load effect on EMI has previously been studied using a Norton-based two-port equivalent circuit model excluding load. In order to make an EMI prediction, the internal impedances of the system should remain constant regardless of the change in load, while only the noise current source should change with the change in load. By using numerical interpolation under these conditions, it is possible to calculate the noise current source at any load. Using the waveform decomposition method, the model parameters for a DC-DC buck converter with a switching frequency of 200 kHz were identified precisely. As the load changed, the internal admittances remained almost constant, whereas the input-port current source decreased with the change in load. Based on the cubic spline interpolation method, the input-port current source was fitted and calculated under any load condition. This approach was verified by predicting the input-port noise voltage for loads between 3.3 Ω and 15.6 Ω. When the input-port current source decreases with load below 80 MHz, the input-port voltage predicted using the input-port current source fitted by interpolation is in good agreement with the measured input-port voltage.

Chapter 6

General Conclusion

In this thesis, a serious study is proposed to address the inadequacy of black-box EMI models.The author focuses on the conducted emissions from DC-DC converters, and the noise-source equivalent-circuit model is used to model DC-DC converters. Overall, the work presented in this dissertation illustrates the wide applicability of two-port noise-source equivalent circuit model for EMI prediction in DC-DC converters. Simulations and experiments have shown that noise-source equivalent circuit model can accurately capture the high frequency behavior of DC-DC converter converters and are much easier to simulate than lumped-circuit models. Models such as these facilitate the simulation of EMI at the system level and can facilitate rapid iterations of EMI design.

(A) An approach is proposed to reduce the switching fluctuations inherent in DC-DC converters in order to improve noise-source parameter identification accuracy.

(B) The DC-DC converter switching fluctuation and its impact on the EMI spectrum is examined in order to determine a realistic noise spectrum.

(C) The proposed approaches are evaluated using converters with boost converters and GaN-based buck converter.

(D) A load-variable equivalent circuit model is developed to accommodate any changes in the value of the load.

Chapter 2 presents a waveform decomposition method for decomposing the time-domain noise signal waveform into ripple noise, turn-on spike noise, and turn-off spike noise. The use of this method enabled the equivalent noise source model to be identified without switching fluctuation effects during parameter identification. It was found that the peak amplitude was closely related to the prediction result, and the error up to 200 MHz was within 3 dB of the prediction.

In Chapter 3, a semi-empirical study has demonstrated that the inherent jitter caused by switching fluctuations of the DC-DC converter reduces the noise amplitude at higher frequencies. In order to eliminate switching fluctuations during time-domain measurements, the black-box model was used in conjunction with the waveform decomposition method. A study is conducted to examine the effect of switching fluctuations on noise during converter operation. Initially, the fluctuation was thought to be a modulation of frequency that spreads the noise spectrum over a wide range of frequencies. In order to calculate the reduction in spike noise power, the ideal switching waveform and the actual switching waveform were used. Finally, using the ideal noise spectrum, the actual noise spectrum is predicted, and the noise reduction obtained is accurate.

In Chapter 4, the application is tested using a boost DC-DC converter and a GaN-based DC-DC converter. The prediction with a capacitor filter condition matches the measured results. It is demonstrated that this technique allows models of a wide variety of DC-DC converters to be developed with a high degree of accuracy, compactness, and linearity.

In Chapter 5, the load effect on EMI has been studied using a Norton-based two-port equivalent circuit model excluding load. A cubic spline interpolation method was used to calculate the input-port current source under a variety of load conditions. This approach was verified by predicting the input-port noise voltage for loads between 3.3 Ω and 15.6 Ω. A good agreement is found between the input-port voltage predicted using the input-port current source fitted by interpolation and the measured input-port voltage when the input-port current source decreases with load below 80 MHz.

Consequently, the author expands the noise-source equivalent circuit model in order to assist engineers in determining the most appropriate modeling approach for the given application. Noise-source equivalent circuit models provide high accuracy over a wide range of frequencies and facilitate simulations with ease. Additionally, the noise-source equivalent circuit model may be helpful in designing and analyzing EMI filters and system-level EMI.

Appendix A

Envelop spectrum in this thesis

In this section, the spectrum of the conducted disturbance is described. Figure A-1 shows the time waveform of the conducted disturbance, its frequency spectrum, and its envelope. This section uses the same measurement conditions in Chapter 2, and the evaluation board BD9G341EFJ-EVK-101 (ROHM Co.) is used as the DC/DC converter. There is no bypass capacitor inserted. According to the voltage spectrum shown in , the conducted disturbance waves are generated at intervals of 200 kHz. Due to the fact that the conduction disturbance is produced in synchronization with the switching of the DC/DC converter, this is the case. As a result, the voltage level is the same as the noise floor at frequencies where there are no conducted disturbances. Due to this reason, it is appropriate to evaluate conducted disturbance waves occurring at intervals of 200 kHz for frequencies with high voltage levels. The envelopes are drawn at intervals of kHz or MHz. In this thesis, the conducted disturbance is evaluated by evaluating this envelope.

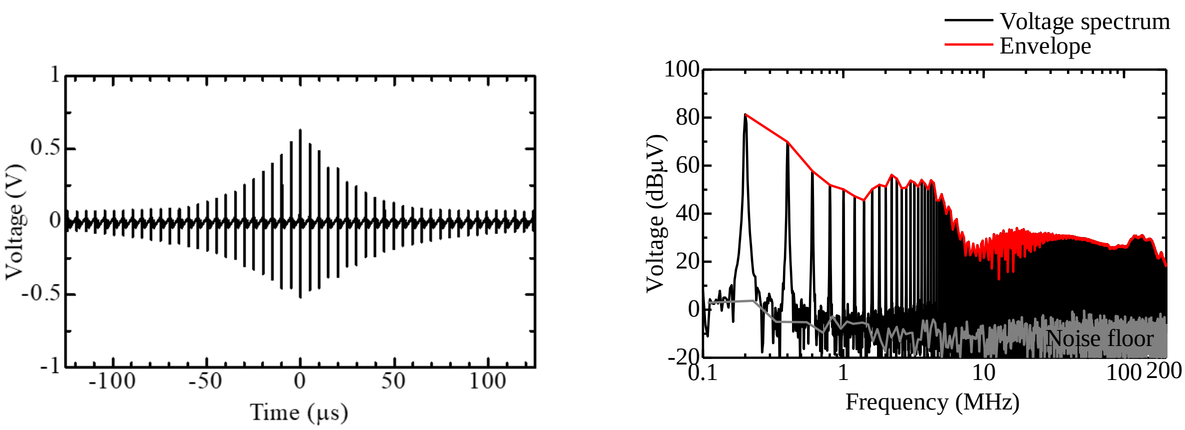

(a) Time-domain signal

(b) Frequency-domain spectrum with envelop line

Figure A.1 Envelop spectrum used in this thesis.

Appendix B

Decomposed time-domain noise signal and frequency-domain spectrum

Since Si-based buck converter working at 200 kHz, the spike signal time length is 5 μs. The obtained time-domain signal is 1 μs, the zero padding is used to make up remaining 4μs. The no filter case noise signal are shown below.

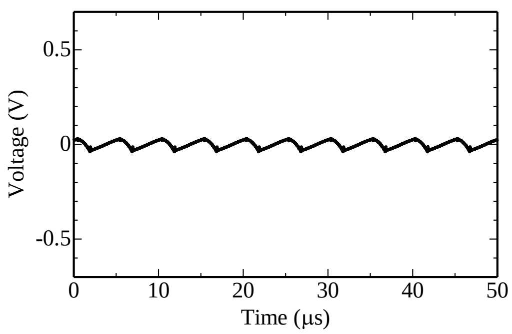

(a) Buck converter ripple noise signal

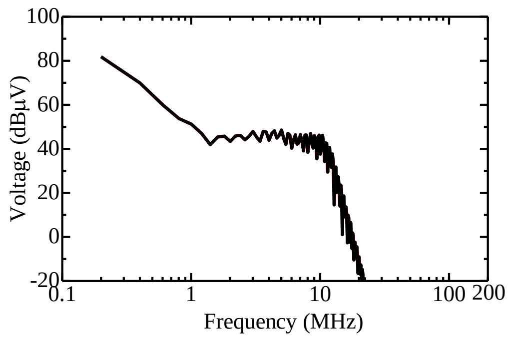

(b) Buck converter ripple noise spectrum

Figure B.1 Buck converter ripple noise.

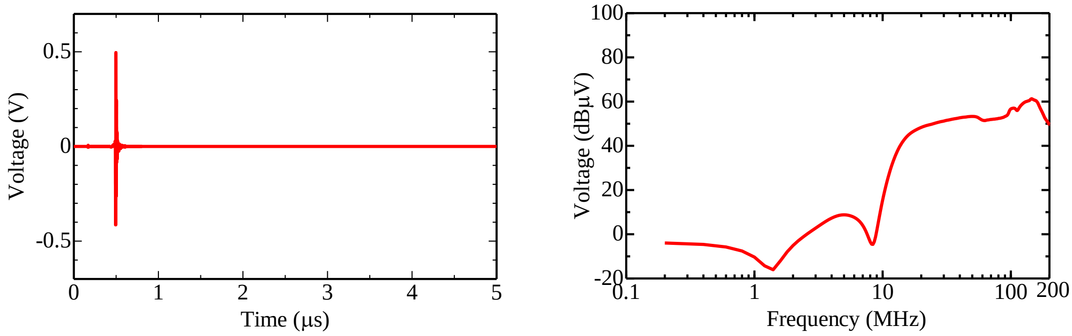

(a) Decomposed buck converter turn-on spike noise signal

(b) Decomposed buck converter turn-on spike noise spectrum

Figure B.2 Buck converter turn-on spike noise.

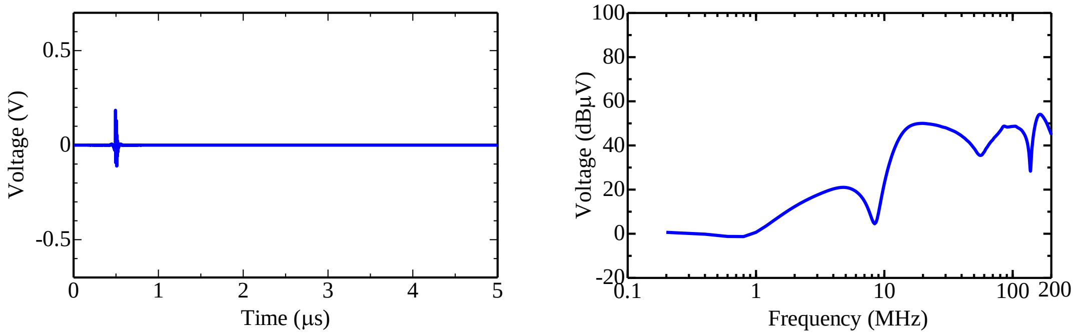

(a) Decomposed buck converter turn-off spike noise signal

(b) Decomposed buck converter turn-off spike noise spectrum

Figure B.3 Buck converter turn-off spike noise.

For GaN-based buck converter working at 200 kHz, the spike signal time length is 0.5 μs. The obtained time-domain signal is 0.25 μs, the zero padding is used to make up remaining 0.25μs. Since the turn-off spike noise is smaller than turn-on spike and it will be overwhelmed by turn-on noise. In general application condition, only the dominated noise are predicted. Thus, in GaN-based converter case, only ripple noise and turn-spike noise are measured for prediction.

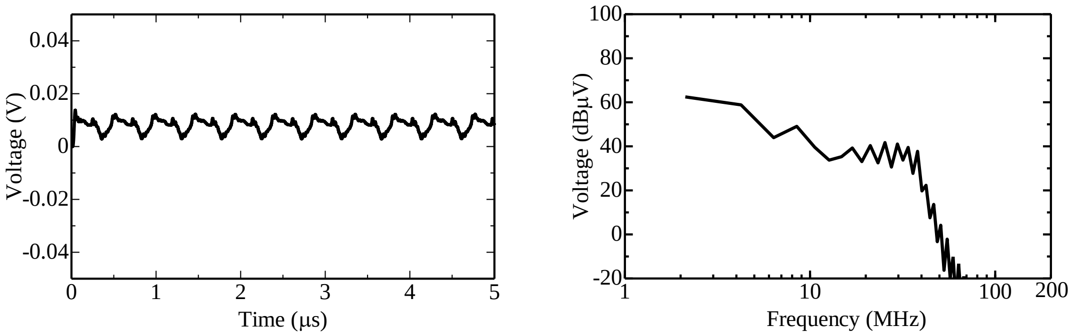

(a) GaN-based buck converter ripple noise signal (b) GaN-based buck converter ripple noise spectrum

Figure B.4 Buck converter ripple noise.

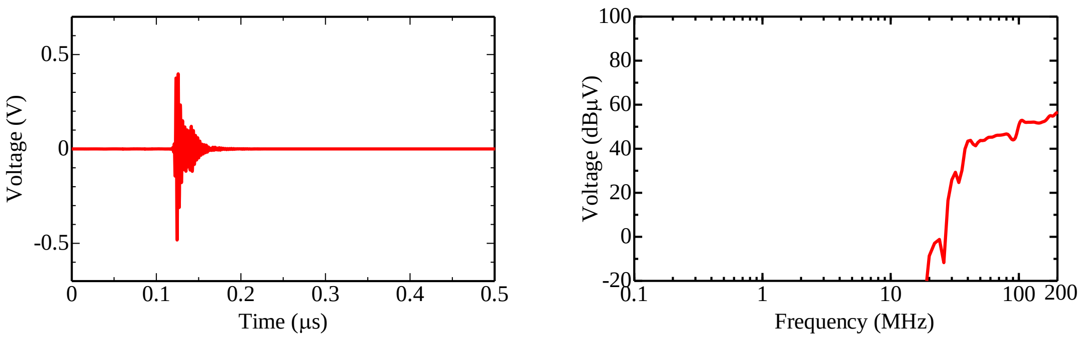

(a) GaN-based buck converter turn-on spike noise signal (b) GaN-based buck converter turn-on spike noise spectrum

Figure B.5 GaN-based buck converter turn-on spike noise.

Appendix C

Filter case measured results for parameter identification

In Chapter 2, the filter case measured results for parameter identification are shown. Same process are repeated, the measured results are in this appendix. Fig. C.1 and Fig. C.2 are measurement results of boost converter. Fig. C.3 and Fig. C.4 are measurement results of GaN-based converter.

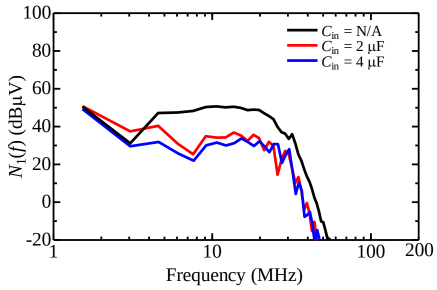

(a) Input-port ripple noise spectrum for parameter identification

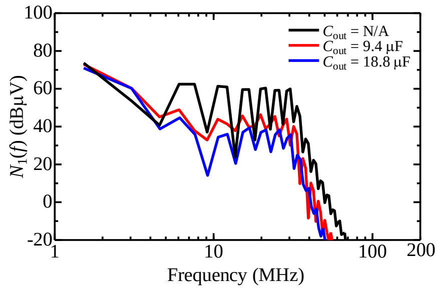

(b) Output-port ripple noise spectrum for parameter identification

Figure C.1 Boost converter ripple noise spectrum for parameter identification.

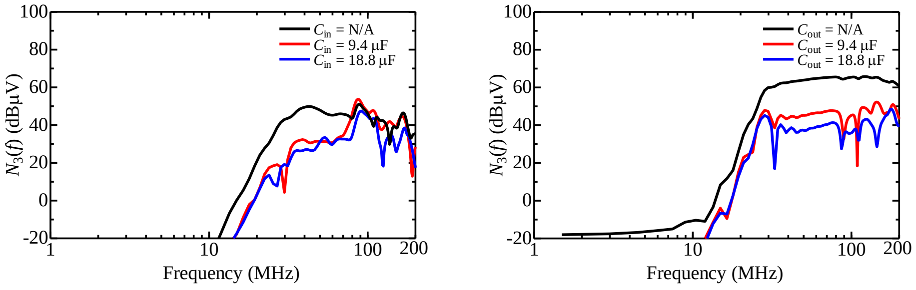

(a) Input-port ripple noise spectrum for parameter identification

(b) Output-port ripple noise spectrum for parameter identification

Figure C.2 Boost converter spike noise spectrum for parameter identification.

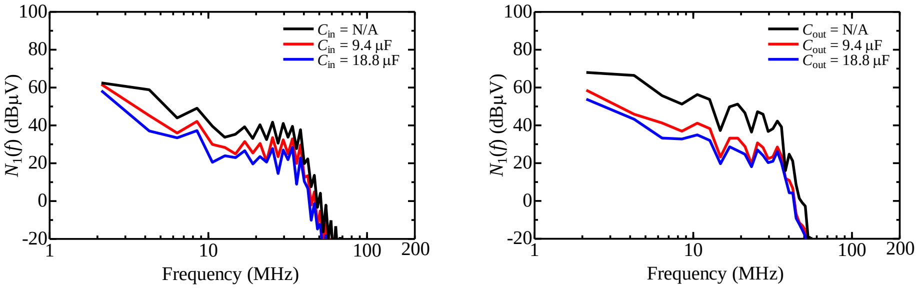

(a) Input-port ripple noise spectrum for parameter identification

(b) Output-port ripple noise spectrum for parameter identification

Figure C.3 Boost converter ripple noise spectrum for parameter identification.

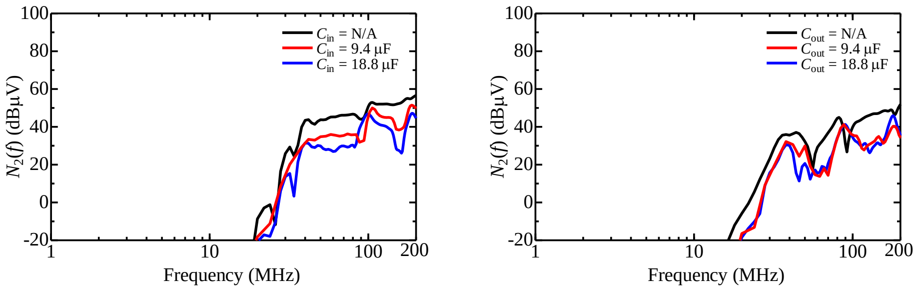

(a) Input-port turn-on noise spectrum for parameter identification

(b) Output-port turn-on noise spectrum for parameter identification

Figure C.4 GaN-based converter turn-on noise spectrum for parameter identification.

Appendix D

The impedance for load connector

To change loads easily, the connector shown Fig. C.1 was used. The frequency characteristics of the connector impedance measured by an impedance analyzer is shown. The results indicate that the parasitic inductance of the resistor with the connector was 0.36 μ H. The connector impedance is considered in the prediction process.

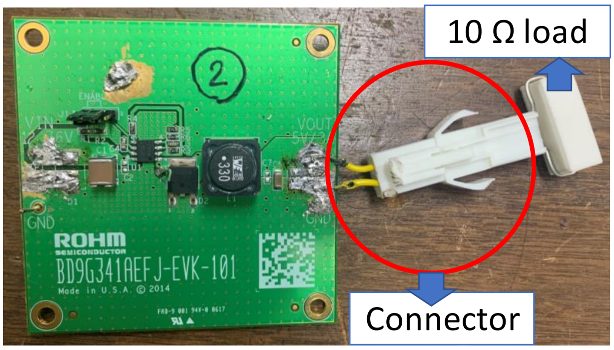

Figure D.1 The view of connector and load.

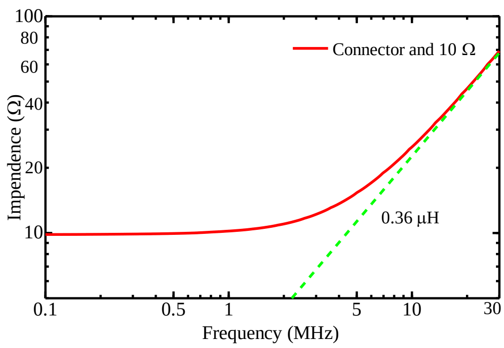

Figure D.2 The impedance of used load.

Bibliography

[1] C. R. Paul, *Introduction to electromagnetic compatibility.* John Wiley & Sons, 2006.

[2] T. Hegarty, "The engineer ' s guide to emi in dc-dc converters (part 2): Noise propagation and filtering," Tech. Rep., 2018.

[3] R. B. Ridley, "Secondary lc filter analysis and design techniques," *IEEE TRANSACTIONS (ON POWER ELECTRONICS, VOL, 3, N ()*, 1988.

[4] D. M. Hockanson, J. L. Drewniak, T. H. Hubing, T. P. Van Doren, F. Sha, and M. J. Wilhelm, "Investigation of fundamental emi source mechanisms driving common-mode radiation from printed circuit boards with attached cables," *IEEE Transactions on electromagnetic compatibility*, vol. 38, no. 4, pp. 557–566, 1996.

[5] E. Zhong and T. A. Lipo, "Improvements in emc performance of inverter-fed motor drives," *IEEE Transactions on Industry Applications*, vol. 31, no. 6, pp. 1247–1256, 1995.

[6] M. Vilathgamuwa, J. Deng, and K. Tseng, "Emi suppression with switching frequency modulated dc-dc converters," *IEEE Industry Applications Magazine*, vol. 5, no. 6, pp. 27–33, 1999.

[7] Z. Li and D. Pommerenke, "Emi specifics of synchronous dc-dc buck converters," in *2005 International Symposium on Electromagnetic Compatibility, 2005. EMC 2005.*, vol. 3. IEEE, 2005, pp. 711–714.

[8] S. Qu and D. Chen, "Mixed-mode emi noise and its implications to filter design in offline switching power supplies," *IEEE Transactions on Power Electronics*, vol. 17, no. 4, pp. 502–507, 2002.

[9] S. Wang, P. Kong, and F. C. Lee, "Common mode noise reduction for boost converters using general balance technique," *IEEE transactions on power electronics*, vol. 22, no. 4, pp. 1410–1416, 2007.

[10] S. Wang, J. D. van Wyk, and F. C. Lee, "Effects of interactions between filter parasitics and power interconnects on emi filter performance," *IEEE Transactions on Industrial Electronics*, vol. 54, no. 6, pp. 3344–3352, 2007.

[11] H.-I. Hsieh, J.-S. Li, and D. Chen, "Effects of x capacitors on emi filter effectiveness," *IEEE Transactions on Industrial Electronics*, vol. 55, no. 2, pp. 949–955, 2008.

[12] F. A. Kharanaq, A. Emadi, and B. Bilgin, "Modeling of conducted emissions for emi analysis of power converters: State-of-the-art review," *IEEE Access*, vol. 8, pp. 189 313–189 325, 2020.

[13] H. Heeb and A. E. Ruehli, "Three-dimensional interconnect analysis using partial element equivalent circuits," *IEEE Transactions on Circuits and Systems I: Fundamental Theory and Applications*, vol. 39, no. 11, pp. 974–982, 1992.

[14] H. Zhu, J.-S. Lai, A. R. Hefner, Y. Tang, and C. Chen, "Analysis of conducted emi emissions from pwm inverter based on empirical models and comparative experiments," in *30th Annual IEEE Power Electronics Specialists Conference. Record.(Cat. No. 99CH36321)*, vol. 2. IEEE, 1999, pp. 861–867.

[15] H. Zhu, J.-S. Lai, A. R. Hefner, Y. Tang, and C. Chen, "Modeling-based examination of conducted emi emissions from hard-and soft-switching pwm inverters," *IEEE Transactions on Industry Applications*, vol. 37, no. 5, pp. 1383–1393, 2001.

[16] J.-S. Lai, X. Huang, S. Chen, and T. W. Nehl, "Emi characterization and simulation with parasitic models for a low-voltage high-current ac motor drive," *IEEE Transactions on Industry Applications*, vol. 40, no. 1, pp. 178–185, 2004.

[17] E. Gubia, P. Sanchis, A. Ursúa, J. López, and L. Marroyo, "Frequency domain model of conducted emi in electrical drives," *IEEE Power Electronics Letters*, vol. 3, no. 2, pp. 45–49, 2005.

[18] J.-S. Lai, X. Huang, E. Pepa, S. Chen, and T. W. Nehl, "Inverter emi modeling and simulation methodologies," *IEEE Transactions on Industrial Electronics*, vol. 53, no. 3, pp. 736–744, 2006.

[19] B. Touré, J.-L. Schanen, L. Gerbaud, T. Meynard, J. Roudet, and R. Ruelland, "Emc modeling of drives for aircraft applications: modeling process, emi filter optimization, and technological choice," *IEEE Transactions on Power Electronics*, vol. 28, no. 3, pp. 1145–1156, 2012.

[20] A. Nejadpak and O. A. Mohammed, "Physics-based modeling of power converters from finite element electromagnetic field computations," *IEEE Transactions on Magnetics*, vol. 49, no. 1, pp. 567–576, 2012.

[21] I. F. Kovačević, T. Friedli, A. M. Muesing, and J. W. Kolar, "3-d electromagnetic modeling of emi input filters," *IEEE Transactions on Industrial Electronics*, vol. 61, no. 1, pp. 231–242, 2013.

[22] X. Gong and J. A. Ferreira, "Investigation of conducted emi in sic jfet inverters using separated heat sinks," *IEEE transactions on industrial electronics*, vol. 61, no. 1, pp. 115–125, 2013.

[23] E. Rondon-Pinilla, F. Morel, C. Vollaire, and J.-L. Schanen, "Modeling of a buck converter with a sic jfet to predict emc conducted emissions," *IEEE Transactions on Power Electronics*, vol. 29, no. 5, pp. 2246–2260, 2013.

[24] A. Boyer, M. G. Sentis, C. Ghfiri, and A. Durier, "Modeling methodology of the conducted emission of a dc-dc converter board," in *2017 11th International Workshop on the Electromagnetic Compatibility of Integrated Circuits (EMCCompo)*. IEEE, 2017, pp. 73–78.

[25] P. R. Mugur, J. Roudet, and J.-C. Crebier, "Power electronic converter emc analysis through state variable approach techniques," *IEEE Transactions on Electromagnetic Compatibility*, vol. 43, no. 2, pp. 229–238, 2001.

[26] J. Meng, W. Ma, Q. Pan, Z. Zhao, and L. Zhang, "Noise source lumped circuit modeling and identification for power converters," *IEEE transactions on industrial electronics*, vol. 53, no. 6, pp. 1853–1861, 2006.

[27] Q. Liu, F. Wang, and D. Boroyevich, "Modular-terminal-behavioral (mtb) model for characterizing switching module conducted emi generation in converter systems," *IEEE Transactions on power electronics*, vol. 21, no. 6, pp. 1804–1814, 2006.

[28] A. C. Baisden, D. Boroyevich, and F. Wang, "Generalized terminal modeling of electromagnetic interference," *IEEE Transactions on Industry Applications*, vol. 46, no. 5, pp. 2068–2079, 2010.

[29] H. Bishnoi, A. C. Baisden, P. Mattavelli, and D. Boroyevich, "Analysis of emi terminal modeling of switched power converters," *IEEE Transactions on Power Electronics*, vol. 27, no. 9, pp. 3924–3933, 2012.

[30] H. Bishnoi, P. Mattavelli, R. Burgos, and D. Boroyevich, "Emi behavioral models of dc-fed three-phase motor drive systems," *IEEE Transactions on Power Electronics*, vol. 29, no. 9, pp. 4633–4645, 2013.

[31] D. Zhang, D. Y. Chen, M. J. Nave, and D. Sable, "Measurement of noise source impedance of off-line converters," *IEEE Transactions on Power Electronics*, vol. 15, no. 5, pp. 820–825, 2000.

[32] V. Tarateeraseth, B. Hu, K. Y. See, and F. G. Canavero, "Accurate extraction of noise source impedance of an smps under operating conditions," *IEEE Transactions on Power Electronics*, vol. 25, no. 1, pp. 111–117, 2009.

[33] A. Ales, J.-L. Schanen, D. Moussaoui, and J. Roudet, "Impedances identification of dc/dc converters for network emc analysis," *IEEE Transactions on Power Electronics*, vol. 29, no. 12, pp. 6445–6457, 2014.

[34] M. Foissac, J.-L. Schanen, and C. Vollaire, "" black box " emc model for power electronics converter," in *2009 IEEE Energy Conversion Congress and Exposition*. IEEE, 2009, pp. 3609–3615.

[35] G. Frantz, D. Frey, J. L. Schanen, B. Revol, H. Bishnoi, and P. Mattavelli, "Emc models for power electronics: From converter design to system level," in *2013 IEEE Energy Conversion Congress and Exposition*. IEEE, 2013, pp. 4247–4252.

[36] T. J. Donnelly, S. D. Pekarek, D. R. Fudge, and N. Zarate, "Thévenin equivalent circuits for modeling common-mode behavior in power electronic systems," *IEEE Open Access Journal of Power and Energy*, vol. 7, pp. 163–172, 2020.

[37] P. Hillenbrand, M. Böttcher, S. Tenbohlen, and J. Hansen, "Frequency domain emi-simulation and resonance analysis of a dcdc-converter," in *2016 International Symposium on Electromagnetic Compatibility-EMC EUROPE*. IEEE, 2016, pp. 176–181.

[38] B. Czerniewski, J.-L. Schanen, H. Chazal, P. Zanchetta, and C. F. d. Freitas, "Identification and validation of a non symmetrical system level emc model for power electronics converter," in *2021 IEEE Energy Conversion Congress and Exposition (ECCE)*, 2021, pp. 2859–2865.

[39] B. Kerrouche, M. Bensetti, and A. Zaoui, "New emi model with the same input impedances as converter," *IEEE Transactions on Electromagnetic Compatibility*, vol. 61, no. 4, pp. 1072–1081, 2019.

[40] H. Zhang and S. Wang, "Emi noise source modeling based on network theory for power converters with mixed-mode characterization," in *2018 IEEE Applied Power Electronics Conference and Exposition (APEC)*, 2018, pp. 984–991.

[41] W. Zhou, X. Pei, Y. Xiang, and Y. Kang, "A new emi modeling method for mixed-mode noise analysis in three-phase inverter system," *IEEE Access*, vol. 8, pp. 71 535–71 547, 2020.

[42] Y. Osaki, Y. Yano, K. Iokibe, and Y. Toyota, "Parameter identification of noise-source linear equivalent circuit of dc-dc converter and its evaluation," in *Proc. of APEMC 2017*, 2017, p. 217.

[43] T. Uematsu, Y. Osaki, Y. Yano, K. Iokibe, and Y. Toyota, "Improvement of prediction accuracy of noise-source equivalent-circuit model based on parameter extraction by port voltage/current measurement," in *Proc. of 2019 Joint International Symposium on Electromagnetic Compatibility and Asia-Pacific International Symposium on Electromagnetic Compatibility*, 2019, p. 199.

[44] S. Zhang, T. Uematsu, K. Iokibe, and Y. Toyota, "Two-port noise source equivalent circuit model for dc/dc buck converter with consideration of load effect," in *2020 International Symposium on Electromagnetic Compatibility-EMC EUROPE*. IEEE, 2020, pp. 1–4.

[45] H. M. Rebholz, S. Tenbohlen, and W. KÖhler, "Time-domain characterization of rf sources for the design of noise suppression filters," *IEEE transactions on electromagnetic compatibility*, vol. 51, no. 4, pp. 945–952, 2009.

[46] A.-M. Sánchez, S. A. Pignari, J.-R. Regué, and M. Ribó, "Device modeling for nonstationary conducted emissions based on frequency- and time-domain measurements," *IEEE Transactions on Electromagnetic Compatibility*, vol. 54, no. 4, pp. 738–746, 2012.

[47] R. Trinchero, I. S. Stievano, and F. G. Canavero, "Emi prediction of switching converters," *IEEE Transactions on Electromagnetic Compatibility*, vol. 57, no. 5, pp. 1270–1273, 2015.

[48] R. Trinchero, I. S. Stievano, and F. G. Canavero, "Enhanced time-invariant linear model for the emi prediction of switching circuits," *IEEE Transactions on Electromagnetic Compatibility*, vol. 62, no. 5, pp. 2294–2302, 2020.

[49] G. Shen, S. Shinde, A. Patnaik, D. Pommerenke, H. Aichele, C. Keller, M. Boettcher, and V. Khilkevich, "Terminal modeling of dc–dc converters with stochastic behavior," *IEEE Transactions on Electromagnetic Compatibility*, vol. 60, no. 6, pp. 2011–2018, 2018.

[50] L. Wan, A. Beshir, X. Wu, X. Liu, F. Grassi, G. Spadacini, and S. Pignari, "Assessment of validity conditions for black-box emi modelling of dc/dc converters," in *2021 IEEE International Joint EMC/SI/PI and EMC Europe Symposium*, 2021, pp. 581–585.

[51] H. Chen, T. Wang, L. Feng, and G. Chen, "Determining far-field emi from near-field coupling of a power converter," *IEEE Transactions on Power Electronics*, vol. 29, no. 10, pp. 5257–5264, 2013.

[52] S. Shinde, K. Masuda, G. Shen, A. Patnaik, T. Makharashvili, D. Pommerenke, and V. Khilkevich, "Radiated emi estimation from dc–dc converters with attached cables based on terminal equivalent circuit modeling," *IEEE Transactions on Electromagnetic Compatibility*, vol. 60, no. 6, pp. 1769–1776, 2017.

[53] J. Yao, S. Wang, and H. Zhao, "Measurement techniques of common mode currents, voltages, and impedances in a flyback converter for radiated emi diagnosis," *IEEE Transactions on Electromagnetic Compatibility*, vol. 61, no. 6, pp. 1997–2005, 2019.

[54] J. He, Z. Guo, and X. Li, “Mechanism model and prediction method of common mode radiation for a nonisolated very-high-frequency dc–dc converter with cables,” *IEEE Transactions on Power Electronics*, vol. 35, no. 10, pp. 10 227–10 237, 2020.

[55] J. Yao, S. Wang, and Z. Luo, “Modeling, analysis, and reduction of radiated emi due to the voltage across input and output cables in an automotive non-isolated power converter,” *IEEE Transactions on Power Electronics*, vol. 37, no. 5, pp. 5455–5465, 2021.

[56] M. Ali, E. Labouré, F. Costa, and B. Revol, “Design of a hybrid integrated emc filter for a dc–dc power converter,” *IEEE Transactions on Power Electronics*, vol. 27, no. 11, pp. 4380–4390, 2012.

[57] S. Negri, G. Spadacini, F. Grassi, and S. A. Pignari, “Prediction of emi filter attenuation in power-electronic converters via circuit simulation,” *IEEE Transactions on Electromagnetic Compatibility*, 2022.

[58] A. Sangswang and C. O. Nwankpa, “Noise characteristics of dc-dc boost converters: experimental validation and performance evaluation,” *IEEE Transactions on Industrial Electronics*, vol. 51, no. 6, pp. 1297–1304, 2004.

[59] D. Bellan, F. Marliani, S. A. Pignari, and G. Spadacini, “Spectral analysis of conducted emissions of dc/dc converters,” in *2010 IEEE International Symposium on Electromagnetic Compatibility*, 2010, pp. 490–494.

[60] S. Zhang, T. Uematsu, K. Iokibe, and Y. Toyota, “Noise-source parameter identification considering switching fluctuation of dc-dc converter,” in *2021 IEEE International Joint EMC/SI/PI and EMC Europe Symposium*, 2021, p. 186.

[61] S. Zhang, K. Iokibe, and Y. Toyota, “An approach to predicting conducted noise from dc-dc converter accounting for switching fluctuation,” in *2021 Asia-Pacific International Symposium on Electromagnetic Compatibility (APEMC)*, 2021, pp. 1–4.

[62] F. Lin and D. Y. Chen, “Reduction of power supply emi emission by switching frequency modulation,” *IEEE transactions on power electronics*, vol. 9, no. 1, pp. 132–137, 1994.

[63] J. Balcells, A. Santolaria, A. Orlandi, D. Gonzalez, and J. Gago, “Emi reduction in switched power converters using frequency modulation techniques,” *IEEE Transactions on Electromagnetic Compatibility*, vol. 47, no. 3, pp. 569–576, 2005.

[64] F. Pareschi, R. Rovatti, and G. Setti, “Emi reduction via spread spectrum in dc/dc converters: State of the art, optimization, and tradeoffs,” *IEEE Access*, vol. 3, pp. 2857–2874, 2015.

[65] J. R. Carson, "Notes on the theory of modulation," *Proceedings of the Institute of Radio Engineers*, vol. 10, no. 1, pp. 57–64, 1922.

[66] *Evaluation Board: High Voltage 3A Buck Converter With Integrated FET*, ROHM Co., Ltd, 2019, rev. 004. [Online]. Available: https://fscdn.rohm.com/en/products/databook/applinote/ic/power/switching_regulator/bd9g341aefj-evk-101-e.pdf

[67] *DEMO MANUAL DC2186A*, Linear Technology Corporation, 2004. [Online]. Available: https://www.analog.com/media/en/technical-documentation/user-guides/DC2186AF.PDF

[68] *EPC9160, 9V-24V Dual Output 5V/ 3.3V Synchronous Buck Converter Evaluation Board,Quick Start Guide*, Efficient Power Conversion Corporation, 2021, rev. 001. [Online]. Available: https://www.analog.com/media/en/technical-documentation/user-guides/DC2186AF.PDF

[69] K. Kostov, J. Rabkowski, and H.-P. Nee, "Conducted emi from sic bjt boost converter and its dependence on the output voltage, current, and heatsink connection," in *2013 IEEE ECCE Asia Downunder*, 2013, pp. 1125–1130.

[70] J. Yousaf, M. Amin, S. Iqbal, H. Durrani, and M. K. Amin, "Conducted emission analysis of dc-dc converters and proper selection of pre-filtering stage," in *Proceedings of 2013 10th International Bhurban Conference on Applied Sciences Technology (IBCAST)*, 2013, pp. 360–363.

[71] M. Amara, C. Vollaire, M. Ali, and F. Costa, "Black box emc modeling of a three phase inverter," in *2018 International Symposium on Electromagnetic Compatibility (EMC EUROPE)*, 2018, pp. 642–647.

[72] Balaji Siva Prasad Emandi, "Improving emi performance through simulation," 2018, https://www.eetimes.com/improving-emi-performance-through-simulation/, Last accessed on 2023-02-03.

[73] M. Schurmann and H. P. Solutions, "Not all jitter is created equal: Understanding jitter in switching power supplies," *Texas Instrument, Appl. Rep. SLUA747A*, 2015.

[74] T. Ueda, "Reliability issues in gan and sic power devices," in *2014 IEEE International Reliability Physics Symposium*, 2014, pp. 3D.4.1–3D.4.6.

Research Activities

Paper

1. **Shuqi Zhang**, Kengo Iokibe, Yoshitaka Toyota "An Approach to Identify Noise-source Parameters of DC-DC Converter and Predict Conducted Emissions with Different Loads," *IEEE Letters on Electromagnetic Compatibility Practice and Applications*, Early access

2. **Shuqi Zhang**, Kengo Iokibe, Yoshitaka Toyota "Conducted Noise Prediction for DC-DC Converter by Noise Source Model Accounting for Switching Fluctuation," *IEEE Transactions on Electromagnetic Compatibility*, Early access

International Conferences

1. **Shuqi Zhang**, Taishi Uematsu, Kengo Iokibe, Yoshitaka Toyota "Two-port Noise Source Equivalent Circuit Model for DC/DC Buck Converter with Consideration of Load Effect," *2020 International Symposium on Electromagnetic Compatibility - EMC EUROPE, 2020*, pp. 1-4, Online, Sep. 2020

2. **Shuqi Zhang**, Taishi Uematsu, Kengo Iokibe, Yoshitaka Toyota "Noise-Source Parameter Identification Considering Switching Fluctuation of DC-DC Converter," *2021 IEEE International Joint EMC/SI/PI and EMC Europe Symposium, 2021*, p. 186, Online, Aug. 2021

3. **Shuqi Zhang**, Kengo Iokibe, Yoshitaka Toyota "An Approach to Predicting Conducted Noise from DC-DC Converter Accounting for Switching Fluctuation," *2021 Asia-Pacific International Symposium on Electromagnetic Compatibility (APEMC), 2021*, pp. 1-4, Online, Sep. 2021

4. **Shuqi Zhang**, Kengo Iokibe, Yoshitaka Toyota "A Load-variable Noise-source Equivalent Circuit Model for DC-DC Converter Considering Cubic Spline Interpolation," *11th IEEE CPMT Symposium Japan (ICSJ 2022)*, pp. 154-157, Kyoto, Japan, Nov. 2022.

Technical Report

1. Taishi Uematsu, **Shuqi Zhang**, Kengo Iokibe, Yoshitaka Toyota “Parameter Identification of Noise-source Equivalent-circuit Model Focusing on Turn-on/Turn-off Timing of DC/DC Converter and Evaluation of Conducted Disturbance Measurement,” *IEICE technical report*, vol. 120, no. 282, EMCJ2020-61, pp. 31-36, Online, Dec. 2020. *(in Japanese)*

2. Mio Ohara, **Shuqi Zhang**, Kengo Iokibe, Yoshitaka Toyota “Investigation of Applicable Range of Conducted Disturbance Prediction Using Noise-source Equivalent-circuit Model of DC/DC Converter,” *Electrical and Information Engineering Societies Chugoku Section Joint Conference*, vol. 72nd, ROMBUNNO.R21-04-05, Online, Oct, 2021. *(in Japanese)*

3. Yanyu Jin, **Shuqi Zhang**, Kengo Iokibe, Yoshitaka Toyota “Investigation of Applicable Types of DC-DC Converters to Noise-source Equivalent-circuit Model for Conducted-noise Prediction,” *IEICE technical report*, Vol. 122 (2023).

Biography

Shuqi Zhang was born in Inner Mongolia Autonomous Region, China, on March 15th, 1994. He received a B.S. degree in electrical engineering from Northeast Electric Power University, Jilin, Jilin, China, in 2011. He then received an M.S. degree in power electronics and power drives from Dalian Jiaotong University, Dalian, Liaoning, China, in 2015. He is currently working toward a Ph.D. degree in electronic and information systems engineering at Okayama University, Okayama, Japan. His research interest is EMC modeling of power converter circuits.